AWARD NUMBER: W81XWH-16-1-0600

TITLE: Dissecting the Mechanisms of Drug Resistance in BRCA1/2-Mutant Breast Cancers

PRINCIPAL INVESTIGATOR: Dr. Alan D'Andrea

CONTRACTING ORGANIZATION:
Dana-Farber Cancer Institute Inc
Boston, MA 02215-5450

REPORT DATE: October 2017

TYPE OF REPORT: Annual

PREPARED FOR: U.S. Army Medical Research and Materiel Command
Fort Detrick, Maryland 21702-5012

REPORT DOCUMENTATION PAGE

Form Approved
OMB No. 0704-0188

1. REPORT DATE	2. REPORT TYPE	3. DATES COVERED
October 2017	Annual	30 Sep 2016 - 29 Sep 2017

4. TITLE AND SUBTITLE

Dissecting the Mechanisms of Drug Resistance in BRCA1/2-Mutant Breast Cancers

5a. CONTRACT NUMBER

5b. GRANT NUMBER
W81XWH-16-1-0600

5c. PROGRAM ELEMENT NUMBER

6. AUTHOR(S)

Alan D'Andrea

Alan_Dandrea@dfci.harvard.edu

5d. PROJECT NUMBER

5e. TASK NUMBER

5f. WORK UNIT NUMBER

7. PERFORMING ORGANIZATION NAME(S) AND ADDRESS(ES)
Dana-Farber Cancer Institute Inc.
450 Brookline Avenue, Boston MA
02215-5450

8. PERFORMING ORGANIZATION REPORT NUMBER

9. SPONSORING / MONITORING AGENCY NAME(S) AND ADDRESS(ES)

U.S. Army Medical Research and Materiel Command
Fort Detrick, Maryland 21702-5012

10. SPONSOR/MONITOR'S ACRONYM(S)

11. SPONSOR/MONITOR'S REPORT NUMBER(S)

12. DISTRIBUTION / AVAILABILITY STATEMENT

Approved for Public Release; Distribution Unlimited

13. SUPPLEMENTARY NOTES

14. ABSTRACT

Poly(ADP-ribose) polymerase (PARP) inhibition provides a promising therapeutic modality for targeting homologous recombination (HR) deficient tumors such as BRCA1 and BRCA2-mutated triple negative breast cancers (TNBCs). Although PARP inhibitors have shown activity in the BRCA-associated TNBCs, several of these tumors develop *de novo* as well as acquired PARP inhibitor (PARPi) resistance. Besides attenuation in intracellular uptake of drugs, the only known mechanism that drives chemotherapy resistance of BRCA1/2-deficient cancers is through the restoration of HR. Recent studies from our laboratories (Nussenzweig and D'Andrea) indicate that deregulation of pathways that promote extensive degradation of nascent DNA strands and alternative end-joining (Alt-EJ) can render BRCA1/2-deficient cells resistant to PARPi in a HR-independent manner. The objective of our project is to collaboratively test the hypothesis that complex processes involving Alt-EJ or replication fork stability promote survival and drives resistance to chemotherapy. A detailed assessment of the

critical mediators that regulate the balance between HR, Alt-EJ and replication fork degradation should identify novel means to overcome acquired chemoresistance in BRCA1/2-mutated breast cancers. During the first year of the DOD funding, we have made progress in identifying the proteins which contribute to the replication fork stability and we have identified new mechanisms of chemoresistance in BRCA2-deficient tumors.

15. SUBJECT TERMS

Breast cancer, BRCA1, BRCA2, PARP inhibitors, chemotherapy, resistance, HR, replication fork stability, EZH2, PAR, FK866, NMNAT-1/2/3

16. SECURITY CLASSIFICATION OF:			**17. LIMITATION OF ABSTRACT**	**18. NUMBER OF PAGES**	**19a. NAME OF RESPONSIBLE PERSON**
					USAMRMC
a. REPORT	**b. ABSTRACT**	**c. THIS PAGE**	Unclassified	69	**19b. TELEPHONE NUMBER** *(include area code)*
Unclassified	Unclassified	Unclassified			

Standard Form 298 (Rev. 8-98)
Prescribed by ANSI Std. Z39.18

Table of Contents

Page

1. INTRODUCTION:

The inactivation of the tumor suppressor genes *BRCA1* and *BRCA2* by mutations or epigenetic silencing is a critical event in breast and ovarian carcinogenesis. *BRCA1* and *BRCA2* encode proteins that are essential for accurate double strand break (DSB) repair by homologous recombination (HR). BRCA1 functions early during DSB resection, BRCA2 functions later in HR by catalyzing RAD51 nucleo-filaments at processed DSBs. Accordingly, HR deficient breast and ovarian tumors are highly sensitive to poly(ADP-ribose) polymerase (PARP) inhibitors, since PARP inhibitors exhibit synthetic lethality in tumors with defective HR DNA repair. PARP inhibitors are currently in development for BRCA- or otherwise HR repair-deficient cancers, with FDA approval of Olaparib, Rucaparib and Niraparib. Of these drugs, Olaparib has been the most widely studied thus far, and it has been approved by the FDA as a monotherapy for treatment of ovarian cancer patients with germline *BRCA1* or *BRCA2* mutations. Nonetheless, *de novo* and acquired PARP inhibitor (PARPi) resistance, is a pressing clinical problem in patients with BRCA-deficient cancers treated with PARP inhibitors. Therefore, identification of the mechanisms underlying PARPi resistance is crucial for improving treatment and predicting tumor responses. Besides attenuation in intracellular uptake and increased efflux of drugs, the other known mechanism of PARPi resistance in BRCA-deficient tumors include restoration of HR due to somatic reversion of *BRCA1/BRCA2* or loss of other genes such as 53BP1, RIF1 or REV7. Recently, it was shown that BRCA1 and BRCA2 protect stalled replication forks from Mre11-mediated degradation, independent of their roles in HR. Accordingly, restoration of either HR capacity or replication fork stability is also associated with PARPi resistance in BRCA-deficient tumors. Indeed, a recent study from the Nussenzweig laboratory indicated that loss of *PTIP* protects replication forks from degradation in both *BRCA1*- and *BRCA2*- deficient cells and confers PARPi resistance. The D'Andrea laboratory has recently identified a novel DNA repair pathway, the so-called PARP/POLQ end-joining pathway, which, when upregulated, provides the HR-deficient breast tumor cell with an alternative mechanism of DNA repair. Collectively, recent studies from both laboratories indicate that deregulation of pathways that promote extensive degradation of nascent DNA strands and alternative end-joining (Alt-EJ) can render BRCA1/2-deficient cells resistant to PARPi in a HR independent manner. *We had therefore hypothesized that replication fork protection and PARP mediated Alt-EJ are novel and potentially interlinked mechanisms by which BRCA1/2-deficient breast cancers acquire resistance to chemotherapy.* Accordingly, the objective of our project is to provide a more detailed assessment of the factors that contribute to replication fork protection and Alt-EJ. This could lead to therapeutic approaches to overcome acquired resistance by targeting new vulnerabilities in both *BRCA1/2*-mutant and *BRCA1/2*–wildtype breast cancer.

2. KEYWORDS:

Breast cancer, BRCA1, BRCA2, PARP inhibitors, chemotherapy, resistance, HR, replication fork stability, EZH2, PAR, FK866, NMNAT-1/2/3

3. ACCOMPLISHMENTS:

The major goal of the project is to identify the molecular mechanisms of PARPi resistance in BRAC1/BRCA2 mutated breast tumors in order to improve therapeutic options for breast cancer patients.
The following specific aims were proposed:

> **Specific Aim 1**. Understand how PTIP-MLL3/4 and PARP1 confers chemoresistance and replication fork (RF) degradation in BRCA1/2-deficient cells.
> **Specific Aim 2**. Determine the interactions of BRCA2, FANCD2, and POLQ in replication fork (RF) stability and Alt-EJ
> **Specific Aim 3**. Assess mechanisms of PARPi resistance in mouse models and patient derived xenografts

- What was accomplished under these goals?

We have described major activities, specific objectives, significant results or key outcomes, conclusions and other achievements related to each specific aim in the following section. Both Drs. Nussenzweig and D'Andrea have noted tasks for which they were responsible (Site 1, NCI, NIH; Site 2, DFCI).

Specific Aim 1: Understand how PTIP-MLL3/4 and PARP1 confers chemo-resistance in BRCA1/2-deficient cells

> **Major Task 1.** Defining the functional domains of PTIP and the contribution of MLL3/4 to drug resistance (site 1, NCI, NIH Dr. Nussensweig)

We performed structure/function studies using PTIP mutants. To identify the region of PTIP that promotes RF degradation in *Brca2*-deficient cells, we expressed EV (empty vector), FL (full-length PTIP), W165R (disrupting interactions with PA1), W663R (disrupting interactions with 53BP1 at DSBs), or Del-BRCT5-6 (disrupting interaction with MLL3/4 independently of DSBs), in *Brca2/Ptip* doubly deficient cells. We observed that only reconstitution of *Brca2/Ptip*-deficient cells with PTIP-Del-BRCT5-6 maintained fork protection. This data was recently published (A. Ray Chaudhuri et al. Nussenzweig, Nature 2016).

Since the PTIP-Del-BRCT5-6 domain disrupts interaction with MLL3/4, we therefore tested whether the recruitment of MRE11 at stalled forks was dependent on MLL3/4. We observed that MRE11 association at RFs was dependent on MLL3/4 as monitored by iPOND and immunofluorescence analysis. We also observed an enrichment of H3K4me1 and H3K4me3 at nascent forks upon HU treatment that was PTIP- and MLL3/4-dependent. Thus, deposition of MRE11 on newly synthesized or stalled chromatin correlates with the establishment of

H3K4me1 and H3K4me3 at RFs. This data was recently published (A. Ray Chaudhuri et al. Nussenzweig, Nature 2016).

To determine whether MLL4 contributes to degradation of stalled forks in *Brca*-deficient cells, we examined RF degradation in *Brca1*$^{-/-}$ *Mll4*$^{-/-}$ and *Brca2*$^{-/-}$*Mll4*$^{-/-}$ B cells. *Brca1*$^{-/-}$*Mll4*$^{-/-}$ and *Brca2*$^{-/-}$ *Mll4*$^{-/-}$ cells displayed a partial rescue of fork degradation To test whether MLL4 methyltransferase activity is critical, we targeted the catalytic SET domain of MLL4 in *Brca1*-deficient B cells. We observed a significant rescue of fork degradation in *Brca1*$^{-/-}$*Mll4*-SET$^{-/-}$ cells, suggesting that the methyltransferase activity is important for promoting fork degradation. In addition, we observed that *Brca2*$^{-/-}$ *Mll4*$^{-/-}$ B cells showed a partial rescue of chromosomal aberrations upon PARPi and cisplatin treatment compared with *Brca2*$^{-/-}$ cells alone. This data was recently published (A. Ray Chaudhuri et al. Nussenzweig, Nature 2016).

Major Task 2: Determine the mechanisms by which PARP1 modulates chemosensitivity in BRCA2 deficient cells

Subtask 1: To test whether PARP1 deficiency protects replication forks from degradation in the absence of BRCA2 (**Site 1, NCI, NIH, Dr. Nussenzweig**)

It is possible that PARP1 triggers genomic instability in Brca2 deficient cells because of excessive poly(ADP-ribose) synthesis or NAD+ depletion. It has been reported that levels of PAR are increased in Brca2 deficient cells, which may result in energy depletion. If such mechanisms reduce NAD+ and ATP levels in Brca2-deficient cells, it might be possible to promote fitness and/or reduce genome instability by overexpression with PARG (an enzyme which cleaves the linkage between ADP-ribose and acceptor proteins), or by supplementing cells with NAD (+) precursors nicotinamide riboside and nicotinamide mononucleotide.

Poly ADP-ribosylation (PARylation) is a type of reversible posttranslational modification that is performed by enzymes in the PAR polymerase (PARP) family, which results in the covalent attachment of polymers of ADP-ribose units on a variety of amino acid residues on target proteins. This modification is mediated by a diverse group of ADP-ribosyl transferase enzymes that use ADP-ribose units derived from NAD+ to catalyze the ADP-ribosylation reaction. It has been previously estimated that ~90% of PAR polymers are

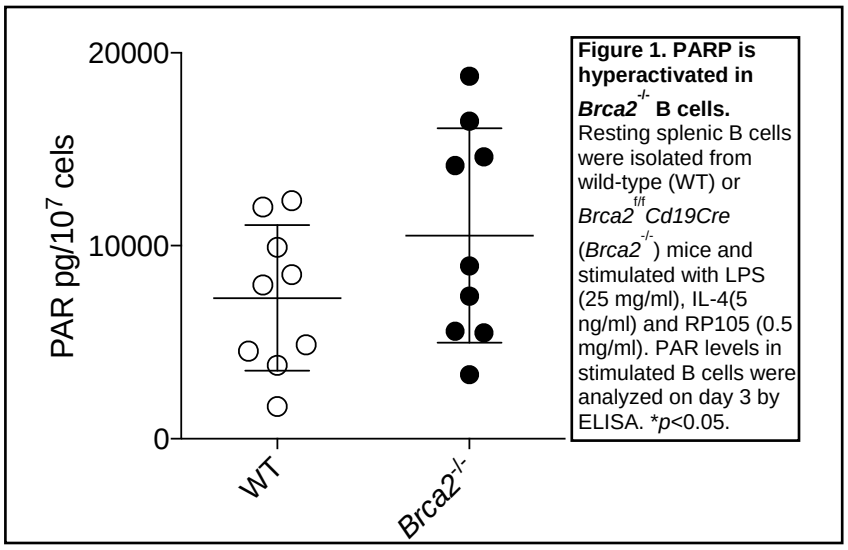

Figure 1. PARP is hyperactivated in *Brca2*$^{-/-}$ B cells. Resting splenic B cells were isolated from wild-type (WT) or *Brca2*$^{f/f}$ *Cd19Cre* (*Brca2*$^{-/-}$) mice and stimulated with LPS (25 mg/ml), IL-4(5 ng/ml) and RP105 (0.5 mg/ml). PAR levels in stimulated B cells were analyzed on day 3 by ELISA. *p<0.05.

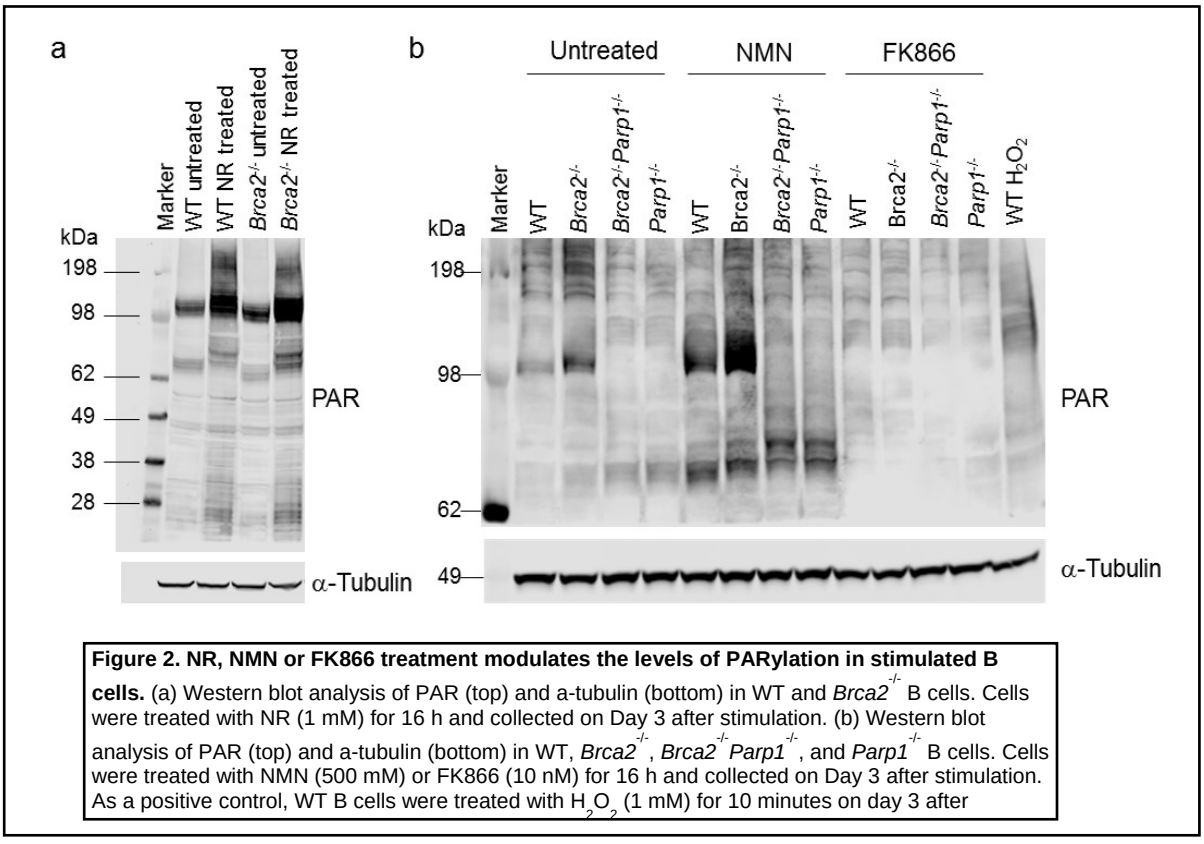

Figure 2. NR, NMN or FK866 treatment modulates the levels of PARylation in stimulated B cells. (a) Western blot analysis of PAR (top) and a-tubulin (bottom) in WT and *Brca2*$^{-/-}$ B cells. Cells were treated with NR (1 mM) for 16 h and collected on Day 3 after stimulation. (b) Western blot analysis of PAR (top) and a-tubulin (bottom) in WT, *Brca2*$^{-/-}$, *Brca2*$^{-/-}$*Parp1*$^{-/-}$, and *Parp1*$^{-/-}$ B cells. Cells were treated with NMN (500 mM) or FK866 (10 nM) for 16 h and collected on Day 3 after stimulation. As a positive control, WT B cells were treated with H_2O_2 (1 mM) for 10 minutes on day 3 after

formed via the catalysis of PARP-1, which is positively correlated with PARP activity. Activated PARP-1 and PARylation regulate various cellular machineries. Interestingly, it has been known that hyperactivation of PARP activity is observed in homologous recombination (HR) defective cells, such as Brca2-deficient cells. Previous studies have also demonstrated that inhibiting PARP-1 activity or knocking out/silencing PARP-1 may rescue the genomic instability and viability of Brca2-deficient cells without restoring HR

activity, suggesting that excessive PARylation may affect genomic instability observed in Brca2-deficient cells.

To confirm hyperactivated PARP activity in BRCA2 defective cells, we assessed PAR polymer in conditionally inactivated Brca2 B lymphocytes (Brca2f/fCd19Cre). We found increased levels of PAR proteins in Brca2-deficient cells reproducibly by ELISA (**Figure 1**).

PARPs are NAD+-dependent enzymes and thus require a source of NAD+ in all cellular compartments in which they function. Recent work has suggested that supplementation with NAD+ precursors nicotinamide riboside (NR) and nicotinamide mononucleotide (NMN) increase intracellular NAD+ levels in murine and human cells. In addition, it has been reported that FK866 effectively causes NAD+ depletion through specific inhibition of nicotinamide phosphoribosyltransferase (NAMPT), a key enzyme in the regulation of NAD+ biosynthesis from natural precursor nicotinamide. We, therefore, treated stimulated B cells with NR, NMN or FK866 and analyzed the levels of PARylation. NR and NMN treatments increased the levels of PARylation, whereas FK866 treatment decreased the levels of PARylation in B cells (**Figure 2**).

These results indicate that cellular NAD+ levels maybe the limiting factor which can modulate the final PARylation output in the cells.

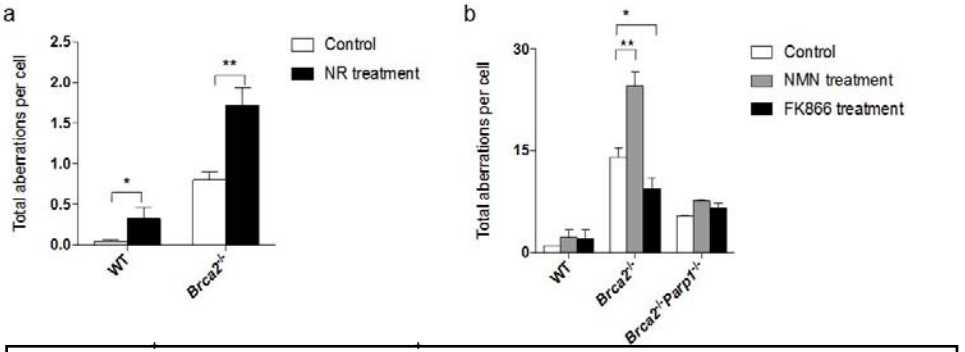

Figure 3. NAD$^+$ supplementation or NAD$^+$ inhibition affects the genomic instability observed in *Brca2*$^{-/-}$ B cells upon cisplatin treatment. (a) Genomic instability measured in metaphase spreads in WT and *Brca2*$^{-/-}$ B cells. LPS, IL-4 and RP105-stimulated B cells were treated with NR (1 mM) and cisplatin (0.5 mM) for 16 h and collected on Day 3. (b) Genomic instability measured in metaphase spreads in WT, *Brca2*$^{-/-}$, *Brca2*$^{-/-}$ *Parp1*$^{-/-}$, and *Parp1*$^{-/-}$ B cells. Stimulated B cells were treated with NMN (500 mM) or FK866 (10 nM) with cisplatin (0.5 mM) for 16 h and collected on Day 3 after stimulation. *p<0.05, **p<0.01.

Next, we assessed chromosomal aberrations in cells treated with NR, NMN or FK866 in response to the DNA damaging agent cisplatin. NR and NMN treatment increased chromosomal aberrations in all genotypes and FK866 treatment decreased genome instability observed in Brca2-deficient cells (**Figure 3**). These results indicate that modulating cellular NAD+ levels through NAD+ supplementation increased cellular PARylation and enhanced genomic instability upon cisplatin treatment. In contrast, inhibition of NAD+ levels by FK866 treatment decreased the levels of PARylation and rescued genomic instability observed in Brca2-deficient cells.

Loss of Brca2 in embryonic stem cells (ESCs) is incompatible with cell survival. To test whether FK866 treatment could promote ESC survival, we used PL2F7 mESCs that have one functionally null allele of Brca2 - the other is a conditional knockout (cko) allele (Brca2cko/ko). We treated these cells with 10 nM of FK866 for 16 h and then deleted the

cko allele by transient expression of CRE. After expression of CRE, we selected the recombinant clones in HAT (hypoxanthine, aminopterin and thymidine) media because CRE-mediated deletion of cko generates a functional HPRT minigene. Genotyping of the colonies did not reveal any Brca2ko/ko clones with DMSO treatment, consistent with the fact that BRCA2 is essential for viability. Remarkably, FK866 pretreatment results in a viable Brca2ko/ko cells in about 4% of clones in comparison to 0% of control (**Figure 4**), although rescued cells grew slower, and the colonies were smaller in size.

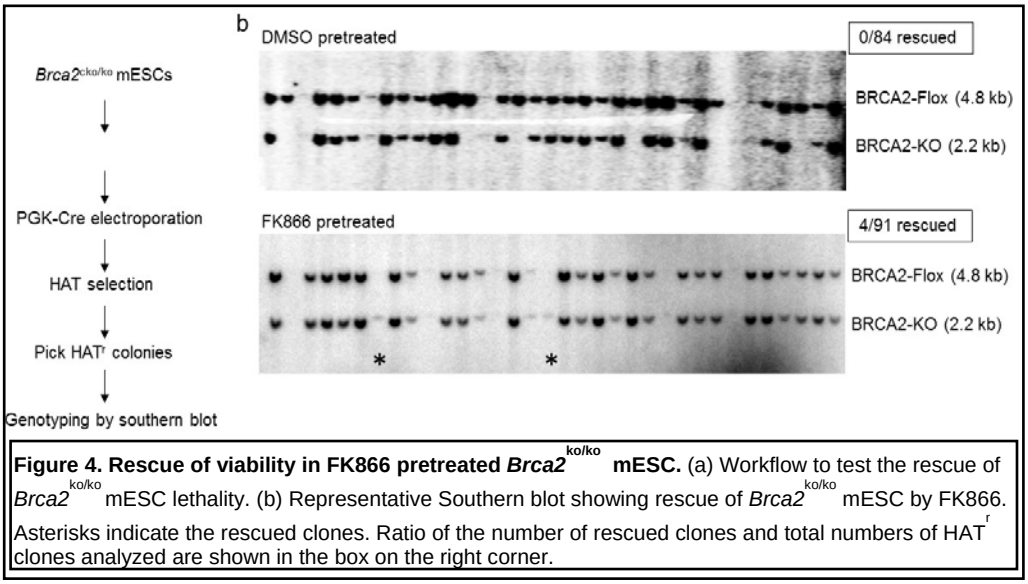

Figure 4. Rescue of viability in FK866 pretreated *Brca2*$^{ko/ko}$ mESC. (a) Workflow to test the rescue of *Brca2*$^{ko/ko}$ mESC lethality. (b) Representative Southern blot showing rescue of *Brca2*$^{ko/ko}$ mESC by FK866. Asterisks indicate the rescued clones. Ratio of the number of rescued clones and total numbers of HAT^{r} clones analyzed are shown in the box on the right corner.

NMNAT-1, NMNAT-2, and NMNAT-3 comprise a small family of NAD+ synthases that produce NAD+ from NMN and ATP. NMNAT-1 is a central enzyme in NAD+ biosynthesis in the nucleus. To test whether NMNAT-1 deficiency in Brca2-deficient cells would have similar functional consequences as observed with NAD+ inhibitor, we knocked down Nmnat-1 in B cells using shRNAs. Absence of NMNAT-1 did not affect chromosomal aberrations observed in wild-type cells upon cisplatin treatment. In striking contrast, loss of NMNAT-1 in Brca2-deficient cells exhibited greater than 2- fold fewer chromosomal aberrations (**Figure 5**).

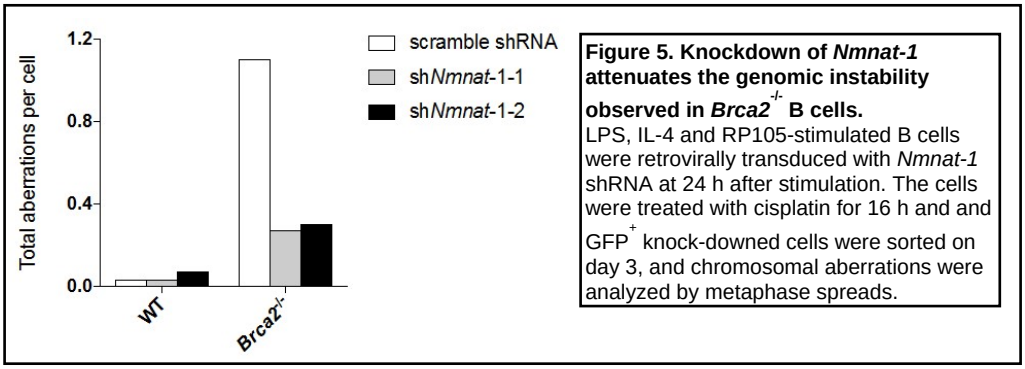

Figure 5. Knockdown of *Nmnat-1* attenuates the genomic instability observed in *Brca2*$^{-/-}$ B cells. LPS, IL-4 and RP105-stimulated B cells were retrovirally transduced with *Nmnat-1* shRNA at 24 h after stimulation. The cells were treated with cisplatin for 16 h and and GFP^{+} knock-downed cells were sorted on day 3, and chromosomal aberrations were analyzed by metaphase spreads.

To analyze the impact of NMNAT-1 deficiency for the viability of Brca2-deficient ESCs, we generated three stably knockdown clones using three different shRNAs against Nmnat-1. We obtained several HAT-resistant mESC clones after cko deletion. Genotyping of the clones revealed

that about 2% were Brca2ko/ko. Thus, deficiencies in NMNAT-1 rescue the lethality of Brca2-deficient ESCs (**Figure 6**).

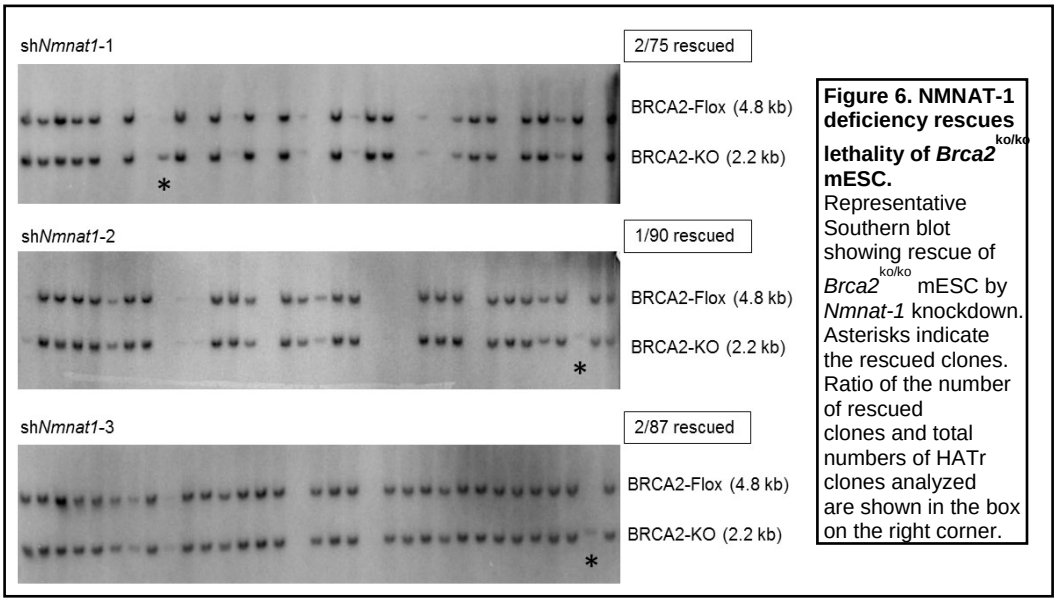

Figure 6. NMNAT-1 deficiency rescues lethality of *Brca2*$^{ko/ko}$ mESC. Representative Southern blot showing rescue of *Brca2*$^{ko/ko}$ mESC by *Nmnat-1* knockdown. Asterisks indicate the rescued clones. Ratio of the number of rescued clones and total numbers of HATr clones analyzed are shown in the box on the right corner.

PAR polymers turn over rapidly in the cell. Thus, not surprisingly, a number of enzymes have evolved to remove covalently linked ADP-ribose and PAR from proteins. These PAR hydrolases include ADP-ribosyl hydrolase 3 (ARH3) and PAR glycohydrolase (PARG). Next, we wanted to down regulate cellular PAR levels by overexpressing PAR hydrolases in Brca2-deficient B cells and analyze genomic stability upon cisplatin treatment. We found that overexpression of PARG, but not ARH3, attenuates the chromosomal aberrations observed in Brca2-deficient cells upon cisplatin treatment (**Figure 7**). These results again indicate that cellular PARylation levels affect genomic instability in Brca2-deficient cells.

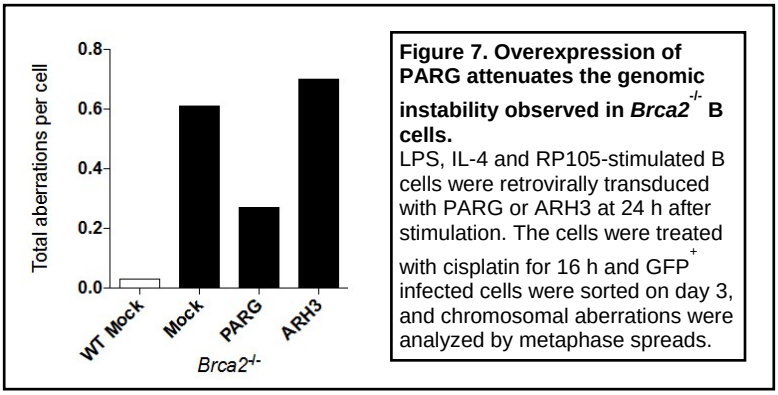

Figure 7. Overexpression of PARG attenuates the genomic instability observed in *Brca2*$^{-/-}$ B cells. LPS, IL-4 and RP105-stimulated B cells were retrovirally transduced with PARG or ARH3 at 24 h after stimulation. The cells were treated with cisplatin for 16 h and GFP^{+} infected cells were sorted on day 3, and chromosomal aberrations were analyzed by metaphase spreads.

Milestone(s) Achieved: These experiments have better defined the relationship between PARylation, Brca2-deficiency and genomic instability that lead to cancer development. Future studies will test whether NAD inhibition, or PARPG overexpression protects replication forks from degradation.

Subtask 2a: To submit and receive ACURO and HRPO approvals (proposed time line: 3-4 months) (**Site 2, DFCI, Dr. D'Andrea**)

ACURO approval: Importantly, we have already obtained an approval from the Institutional Animal Care and Use Committee (IACUC) (protocol # 08-036) for performing

all of the proposed animal experiments at site 2, DFCI. The ACURO documents/forms have been submitted to DOD for approval. The USAMRMC Animal Care and Use Review Office (ACURO) has received the appropriate forms/documents involving animal studies and it is currently being reviewed. We have already addressed the comments after the initial review by the ACURO office and are currently waiting for approval. Animal work under the DOD funding will not be initiated until notification of approval from ACURO.

HRPO approval: We have already submitted Human Research Protection Office (HRPO) forms and approval has been obtained via phone conversation. It was determined that we need not submit any more documents for HRPO approval.

Subtask 2b: To generate PARP1/BRCA1 and PARP1/FANCD2 double knockout mice to monitor replication fork protection-250 mice (proposed time line: 12-18 months) (**Site 2, DFCI, Dr. D'Andrea**)

We are still waiting for ACURO approval. Therefore, these animal experiments have not been yet initiated.

Milestone(s) Achieved: ACURO forms for animal studies have been submitted and they are currently being reviewed. The HRPO approval has been obtained.

Major Task 3: Determine the changes in replisome composition associated replication fork degradation and protection

Subtask 1: Measuring MRE11 chromatin binding in BRCA2-, FANCD2-, BRCA2/PARP1-, BRCA2/PTIP-deficient cells treated with HU and cisplatin by high throughput microscopy (time line: 1-6 months). The progress is described in following section (Subtask 2) (**Site 2, DFCI, Dr. D'Andrea**).

Subtask 2: To determine the global composition of proteins at active and stalled replication forks using iPOND with mass spectrometry using WT vs. BRCA2- vs. FANCD2- vs. POLQ-deficient cells (proposed time line: 6-18 months) (**Site 2, DFCI, Dr. D'Andrea**).

Dr. D'Andrea has made significant progress related to this task. Indeed, we have validated known mechanisms of PARP inhibitor resistance (e.g. PTIP deficiency) using DNA fiber assays, biochemical assays and cell-based assays. In addition, we have identified a novel role of EZH2 in replication fork stability and have uncovered a new mechanism of PARPi resistance in BRCA2-deficient tumors.

We initially examined gene expression profiles of chromatin modifiers in cancers frequently associated with defects in HR (i.e. mutations in BRCA1/2 genes). EZH2 scored as the top overexpressed chromatin modifier in subgroups of ovarian, breast, and uterine cancers associated with HR deficiency. EZH2 expression correlated with tumor grade, POLQ and Ki67 expression (high POLQ expression is a surrogate marker for HR defect) and increase in tumors harboring alterations in BRCA1/2 genes. We therefore hypothesized that EZH2

may regulate genomic stability in BRCA1/2-deficient tumors. HR-deficient HeLa cells (siBRCA1 and siBRCA2) and HR-proficient control cells (siScr) were exposed to the EZH2 inhibitor GSK126, and clonogenic survival was measured under increasing concentrations of PARPi. While EZH2 inhibition had no effect on siScr or siBRCA1 transfected cells, it induced PARPi resistance in siBRCA2-transfected HeLa cells (data not shown). These results were recapitulated in a panel of BRCA2-deficient (e.g.VU423) but not BRCA1-deficient ovarian and breast cancer cell lines (**Figure 8, data not shown**). Interestingly, EZH2 inhibition also conferred resistance of BRCA2-deficient cells to cisplatin (data not shown).

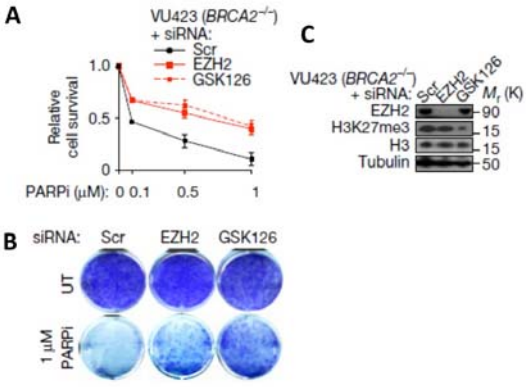

Figure 8. EZH2 depletion or inhibition of EZH2 activity causes PARPi resistance if BRCA2-deficient breast cancer cells. (A, B) Clonogenic assay and representative images of BRCA2-deficient VU423 cells expressing scrambled (Scr) siRNA, siRNAs against EZH2 or treated with GSK126 under increasing concentrations of a PARP inhibitor rucaparib. (C) Immunoblot analysis of cells expressing the above mentioned siRNAs at 72 hrs after transfection.

We next determined whether EZH2 depletion results in PARPi resistance in BRCA2-/- cells due to restoration of HR capacity or due to stablization/protection of replication fork. We performed a DR-GFP reporter assay and assessed RAD51 foci (a marker of HR activity) to evaluate HR status after EZH2 knockdown. EZH2 depletion did not increase HR frequency in BRCA1/2-deficient tumors nor it induced RAD51 foci after DNA damage indicating that PARPi resistance mediated by EZH2 loss does not result from restoration of HR (data not shown). By using the DNA fiber assay, we observed that EZH2 depletion or inhibition increased replication fork protection after hydroxyurea (HU) treatment in BRCA2-deficient cells, similarly to PTIP knockdown (**Figure 9**).

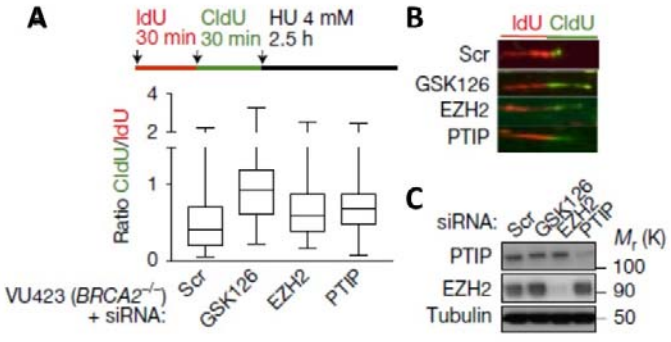

Figure 9. EZH2 loss promotes replication fork protection in BRCA2-deficient tumors. (A) Schematic and box plot for fork protection experiments. (B) Representative fibers (one over n=3 independent experiments) of BRCA2-deficient VU423 cells expressing scrambled (Scr) siRNA, siRNAs against EZH2 or PTIP or treated with GSK126 are shown. (C) Relative immunoblot analysis of the cells is shown.

Achievement of fork stability requires the simultaneous stalling of replication forks and the blockage of replication restart. Accordingly, EZH2 depletion or inhibition promoted fork stalling and reduced fork

restart in BRCA2-deficient cells (data not shown). In addition, we determined that that EZH2 depletion increases fork protection and decreases fork restart specifically in BRCA2-deficient cells and independently of the MLL3/4-PTIP-MRE11 pathway. We next performed an accelerated native isolation of protein on nascent DNA (aniPOND) assay to assess the localization of EZH2 and MUS81 at the replication fork. aniPOND is a biochemical assay that allows for the isolation and detection of proteins associated with sites of ongoing DNA replication. Using aniPOND experiments, we determined that EZH2 localizes to the stalled replication forks, recruits a nuclease MUS81 and promotes a degradation of stalled replication forks. Accordingly, low EZH2 levels reduce H3K27 methylation, prevent MUS81 recruitment at stalled forks and cause fork stabilization. As a consequence, loss of function of the EZH2/MUS81 axis promotes PARPi resistance in BRCA2-deficient cells. Using non-DOD funding, we have also confirmed these results in a murine model. We have determined that inhibition of Ezh2 in a murine Brca2-/- breast tumor model is associated with acquired PARP inhibitor resistance (data not shown, see Appendix).

Finally, to evaluate the impact of EZH2 loss *in vivo*, we analyzed the progression-free survival (PFS) after platinum-based chemotherapy (a surrogate measure of chemoresistance) of ovarian carcinoma patients harboring BRCA1/2 mutations. Interestingly, in BRCA2-deficient tumors, but not BRCA1-deficient or BRCA1/2-wild-type, low EZH2 expression correlated with poor response to chemotherapy (see Appendix for the data). These data suggested that low EZH2 levels worsen the prognosis of BRCA2-deficient patients by exhibiting chemotherapy resistance. Taken together, we identified EZH2 expression as a potential biomarker of BRCA2-deficient tumor response to chemotherapy.

Milestone(s) Achieved: We have identified a novel role of EZH2 at replisomes in BRCA2-deficient tumors. Specifically, we have determined that EZH2 localizes at stalled forks and mediates recruitment of the MUS81 nuclease. Low EZH2 levels prevent MUS81 recruitment at stalled forks and cause fork stabilization. As a consequence, loss of function of the EZH2/MUS81 axis promotes PARPi resistance in BRCA2-deficient cells. Accordingly, low EZH2 or MUS81 expression levels predict chemoresistance and poor outcome in patients with BRCA2-mutated tumors. We have identified EZH2 expression as a biomarker of BRCA2-deficient tumor response to chemotherapy.

Specific Aim 2: Determine the interactions of BRCA2, FANCD2, and POLQ in Replication Fork stability and Alt-EJ

Major Task 4: To determine whether the concurrent deletion of BRCA2 and POLQ results in synthetic lethality and reduced breast tumorigenesis

Subtask 1: To determine whether BRCA2 and POLQ are also synthetic lethal in tumorigenesis by using the conditional BRCA2/p53 knockout mouse model (K14CRE;BRCA2f/f;p53f/f, KB2P) (proposed time line: 12-15 months) (**Site 2, DFCI, Dr. D'Andrea**).

Conditional BRCA2/p53 knockout mice develop breast cancer within 100-300 days after birth. We aim to breed these mice with POLQ knockout mice and evaluate breast cancer progression in triple knockout mice. We anticipate that concurrent knockout of BRCA2/p53 and POLQ will result in synthetic lethality and the triple knockout mice will be tumor free. We are still waiting for ACURO approval. Therefore, these animal experiments have not been yet initiated. However, we have already sufficient number of POLQ knockout mice through our breeding colony of POLQ mutant mice. POLQ mice are being bred using a non-DOD funding source. Of note, during the first year of the DOD funding, we have confirmed all the cellular and biochemical phenotypes of POLQ deficiency.

Milestone(s) Achieved: We have confirmed a role of POLQ protein in Alt-EJ and in replication fork stability.

Major Task 5: To determine the mechanism of replication fork instability in FANCD2-deficient cells

Subtask 1: To test that PTIP/MRE11-mediated nucleolytic degradation is responsible for the replication fork instability in FANCD2-/- cells (proposed time line: 12-18 months). We had proposed to generate double knockouts in B-cells by crossing pTIPf/f-FANCD2-/- mice with the CD19 CRE transgenic mice and use B-cells from the double knockout mice for their competence in HR and fork stability. As we are still waiting for an ACRURO approval, these animal studies have not been initiated (**Site 2, DFCI, Dr. D'Andrea**).

Milestone(s) Achieved: None

Major Task 6: To identify and characterize proteins which cooperate with FANCD2 and POLQ in replication fork stability and Alt-EJ

Subtask 1: To identify and characterize proteins which cooperate with FANCD2 and POLQ in replication fork stability and Alt-EJ using iPOND/mass spectrometry (time line:6-18 months) (**Site 2, DFCI, Dr. D'Andrea**).

We have not yet performed the experiments proposed for this subtask.

Subtask 2: Validation of FANCD2 and POLQ interacting proteins identified by mass spec using coimmunoprecipitation, shRNA knockdown, changes in POLQ nuclear foci and Alt-EJ template assays (proposed time line: 18-30 months) (**Site 2, DFCI, Dr. D'Andrea**).

We have not yet performed the experiments proposed for this subtask.

Milestone(s) Achieved: None

Specific Aim 3: Assess mechanisms of PARPi resistance in mouse models and patient derived xenografts

Major Task 7: Evaluate replication fork stability relative to PARPi/cisplatin response in genetically engineered mouse models

Subtask 1: To test whether resistance in KB2P mouse models to PARPi correlates with RF protection and/or up-regulation of Alt-NHEJ using an organoid culture model to propagate tumors (proposed time line: 24-30 months) (**Site 2, DFCI, Dr. D'Andrea**).

We have set up immunohistochemistry (IHC)-based RAD51 foci assay to measure HR and a DNA fiber assay to measure RF protection in organoid cultures from primary ovarian cancer cells (see the details in "Major Task 8").

Milestone(s) Achieved: We have established assays in primary organoid cultures.

Major Task 8: Evaluate Replication Fork Stability and HR competence in PARP Inhibitor Sensitive and Resistant TNBC-PDX models

Subtask 1: To test a triple negative breast cancer-PDX model for resistance to PARPi and platinum by treating with vehicle, cisplatin, and olaparib and measuring RAD51 foci formation and replication fork fiber lengths (proposed time line: 30-36 months) (**Site 2, DFCI, Dr. D'Andrea**).

We aim to evaluate replication fork stability and HR competence in PARP inhibitor sensitive and resistant triple negative breast cancer (TNBC)-PDX models. We plan to test a triple negative breast cancer-PDX models for resistance to PARPi and platinum (Cisplatin) by treating PDX-bearing mice with vehicle, cisplatin, and olaparib and measuring RAD51 foci formation for HR competence and replication fork fiber lengths in tumors. Since we are still waiting for ACURO approval, these animal studies have not been initiated. Meanwhile, we have set up assays to evaluate replication fork stability and HR in tumor tissues. Importantly, we have developed a RAD51-based immunohistochemical (IHC) functional assay to determine HR-mediated DNA repair proficiency and PARP inhibitor sensitivity in PDX samples and primary tumors from ovarian cancer patients. Using this assay, we have determined that in ovarian cancer PDX models, presence of RAD51 foci correlates with PARP inhibitor response (see an example in **Figure 10**).

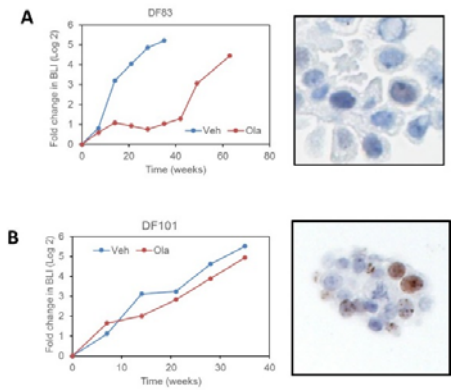

Figure 10. Detection of RAD51 foci by immunohistochemistry in ovarian cancer PDX models. (A) Olaparib sensitivity (left panel) and RAD51 staining of the DF83 PDX sample (right panel) are shown. Note the absence of RAD51 staining or RAD51 foci in this olaparib sensitive PDX model. (B) Olaparib sensitivity (left panel) and RAD51 staining of the DF101 PDX sample (right panel) are shown. Note the presence of RAD51 staining or RAD51 foci in this olaparib resistant PDX model.

We have also adopted the cell-based replication fork stability assay in primary organoid cultures derived from ovarian cancer patients and is currently optimizing it in PDX tumors.

Milestone(s) Achieved: We have established a RAD51 foci assay in primary PDX samples. In addition, we have established a replication fork stability assay in primary organoid cultures from ovarian cancer patients. Both of these assays will be useful in future in determining the replication fork stability and HR competence in PARP inhibitor or Cisplatin sensitive and resistant TNBC-PDX models

Summary of the key research accomplishments: During the first year of the DOD funding, we have made progress in identifying the proteins which contribute to the replication fork stability and we have identified a new mechanism of chemoresistance in BRCA2-deficient tumors. We have demonstrated that modulating cellular NAD+ levels can enhance or rescue genomic instability upon cisplatin treatment in Brca2-deficient cells. We have also determined that loss of function of EZH2 in BRCA2-deficient cancer cells promotes PARPi resistance. Importantly, our results identify EZH2 expression as a biomarker of BRCA2-deficient tumor response to chemotherapy. We have published a manuscript describing our EZH2 results.

- **What opportunities for training and professional development did the project provide**?

Nothing to report

- How were the results disseminated to communities of interest?

Results were shared with the scientific community via informal discussions, posters and presentations at scientific meetings and through publications in peer-reviewed journals

- What do you plan to do during the next reporting period to accomplish the goals and objectives?

The major goal of our project is to identify novel molecular mechanisms of PARPi resistance in BRCA1/2 mutated breast cancer. Therefore, during the upcoming grant funding year, we will rigorously study the interplay between PTIP, POLQ, PARP1, FANCD2, BRCA1/BRCA2 and EZH2/MUS81 axis in maintaining replication fork stability and Alt-EJ. In addition to the cell-based and biochemical assays such as iPOND and fiber assays, we will also use murine models for these studies. For example, we will generate PARP1/BRCA1 and PARP1/FANCD2 double knockout mice to monitor genomic stability and replication fork protection in the B-cells from these mice. We will also generate conditional triple knockout mice with deficiency for POLQ, BRCA2 and p53 in the breast tumors to determine whether POLQ and BRCA2 are synthetic lethal in tumorigenesis.

4. IMPACT:

Nothing to Report

What was the impact on the development of the principal discipline(s) of the project?

We have identified low EZH2 expression as a novel mechanism of chemotherapy resistance in BRCA2-deficient tumors. This finding has a high impact on identifying a patient population for a chemotherapy response.

What was the impact on other disciplines?

Nothing to Report

What was the impact on technology transfer?

Nothing to Report

What was the impact on society beyond science and technology?

Nothing to Report

5. CHANGES/PROBLEMS:

Changes in approach and reasons for change

Nothing to Report

Actual or anticipated problems or delays and actions or plans to resolve them

We (**site 2, DFCI**) had proposed that we will obtain ACURO approval for animal studies within 3-4 months. However, this has been delayed and we were unable to initiate animal studies. Our application for ACURO approval has been already under review. Once this is approved, we should be able to perform animal studies.

Changes that had a significant impact on expenditures

Nothing to Report

Significant changes in use or care of human subjects, vertebrate animals, biohazards, and/or select agents:

Nothing to Report

Significant changes in use or care of human subjects:

Not applicable

Significant changes in use or care of vertebrate animals:

Nothing to Report

Significant changes in use of biohazards and/or select agents:

Nothing to Report

6. PRODUCTS

Publication:

Rondinelli B, Gogola E, Yucel H, Duarte AA, van de Ven M, van der Sluijs R, Konstantinopoulos PA, Jonkers J, Rottenberg S, D'Andrea AD. EZH2 promotes degradation of stalled replication forks by recruiting MUS81 through histone H3 trimethylation. Nature Cell Biology, 2017, Oct 16. doi: 10.1038/ncb3626. [Epub ahead of print]

Acknowledgement of DOD support: Yes
Acknowledgement of federal support: Yes

Books or other non-periodical, one-time publications.

Nothing to Report

Other publications, conference papers, and presentations.

Dr. Alan D'Andrea (Site 2, DFCI)
Presentation at Conferences:

2016	AACR Special Conference on DNA Repair: Tumor Development and Invited Seminar: University of Chicago, Chicago, IL NCI Chromosome Biology Symposium: Nuclear Structure, Genome Integrity and Cancer, Bethesda, MD
2017	Invited Seminar, University of California, San Francisco, CA Gordon Research Conference on Mammalian DNA Repair, Ventura, CA

Invited Seminar, Ludwig Center at Harvard, Boston, MA
Invited Seminar, Ohio State University Wexner Medical Center, Research Training Day, Columbus, OH
Northeast Regional Genome Instability and Cancer Conference, The Geisel School of Medicine at Dartmouth, Lebanon, NH
International Academy of Advanced Oncology (IAAO) Paradigm Shift in Therapeutic Strategies and Novel Treatments for Cancer, Tokyo, Japan
AACR Breast Cancer Conference, Hollywood, CA
AACR-NCI-EORTC Meeting, Philadelphia, PA
Chabner Colloquium, Boston, MA

- **Website(s) or other Internet site(s)**

Nothing to Report

- **Technologies or techniques**

Nothing to Report

- **Inventions, patent applications, and/or licenses**

Nothing to Report

- **Other Products**

Nothing to Report

7. PARTICIPANTS & OTHER COLLABORATING ORGANIZATIONS

Name:	Alan D D'Andrea
Project Role:	Principal Investigator (Partnering PI)
Researcher Identifier (e.g. ORCID ID):	N/A
Nearest person month worked:	0.2 calendar months
Contribution to Project:	Dr. D'Andrea was responsible for the project management and collaboration with Dr. Nussenzweig.
Funding Support:	Supported by the following grants:

Name:	Beatrice Rondinelli
Project Role:	Post-doctoral fellow
Researcher Identifier (e.g. ORCID ID):	N/A
Nearest person month worked:	12 calendar months
Contribution to Project:	Dr. Rondinelli has performed work in the area on examining the role of EZH2 in replication fork stabilization and PARP inhibitor resistance.
Funding Support:	Supported by Ovarian Cancer Research Fund Fellowship

Name:	Emma Roberts
Project Role:	Research Technician
Researcher Identifier (e.g. ORCID ID):	N/A
Nearest person month worked:	9 calendar months
Contribution to Project:	Ms. Roberts has assisted Dr. Rondinelli in performing cell-based and biochemical assays.
Funding Support:	Supported by this DoD grant and Breast Cancer Research Foundation grant

Has there been a change in the active other support of the PD/PI(s) or senior/key personnel since the last reporting period?

Dr. D'Andrea had the following changes in his active other support since the last reporting period:

Following grants were newly awarded/renewed:

Breast Cancer Research Foundation (PI: D'Andrea) 10/1/11-9/30/18 0.24 calendar
(BCRF) $208,334
Extending the use of PARP Inhibitors for Triple Negative Breast Cancer Therapy

Lilly Wave 2 (PI: D'Andrea) 3/27/17-3/28/19 0.24 calendar
$171,428

Preclinical Study of the CHK1 inhibitor LY2606368 in Combination with the ATR Inhibitor VX-970 in Cell Line and Patient-Derived Xenograft Models of Triple-Negative Breast and Ovarian Cancer

5P01HL048546 (PI: Grompe)
Pathophysiology and Treatment of Fanconi/Project 2 and Core
NIH 9/1/16-5/31/21 2.76 calendar
$383,000

Prostate Cancer Foundation Challenge Award (PI: Van Allen)
9/01/16 – 8/31/18 0.36 calendar
$66,666
Exploiting DNA Repair Defects in Metastatic Prostate Cancer to Promote Immunotherapeutic Responses

Rivkin Center for Ovarian Cancer (PI: D'Andrea) 4/1/2017-3/31/2018 0.12 calendar
$75,000
Novel Mechanism of PARP-inhibitor Resistance in BRCA2-deficient ovarian and breast cancer

Fanconi Anemia Research Fund, Inc. (PI: D'Andrea) 4/1/2017-3/31/2019 0.2 calendar
$87,500
TGF-beta pathway inhibitors for the treatment of bone marrow failure in Fanconi Anemia

Following grants were completed:

2R56 DK43889-23 (PI: D'Andrea) 9/08/15 – 8/31/17*
0.6calendar
NIH $ 80,000
*No cost extension
Mechanisms of Bone Marrow Failure in Fanconi Anemia

What other organizations were involved as partners?

Nothing to report

8. SPECIAL REPORTING REQUIREMENTS:

COLLABORATIVE AWARDS: We have marked the tasks assigned to us and accordingly we have provided a progress made for each task.

QUAD CHARTS: Not applicable

9. APPENDICES: We have attached a recent manuscript (Rondinelli B et al, 2017) which is published in Nature Cell Biology. This publication describes in detail the experimental methods and results described in this annual report.

nature cell biology

EZH2 promotes degradation of stalled replication forks by recruiting MUS81 through histone H3 trimethylation

Beatrice Rondinelli[1,2], Ewa Gogola[3], Hatice Yücel[1], Alexandra A. Duarte[3], Marieke van de Ven[4], Roxanne van der Sluijs[1,5], Panagiotis A. Konstantinopoulos[2,6], Jos Jonkers[3], Raphaël Ceccaldi[1,2], Sven Rottenberg[3,7] and Alan D. D'Andrea[1,2,8]

The emergence of resistance to poly-ADP-ribose polymerase inhibitors (PARPi) poses a threat to the treatment of BRCA1 and BRCA2 (BRCA1/2)-deficient tumours[1]. Stabilization of stalled DNA replication forks is a recently identified PARPi-resistance mechanism that promotes genomic stability in BRCA1/2-deficient cancers[2]. Dissecting the molecular pathways controlling genomic stability at stalled forks is critical. Here we show that EZH2 localizes at stalled forks where it methylates Lys27 on histone 3 (H3K27me3), mediating recruitment of the MUS81 nuclease. Low EZH2 levels reduce H3K27 methylation, prevent MUS81 recruitment at stalled forks and cause fork stabilization. As a consequence, loss of function of the EZH2/MUS81 axis promotes PARPi resistance in BRCA2-deficient cells. Accordingly, low *EZH2* or *MUS81* expression levels predict chemoresistance and poor outcome in patients with BRCA2-mutated tumours. Moreover, inhibition of Ezh2 in a murine *Brca2*$^{-/-}$ breast tumour model is associated with acquired PARPi resistance. Our findings identify EZH2 as a critical regulator of genomic stability at stalled forks that couples histone modifications to nuclease recruitment. Our data identify *EZH2* expression as a biomarker of BRCA2-deficient tumour response to chemotherapy.

The discovery that poly(adenosine diphosphate (ADP)-ribose) polymerase inhibitors (PARPi) could kill cancer cells with BRCA1 and BRCA2 mutations[3] led to the implementation of several clinical trials for the treatment of BRCA1/2-mutated cancers[1,4]. However, the enthusiasm generated by preclinical data has been tempered by the occurrence of resistance to PARPi in the clinic, which greatly reduces drug efficacy and worsens patient outcome[1,4].

The mechanism underlying the sensitivity of BRCA1/2-deficient tumours to PARPi relies on the dual function of BRCA1 and BRCA2 (BRCA1/2) proteins in protecting genomic integrity through homologous recombination (HR)-mediated DNA repair[5] and replication fork stabilization[6]. As a consequence, loss of BRCA1/2 proteins induces a defect in both HR and fork stabilization[6]. Conversely, restoration of either HR capacity[7] or replication fork stability is associated with cellular resistance to PARPi[2]. Although a multitude of DNA repair factors have been shown to participate in replication fork protection and fork restart, ultimately hindering the accumulation of replication stress and genomic instability, the evidence that replication fork protection can promote PARPi resistance only recently emerged[2].

Chromatin modifiers perform an essential role in the maintenance of genomic stability[8], including the stabilization of replication forks. For instance, depletion of histone H4 induces replication fork collapse[9] while methylation of Lys4 on histone 3 (H3K4) induces MRE11-mediated fork degradation[2]. In accordance with these studies, loss of chromatin factors promotes chemoresistance in different tumours[10,11], including BRCA1/2-deficient tumours[2]. As part of the Polycomb repressive complex 2 (PRC2), enhancer of zeste homologue 2 (EZH2) methylates histone H3 on Lys27 (H3K27)[12] and exerts a broad transcriptional repressor activity, whose relevance in oncogenesis was established for various types of cancer[13]. Beyond transcription, EZH2 also localizes to sites of DNA damage[14,15] and mediates H3K27 methylation at replication forks[16]. We therefore hypothesized that EZH2 may regulate genomic stability at stalled forks.

We herein applied the same strategy used to characterize the essential role of Polθ and FANCD2 in the survival of BRCA1/2-deficient tumours[17,18] to examine gene expression profiles of chromatin modifiers (Supplementary Table 1) in cancers frequently

[1]Department of Radiation Oncology, Dana-Farber Cancer Institute, Harvard Medical School, Boston, Massachusetts 02215, USA. [2]Center for DNA Damage and Repair, Dana-Farber Cancer Institute, Harvard Medical School, Boston, Massachusetts 02215, USA. [3]Division of Molecular Pathology and Cancer Genomics Netherlands, The Netherlands Cancer Institute, Amsterdam 1066 CX, the Netherlands. [4]Mouse Clinic for Cancer and Aging (MCCA), Preclinical Intervention Unit, The Netherlands Cancer Institute, Amsterdam 1066 CX, the Netherlands. [5]University of Amsterdam, Amsterdam 1012 WX, the Netherlands. [6]Department of Medical Oncology, Medical Gynecologic Oncology Program, Dana-Farber Cancer Institute, Harvard Medical School, Boston, Massachusetts 02215, USA. [7]Institute of Animal Pathology, Vetsuisse Faculty, University of Bern, Bern 3012, Switzerland.
[8]Correspondence should be addressed to A.D.D. (e-mail: alan_dandrea@dfci.harvard.edu)

Received 1 August 2017; accepted 13 September 2017; published online 16 October 2017; DOI: 10.1038/ncb3626

associated with defects in HR (that is, mutations in *BRCA1/2* genes)[19]. EZH2 scored as the top overexpressed chromatin modifier in subgroups of ovarian, breast and uterine cancers associated with HR deficiency. *EZH2* expression correlated with tumour grade, *Polθ* and *Ki67* expression[17] (high *Polθ* expression is a surrogate marker for HR defect) and increased in tumours harbouring alterations in *BRCA1/2* genes (Fig. 1a and Supplementary Figs 1a–e and 6). We acknowledge that *EZH2* overexpression in HR-deficient cancers may not be directly related to the defect in HR, but rather to a subsequent proliferation signature that characterizes these tumours.

On the basis of gene expression data, we hypothesized that EZH2 may regulate genomic stability in BRCA1/2-deficient tumours. HR-deficient HeLa cells (*BRCA1* siRNA (siBRCA1) and siBRCA2) and HR-proficient control cells (siScr) were exposed to the EZH2 inhibitor GSK126[20], and clonogenic survival was measured under increasing concentrations of PARPi. While EZH2 inhibition had no effect on siScr- or siBRCA1-transfected cells, it induced PARPi resistance in siBRCA2-transfected HeLa cells (Fig. 1b and Supplementary Fig. 6). These results were recapitulated in a panel of BRCA2-deficient but not BRCA1-deficient ovarian and breast cancer cell lines (Fig. 1c and Supplementary Figs 1f–m and 6). Interestingly, EZH2 inhibition also conferred resistance of BRCA2-deficient cells to cisplatin (Supplementary Fig. 1n,o). Next, we asked whether loss of the methyltransferase activity of EZH2 played a role in mediating the observed PARPi resistance. BRCA2-deficient (VU423) cell lines expressing wild-type (WT) but not methyltransferase-dead mutant of EZH2 (ΔHMT) or empty vector (EV) restored PARPi sensitivity (Supplementary Figs 1p and 6), demonstrating that loss of the methyltransferase activity of EZH2 mediates PARPi resistance. Moreover, EZH2 inhibition reduced the levels of chromosomal aberrations in BRCA2-knockdown or -deficient cells exposed to damaging agents (Fig. 1d,e and Supplementary Fig. 1q,r), suggesting that EZH2 depletion limits genomic instability in these cells. We next tested whether the role of EZH2 in mediating PARPi resistance was dependent on its known biological functions as part of the PRC2 complex[21]. Downregulation of the subunit SUZ12 similarly induced PARPi resistance in BRCA2-deficient cells, indicating that the PARPi resistance following EZH2 loss is mediated by decreased activity of the PRC2 complex itself (Fig. 1f and Supplementary Fig. 6). To evaluate the impact of EZH2 loss *in vivo*, we analysed the progression-free survival after platinum-based chemotherapy (a surrogate measure of chemoresistance) of ovarian carcinoma patients harbouring BRCA1/2 mutations. Interestingly, in BRCA2-deficient tumours, but not BRCA1-deficient or BRCA1/2-wild-type, low *EZH2* expression correlated with poor response to chemotherapy (Fig. 1g). These data establish that low *EZH2* levels worsen the prognosis of BRCA2-deficient patients by promoting chemotherapy resistance and limiting genomic instability. They also identify *EZH2* expression as a potential biomarker of BRCA2-deficient tumour response to chemotherapy.

Restoration of HR capacity represents one of the most common PARPi-resistance mechanisms[7]. We therefore assessed whether EZH2 depletion could restore HR repair[7]. Unlike 53BP1 loss, EZH2 depletion did not increase HR frequency in BRCA1/2-deficient tumours (Supplementary Fig. 2a) nor did it induce RAD51 foci (a marker of HR activity) after DNA damage (Supplementary Fig. 2b,c), indicating that PARPi resistance mediated by EZH2 loss does not result from restoration of HR.

Loss of the chromatin modifier-containing MLL3–4/PTIP/MRE11 pathway protects replication forks from degradation and has emerged as a previously uncharacterized PARPi-resistance mechanism[2]. On the basis of these data, we next tested whether EZH2 depletion could similarly stabilize replication forks through fork protection. By using the DNA combing assay[6], we observed that EZH2 depletion or inhibition increased replication fork protection in BRCA2-deficient cells, similarly to PTIP knockdown (Fig. 2a and Supplementary Fig. 6), and that the effect was not present in BRCA1-deficient nor in BRCA1/2-wild-type cells (Supplementary Figs 2d–f and 6). Importantly, WT but not ΔHMT EZH2 rescued replication fork protection mediated by EZH2 knockdown, indicating that loss of EZH2 methyltransferase activity protects forks from degradation (Fig. 2b). Achievement of fork stability requires the simultaneous stalling of replication forks and the blockage of replication restart[22]. Accordingly, EZH2 depletion or inhibition promoted fork stalling and reduced fork restart in BRCA2-deficient cells (Fig. 2c,d and Supplementary Fig. 6). We next investigated whether the replication fork protection conferred by EZH2 depletion resulted from the disruption of the MLL3–4/PTIP/MRE11 pathway, which was recently shown to confer replication fork protection[2]. Of note, EZH2 depletion further accentuated the fork protection conferred by MRE11 depletion, suggesting that EZH2 and the MLL3–4/PTIP/MRE11 complex belong in distinct pathways, both acting at the stalled replication fork (Fig. 2e). Taken together, our results indicate that EZH2 depletion increases fork protection and decreases fork restart specifically in BRCA2-deficient cells and independently of the MLL3–4/PTIP/MRE11 pathway.

During normal DNA replication, EZH2 promotes H3K27 methylation (H3K27me2 and me3) of newly incorporated nucleosomes[16,23–25]. As our data indicate that EZH2 stabilizes stalled replication forks, we asked whether EZH2 was present at sites of stalled DNA replication. Accelerated native isolation of protein on nascent DNA (aniPOND) experiments[26] following fork stalling with hydroxyurea (HU) revealed PCNA unloading[23] and increased levels of EZH2 and H3K27me3, consistent with enhanced EZH2 activity at stalled forks (Fig. 2f and Supplementary Fig. 6). Moreover, EZH2 co-localizes with phosphorylated RPA2 (pSer33-RPA2 and pSer4/8-RPA2; Fig. 2g and Supplementary Fig. 2h), a marker of stalled replication forks[27]. Co-localization signals were reduced in siEZH2-transfected cells, thus indicating the specificity of the signal (Fig. 2g and Supplementary Fig. 2h).

We next explored the function of EZH2 at stalled replication forks. Building on pioneering works on the role of EZH2 in DNA replication and S phase progression[16,23–25], we observed that EZH2 promoted fork restart in BRCA2-deficient (VU423) cells in a methyltransferase-dependent manner (Fig. 3a and Supplementary Fig. 6). Collectively, these data indicate that EZH2 localizes at stalled replication forks where it methylates H3K27 and that this event is required for replication fork restart. Fork degradation activity is fundamental to achieve fork restart and resume DNA replication after the removal of replication inhibitors[22]. For this reason, we evaluated whether EZH2 expression could also affect fork degradation. Interestingly, WT EZH2 promoted replication fork degradation in BRCA2-deficient (VU423) cells (Supplementary Figs 3b and 6) and this effect is

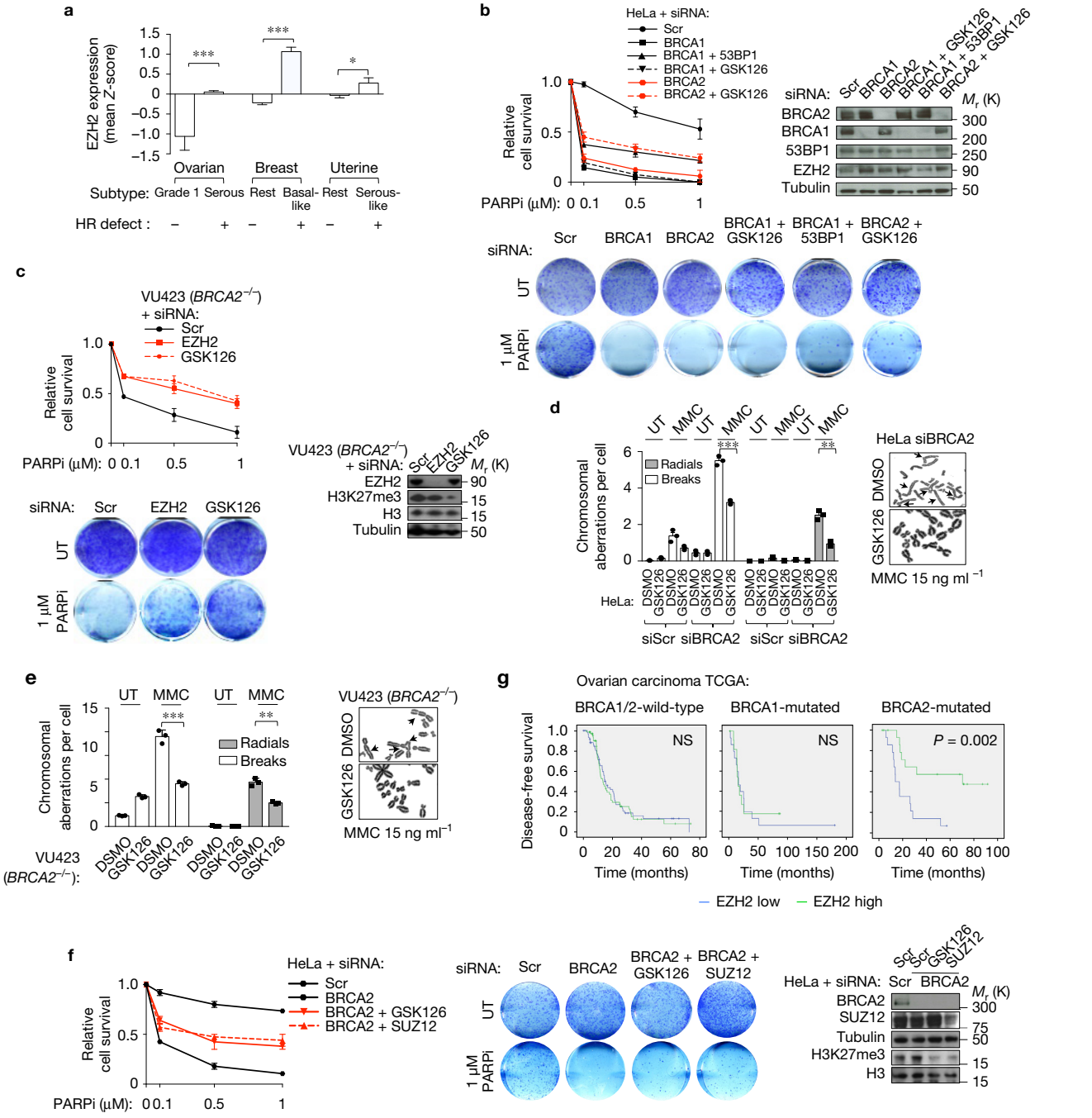

Figure 1 EZH2 depletion induces PARPi resistance and genomic stability in BRCA2-deficient tumours. (**a**) *EZH2* gene expression in subtypes of ovarian (grade 2/3 serous $n=143$ compared with grade 1 $n=20$; $P=0.00031$), breast (basal-like $n=80$ compared with the rest $n=421$; $P=0.00043$) and uterine (serous-like $n=60$ compared with the rest $n=172$; $P=0.038$) carcinomas. For each tumour group, expression values are represented as the mean ± s.e.m. of Z scores. $^{***}P=0.000271$, $^{***}P=0.000418$, $^{*}P=0.031$. (**b**) Clonogenic assay (top left) and representative images (bottom) of HeLa cells expressing scrambled (siScr) siRNA, siRNAs against EZH2, BRCA1 and BRCA2 or treated with GSK126 (5 μM) under increasing concentrations of the PARP inhibitor rucaparib. Immunoblot analysis (top right) of cells expressing the above-mentioned siRNAs at 72 h following transfection. (**c**) Clonogenic assay (top left) and representative images (bottom) of VU423 cells expressing scrambled (siScr) siRNA, siRNAs against EZH2 or treated with GSK126 under increasing concentrations of rucaparib. Immunoblot analysis (top right) of cells expressing the above-mentioned siRNAs at 72 h following transfection. (**d**,**e**) Chromosome breakage analysis (left) and representative images of one out of three independent experiments (right) of HeLa (**d**) and VU423 cells (**e**) transfected with the indicated siRNAs and treated with mitomycin C (MMC) or left untreated (UT). The arrows indicate chromosomal aberrations. Left to right, $^{***}P=0.00061$ and $^{**}P=0.0053$ for **d** and $^{***}P=0.00042$ and $^{**}P=0.0029$ for **e**. (**f**) Clonogenic assay (left), representative pictures of one out of three independent experiments (middle) and western blot analysis (right) of HeLa cells transfected with the indicated siRNAs or treated with GSK126 under increasing concentrations of rucaparib. (**g**) Progression-free survival after platinum chemotherapy of ovarian carcinoma TCGA patients. Unprocessed original scans of blots are shown in Supplementary Fig. 6. Data in **a**,**d** and **e** were analysed using two-sided Student's *t*-test. Data in **b**–**f** represent mean ± s.e.m. of $n=3$ independent experiments. In **g**, statistical significance was assessed by the two-sided log-rank test. In **a**,**d** and **e**, $^{*}P<0.05$, $^{**}P<0.01$ and $^{***}P<0.001$ with exact P values (with a confidence interval of 95%) noted in legends for relevant panels.

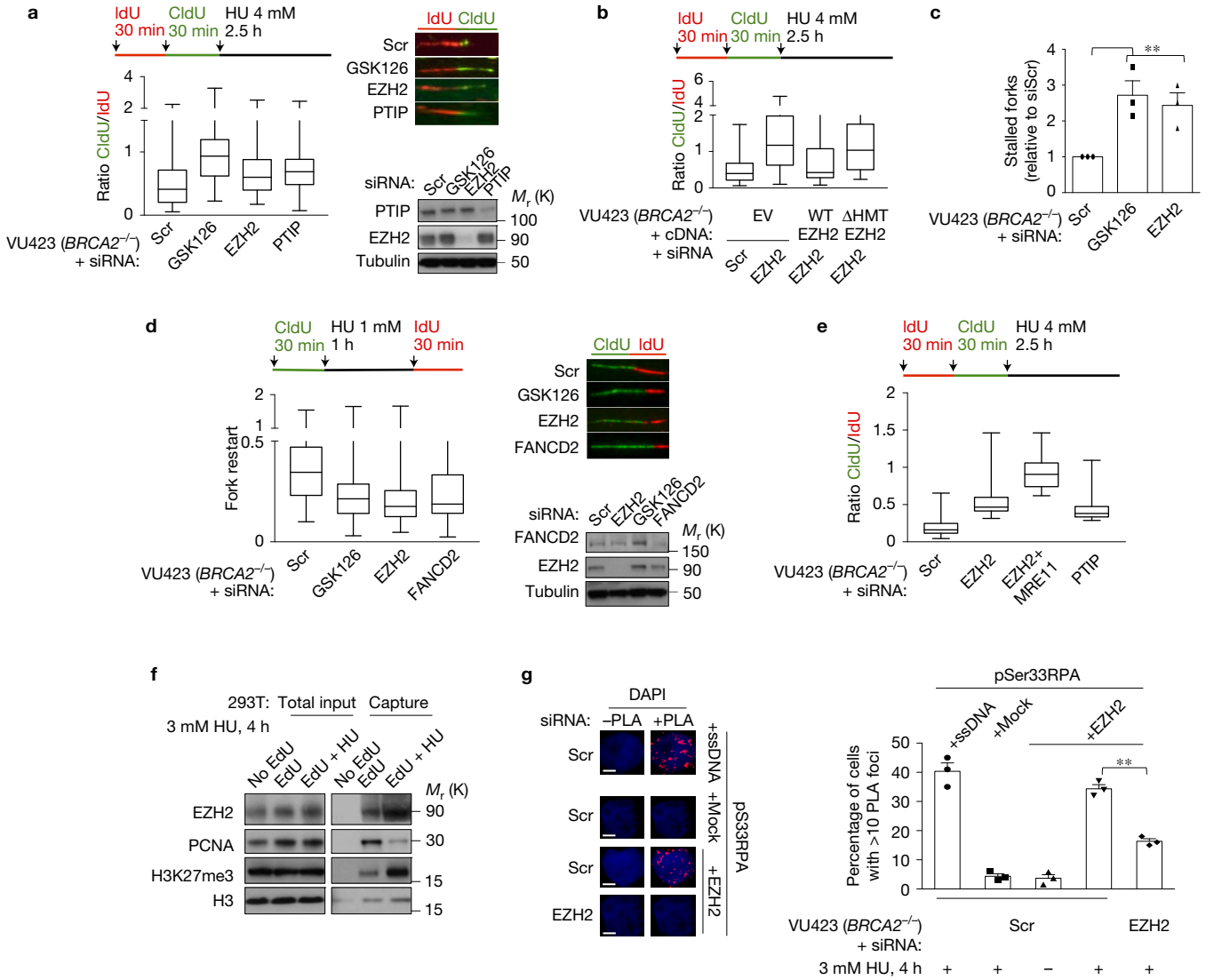

Figure 2 EZH2 loss promotes replication fork protection in BRCA2-deficient tumours through direct activity at stalled forks. (**a**) Schematic and box plots for fork protection experiments (left). Representative fibres (top right) and immunoblot analysis (bottom right) of one out of three independent experiments are shown. $P=0.000056$. (**b**) Fork protection experiment in VU423 cells stably expressing EZH2 cDNAs and transfected with siRNAs. $P=0.00048$. (**c**) VU423 cells transfected or treated as indicated were subjected to fork restart assay. Bars represent the number of stalled forks as fold change over siScr, which was arbitrarily set to 1; $^{**}P=0.0054$. (**d**) Schematic and box plots (left) for fork restart experiments of VU423 cells expressing the indicated siRNA or treated with GSK126. Representative fibres of one out of three independent experiments are shown (top right), together with the immunoblot of cell lysates (bottom right). $P=0.000032$. (**e**) Schematic for the labelling of cells with IdU and CldU for fork protection experiments. Box plots for CldU to IdU ratio following HU treatment for BRCA2-deficient (VU423) cell line expressing the indicated siRNAs. $P=0.000059$. (**f**) aniPOND in HEK 293T cells showing recruitment of proteins at replicating (EdU) and stalled (EdU + HU) forks. Western blots of one out of three independent experiments with similar results are shown. (**g**) Representative PLA images of one out of three independent experiments (left) and quantification of foci (right). Scale bars, 1 μm. Error bars show quantification of cells with more than $n>10$ PLA foci. One hundred cells were counted per condition. $^{**}P=0.0068$. Box plots in **a**,**b**,**d** and **e** display a median bar, a first–third quartile box and minimum-to-maximum value whiskers. The analysis was performed on 100 fibres per condition on $n=3$ independent experiments. Significance of difference among all the groups was assessed with the non-parametric Kruskal–Wallis test. Data in **c** represent mean ± s.e.m. of $n=3$ independent experiments, analysed by two-sided Student's t-test. Data in **g** represent mean ± s.e.m. of $n=3$ independent experiments analysed with the χ^2 significance test for trends in proportions. In **c** and **g**, $^{**}P<0.01$ with exact P values (with a confidence interval of 95%) noted in the legends for the relevant panels. Unprocessed original scans of blots are shown in Supplementary Fig. 6.

mediated by its methyltransferase activity since expression of ΔHMT EZH2 had no effect on fork degradation (Supplementary Figs 3b and 6). We next tested whether EZH2 cooperates with nucleases to promote fork degradation and restart. From a panel of nucleases previously shown to process stalled forks and promote fork restart[28,29], the specific knockdown of the endonuclease MUS81 alleviated the EZH2-mediated fork degradation and restart in BRCA2-deficient (VU423) cells (Fig. 3b and Supplementary Figs 3c,d and 6). Finally, we found that a histone H3 peptide specifically di- or trimethylated on Lys27 (H3K27me2 and me3) precipitated the MUS81 endonuclease, while its unmethylated form (H3) did not (Fig. 3c and Supplementary Figs 3e and 6). The MRE11 nuclease showed no preferential binding to

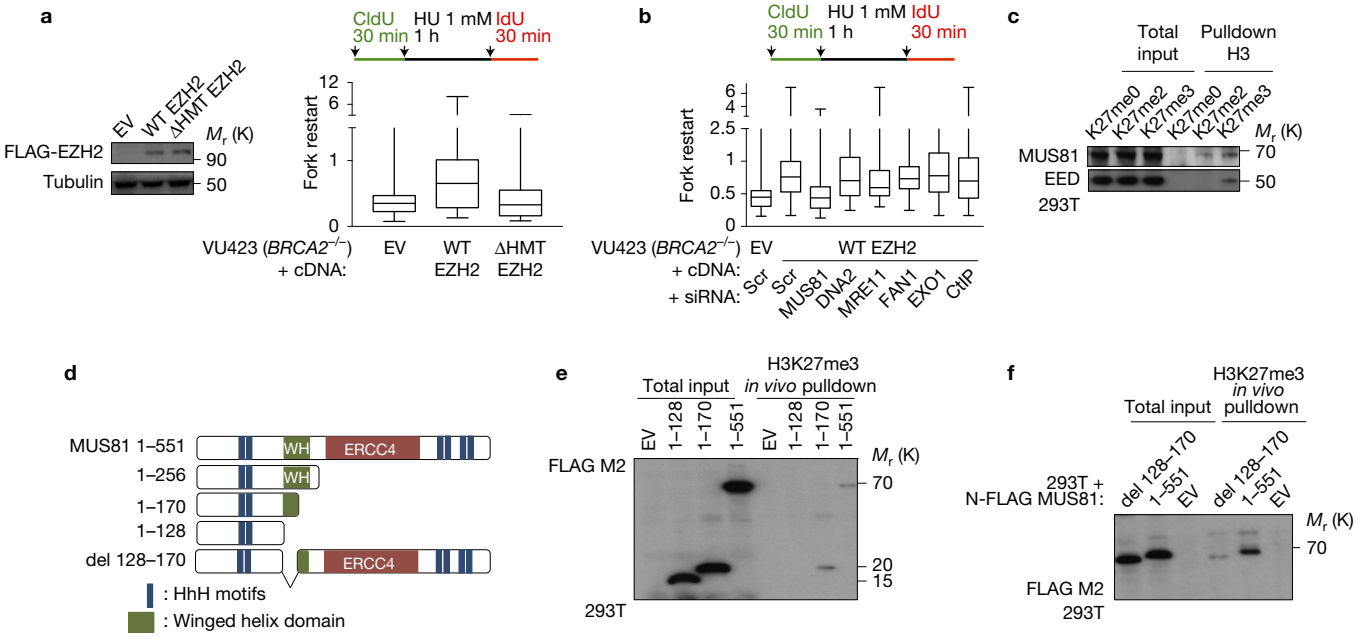

Figure 3 EZH2 promotes MUS81 recruitment and replication fork restart in BRCA2-deficient cells through methylation of H3K27 at stalled replication forks. (**a**) Immunoblot analysis (left) of VU423 cells transduced with EV, WT or ΔHMT EZH2 and schematic of fork restart experiments with CldU and IdU incorporation (right). Box plots show the IdU to CldU ratio. $P=0.0002$. (**b**) Schematic for the labelling with IdU and CldU of cells expressing EV or WT EZH2 for fork restart experiments. Box and whiskers show the nucleoside ratio of cells expressing the indicated cDNA and transfected with nuclease siRNAs (MUS81_5 was used to knockdown MUS81). $P=0.000071$. (**c**) Pulldown of one out of three independent experiments with similar results performed in 293T whole-cell lysate with unmethylated, dimethylated and trimethylated histone H3 at Lys27 (K27me2 or K27me3) as baits. EED binding to H3K27me3 is used as a positive control. (**d**) Domain structure of full-length MUS81 and of the truncated and deletion mutants generated. ERCC4 represents the nuclease domain while HhH depicts the harpin-helix-harpin motifs. (**e**) Pulldown of one out of three independent experiments with similar results performed with trimethylated histone H3 at Lys27 (H3K27me3) in 293T whole-cell lysate expressing full-length or truncated MUS81. (**f**) Pulldown experiment of one out of three independent experiments with similar results performed with trimethylated histone H3 at Lys27 (H3K27me3) in 293T whole-cell lysate expressing the 128–170 deletion mutant (del 128–170) or full-length (1–551) MUS81. The box plots in **a** and **b** display a median bar, a first–third quartile box and minimum-to-maximum value whiskers. The analysis was performed by measuring analogue tracts on 100 fibres per condition in $n=3$ independent experiments. Significance of difference among all the groups was assessed with the non-parametric Kruskal–Wallis test. Unprocessed original scans of blots are shown in Supplementary Fig. 6.

histone H3 in its unmethylated or methylated form, further indicating that MUS81 and MRE11 participate in two distinct degradation pathways at stalled forks (Supplementary Figs 3e and 6). Through pulldown experiments with truncating mutants or a deletion mutant of MUS81, we narrowed down a region that mediates its interaction with methylated H3K27 and that overlaps with the winged helix (WH) domain of MUS81 (Fig. 3d–f and Supplementary Figs 3f–h and 6). These data show that methylation of Lys27 promotes the interaction of histone H3 with MUS81, either directly or indirectly. Collectively, our findings suggest that EZH2 methylates H3K27 at stalled forks resulting in the recruitment of MUS81 and ultimately in the restart of DNA replication.

As we showed that EZH2 cooperates with MUS81, we next analysed the consequences of EZH2 depletion on MUS81 recruitment at stalled forks. By performing aniPOND[26] in EZH2-knockdown or -inhibited cells (EZH2_1 or GSK126 treated) after fork stalling, we observed increased binding of RAD51 as well as binding of the nucleases MRE11 and MUS81 (refs 30,31). Importantly, EZH2 depletion reduced MUS81 recruitment to stalled forks but had no effect on RAD51 or MRE11 recruitment (Fig. 4a and Supplementary Figs 4a and 6). Depletion or inhibition of EZH2 reduced the number of cells forming MUS81 but not MRE11 replication stress foci (Fig. 4b and Supplementary Figs 4b and 6). Again, WT but not ΔHMT EZH2 restored MUS81 foci, suggesting that EZH2 methyltransferase activity is required for MUS81 recruitment to stalled forks and foci assembly (Fig. 4c). Importantly, EZH2 depletion did not affect MUS81 and MRE11 protein expression levels, thus excluding any EZH2-mediated transcriptional activity on these genes (Supplementary Figs 4c and 6).

Loss of MUS81 specifically confers replication fork protection and PARPi resistance in BRCA2- but not BRCA1-deficient cells, thus functionally linking the effect of EZH2 depletion on fork protection and PARPi resistance to the impairment of MUS81 recruitment at stalled forks (Fig. 4d,e). Moreover, low *MUS81* levels correlate with poor prognosis specifically in patients with BRCA2-deficient, but not BRCA1-deficient nor BRCA1/2-wild-type ovarian tumours (Supplementary Fig. 4d). Our data show that EZH2 and MUS81 function in a common pathway at stalled replication forks and that loss of this pathway promotes replication fork protection and PARPi resistance in BRCA2-deficient tumours.

We next decided to evaluate the relevance of our findings in a panel of olaparib (PARPi)-naive and -resistant tumours derived from the Brca2-deficient KB2P (*K14cre; Brca2F/F; p53F/F*) mammary tumour mouse model[32]. We first evaluated *Ezh2* and *Mus81* gene expression in the two groups. Immunohistochemical analysis and gene expression profiling revealed that both the genes were downregulated in PARPi resistant versus naive KB2P tumours (Fig. 5a,b). Finally, we took

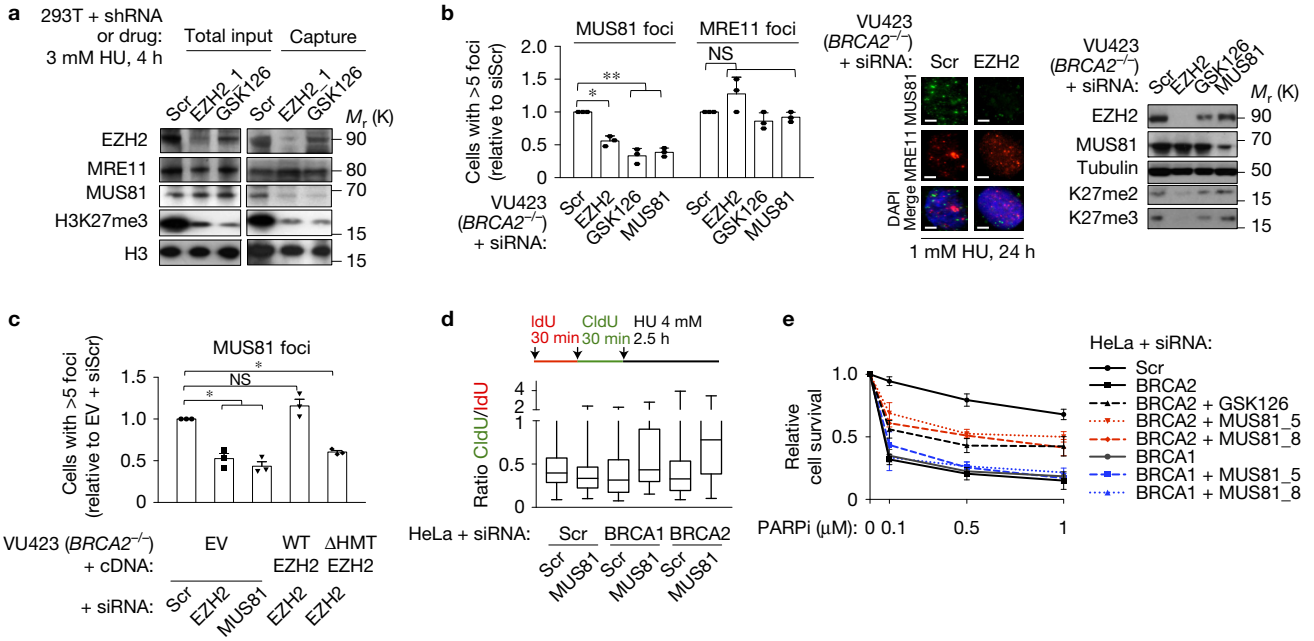

Figure 4 Reduced MUS81 recruitment at stalled replication forks mediates replication fork protection and PARPi resistance. (**a**) aniPOND of one out of three independent experiments with similar results in 293T cells transduced with shScr or shEZH2_1 or treated with GSK126. (**b**) VU423 cells were transfected or treated with GSK126 and subjected to HU-mediated replication stress. Bars (left) represent quantification of VU423 cells with more than 5 foci; 100 cells per independent experiments were scored. The number of positive cells is expressed as fold change of siScr-transfected sample, whose value was set to 1. $^{*}P=0.027$, $^{**}P=0.0038$. NS, not significant. Representative MUS81^{+} and MRE11^{+} nuclei (middle) and western blot analysis on cell lysates of one out of three representative experiments are shown (right). Scale bars, 1 μm. (**c**) Complementation of MUS81 foci in cells transfected with siRNAs and transduced with EV, WT or ΔHMT EZH2. Bars represent quantification of cells with more than 5 foci; 100 cells per independent experiments were scored. The number of positive cells is expressed as fold change of EV + siScr-transfected sample, whose value is set to 1. $^{*}P=0.031$ for EV + siScr versus EV + siEZH2, $^{*}P=0.038$ for EV + siScr versus EV + siMUS81, $^{*}P=0.018$ for EV + siScr versus ΔHMT EZH2 + siEZH2. (**d**) Schematic for IdU/CldU labelling of cells for fork protection experiments. Box plots for CldU to IdU ratio following HU treatment for HeLa cells expressing the indicated siRNAs. $P=0.000046$. (**e**) Clonogenic growth of HeLa cells expressing the indicated siRNAs or treated with GSK126 under increasing concentrations of rucaparib. The data in **b** and **c** represent the mean ± s.e.m. of $n=3$ independent experiments. Significance was assessed with the two-sided Student's *t*-test. The box plots in **d** display a median bar, a first–third quartile box and minimum-to-maximum value whiskers. The analysis was performed by measuring analogue tracts on 100 fibres per condition on 3 independent experiments. Significance of difference among all the groups was assessed with the non-parametric Kruskal–Wallis test. Data in **e** represent mean ± s.e.m. of $n=3$ independent experiments. In **b** and **c**, $^{*}P<0.05$ and $^{**}P<0.01$ and NS, non-significant, with exact *P* values (with a confidence interval of 95%) noted in legends for relevant panels. Unprocessed original scans of blots are shown in Supplementary Fig. 6.

advantage of the KB2P model to monitor the effect of Ezh2 inhibition on the relapse of Brca2-deficient (KB2P) tumours treated with PARPi (olaparib, Supplementary Fig. 5a). Importantly, mice treated with the Ezh2 inhibitor (GSK126) in combination with PARPi experienced earlier tumour relapse (as measured by disease-free survival) and exhibited shorter overall survival than mice treated with PARPi alone (Fig. 5c,d and Supplementary Fig. 5b). Of note, GSK126 treatment alone did not affect the growth of KB2P-derived tumours, suggesting that the effect of Ezh2 inhibition on tumour relapse is not related to proliferation (Supplementary Fig. 5c). Taken together, these results indicate that inhibition of the Ezh2/Mus81 axis *in vivo* promotes PARPi resistance in Brca2-deficient tumours.

Dysregulation of the EZH2/methylH3K27 axis is a recurrent event in cancer. Overexpression of EZH2 is associated with aggressive and advanced cancer stages[13,21] while gain-of-function mutations of EZH2 that increase H3K27 trimethyl levels characterize other specific tumour types[21]. In parallel, EZH2 or histone H3 loss-of-function mutations that reduce the activity of the EZH2/methylH3K27 axis were reported to foster tumour progression and drug resistance in glioblastoma and leukaemia subtypes[10,33]. These data reinforce previous evidence indicating that chromatin modifiers exert differential functions, depending on the cellular context[21].

In this work, we show that the chromatin modifier EZH2 plays an essential role in regulating genomic stability by mediating H3K27 methylation at stalled replication forks, serving as a platform for the recruitment of the endonuclease MUS81. The EZH2/MUS81 axis is essential for replication fork restart in BRCA2-deficient tumours. Concurrently, loss of EZH2 prevents MUS81 recruitment to stalled replication forks and enhances replication fork protection. As a result, loss of the EZH2/MUS81 axis confers PARPi resistance in BRCA2-deficient tumours (Fig. 5e). Accordingly, low EZH2 or MUS81 levels are associated with chemoresistance and poor prognosis in mice and humans harbouring BRCA2-deficient tumours. Our data demonstrate that the EZH2–MUS81 axis is a previously uncharacterized pathway that maintains genomic stability at stalled replication forks. These results broaden our knowledge of how chromatin controls replication fork stability and PARPi resistance and identify EZH2 as a predictor of response to chemotherapy in BRCA2-deficient tumours. MUS81

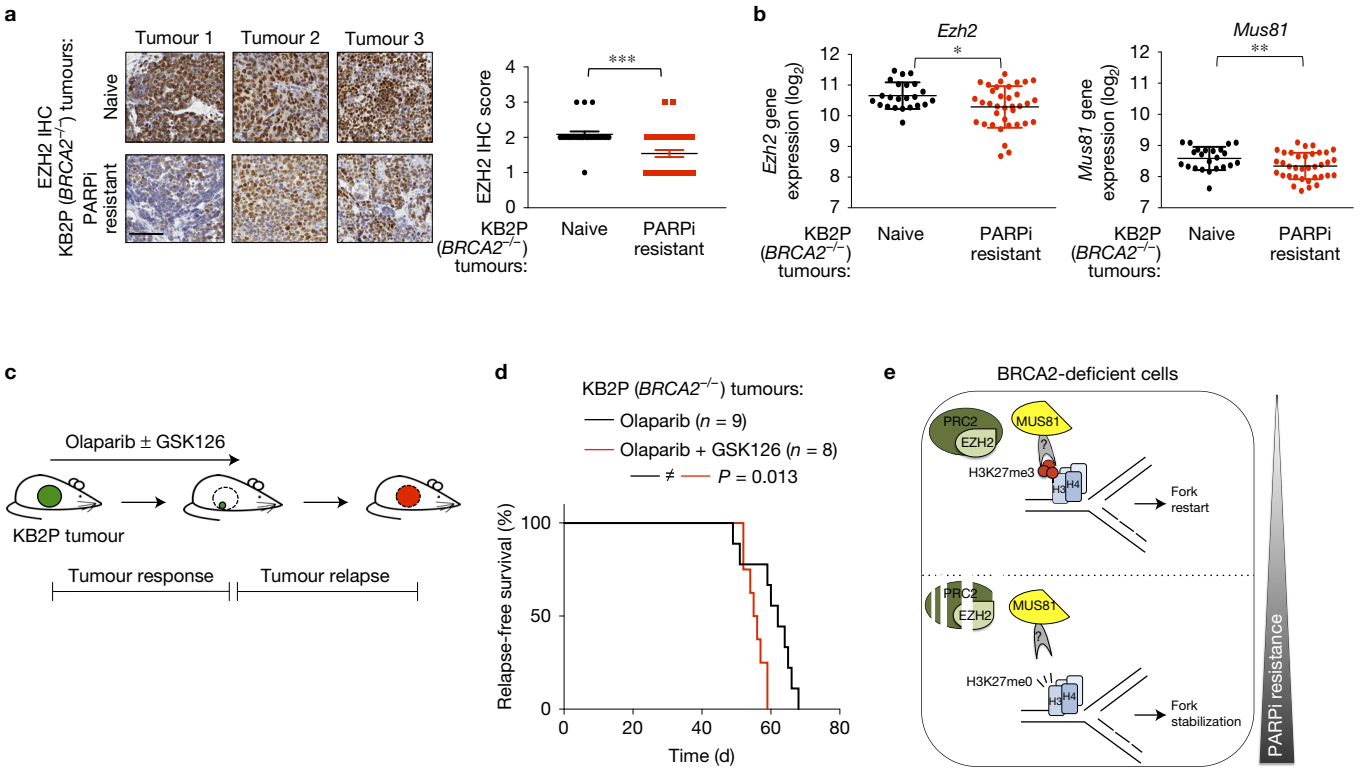

Figure 5 Ezh2 inhibition drives relapse of KB2P-derived breast tumours in mice following PARPi treatment. (**a**) Representative staining (left) and quantification (right) of EZH2 expression by immunohistochemistry (IHC) in naive ($n=24$) versus PARPi (olaparib)-resistant ($n=37$) KB2P-derived tumours. Scale bar, 50 μm. $^{***}P=0.00051$. (**b**) Normalized gene expression of *Ezh2* and *Mus81* using RNA-seq of a panel of naive ($n=24$) and resistant ($n=37$) KB2P-derived tumours. $^{*}P=0.028$ for Ezh2 and $^{**}P=0.0059$ for Mus81. (**c**) Outline of the PARPi treatment in mice. Following tumour outgrowth to approximately 200 mm^3, mice were treated with either olaparib alone ($n=9$) or olaparib + GSK126 ($n=8$). Relapse-free survival was defined as the time needed for the tumours to grow back to the initial volume (200 mm^3) after the administered treatment. (**d**) Relapse-free survival of mice carrying orthotopically injected KB2P-derived tumours that were treated as indicated. (**e**) Model for EZH2-mediated PARPi resistance in BRCA2-deficient cells. EZH2 methylates Lys27 on histone 3 (H3K27me2/3) at stalled forks. Methylated H3K27 allows the binding of the endonuclease MUS81, ultimately promoting fork degradation and restart. Following EZH2 downregulation, Lys27 on histone 3 remains unmethylated (H3K27me0). As a consequence, MUS81 recruitment to stalled forks is reduced, resulting in increased fork stabilization. In agreement with this, low EZH2 or MUS81 levels at stalled forks cause PARPi resistance. Data in **a** and **b** represent mean ± s.d. and significance was determined by the two-sided Mann–Whitney test. Significance in **d** was determined by the two-sided log-rank (Mantel–Cox) test, for which the *P* value is indicated and the confidence interval is 95%. In **a** and **b**, $^{*}P<0.05$, $^{**}P<0.01$ and $^{***}P<0.001$, with exact *P* values (with a confidence interval of 95%) noted in the legends for the relevant panels.

endonuclease activity is known to promote HR-mediated repair of stalled forks and to preserve genome stability[34]. We hypothesize that prolonged MUS81 activity at the replication fork in BRCA2-deficient cells may be toxic, resulting in uncontrolled fork degradation or collapse, as observed for MRE11 (ref. 35).

We establish that the EZH2/MUS81 axis acts independently of the recently characterized MLL3–4/PTIP/MRE11 pathway of chemoresistance. The evidence that two distinct pathways control fork stability suggests that this process is tightly regulated in the cell. Recent work[2], along with our data, indicates that chromatin modifications have an active role in this regulation. Therefore, it will be critical to comprehensively unravel how chromatin modifications affect fork stability and ultimately control genomic stability at stalled forks. Our work describes a previously unrecognized function of EZH2 in driving PARPi resistance in BRCA2-deficient tumours. As such, it raises concerns about the use of EZH2 inhibitors in combination with PARPi or other chemotherapeutics routinely used for the treatment of BRCA2-deficient cancers. According to our data, EZH2 levels can be useful in predicting BRCA2-mutated tumour response to chemotherapy, ultimately allowing a better stratification of patients in clinical trials. Future studies on human samples deriving from the current clinical trials with PARPi will reveal the relevance of EZH2/MUS81 loss in promoting resistance in patients harbouring BRCA2-mutated ovarian and breast carcinomas. □

METHODS

Methods, including statements of data availability and any associated accession codes and references, are available in the online version of this paper.

Note: Supplementary Information is available in the online version of the paper

ACKNOWLEDGEMENTS

We thank all the members of the D'Andrea laboratory for their useful comments, suggestions and help. We thank D. Chowdhury and G. I. Shapiro for helpful discussions on the project and their laboratories for help and reagents (the Shapiro laboratory also provided MDA-MB-436 EV and HA-BRCA1). We thank K. Mouw for helpful discussions and critical reading of the manuscript. We thank S. Orkin (DFCI, Boston, USA) and M. I. Aladjem (NCI, NIH, Bethesda, MD) for providing us with the siEZH2-resistant WT, ΔHMT EZH2 cDNA and with full-length MUS81 plasmids, respectively. We thank the people from the Preclinical Intervention Unit

of the Mouse Clinic for Cancer and Ageing (MCCA) at the NKI for their technical support with the animal studies and J. R. de Ruiter for help with RNA-Seq analysis of the KB2P tumour panel. We thank P. Germain for a preliminary analysis on ovarian carcinoma TCGA gene expression data. B.R. is a recipient of an Italian Association for Cancer Research (AIRC) Fellowship for Abroad and an Ovarian Cancer Research Fellowship (OCRF) Ann Schreiber Mentored Investigator Award. This research was supported by a Stand Up To Cancer-Ovarian Cancer Research Fund Alliance-National Ovarian Cancer Coalition Dream Team Translational Research Grant (Grant Number: SU2C-AACR-DT16-15). Stand Up To Cancer is a programme of the Entertainment Industry Foundation. Research grants are administered by the American Association for Cancer Research, the scientific partner of SU2C. This work was also supported by grants from the US National Institutes of Health (R01DK43889, R01HL052725, P01HL048546, P50CA168504), the United States Department of Defense (BC151331P1), the Breast Cancer Research Foundation, and the Ludwig Center at Harvard (to A.D.D.), the Dutch Cancer Society (2014-6532 to S.R. and J.J.), the Swiss National Science Foundation (310030_156869 to S.R.), and the European Union (ERC CoG-681572 to S.R.).

AUTHOR CONTRIBUTIONS

B.R. conceived the study, performed experiments, analysed data and wrote the manuscript. E.G. and A.A.D. performed and analysed the animal, gene expression and IHC experiments under the supervision of M.v.d.V., J.J. and S.R. H.Y. and R.v.d.S. performed experiments, A.D.D. and M.v.d.V. contributed to mouse work, P.A.K. curated TCGA data sets for Fig. 1g and Supplementary Fig. 5d and provided clinical perspectives. R.C. performed bioinformatic analysis on TCGA gene expression, reviewed data and provided expertise, S.R. reviewed *in vivo* and IHC data and provided expertise, and A.D.D. conceived the study and wrote the manuscript. All authors approved the final version of the manuscript.

COMPETING FINANCIAL INTERESTS

The authors declare no competing financial interests.

Published online at http://dx.doi.org/10.1038/ncb3626

1. Lord, C. J. & Ashworth, A. Mechanisms of resistance to therapies targeting BRCA-mutant cancers. *Nat. Med.* **19,** 1381–1388 (2013).
2. Ray Chaudhuri, A. *et al.* Replication fork stability confers chemoresistance in BRCA-deficient cells. *Nature* **535,** 382–387 (2016).
3. Farmer, H. *et al.* Targeting the DNA repair defect in BRCA mutant cells as a therapeutic strategy. *Nature* **434,** 917–921 (2005).
4. Konstantinopoulos, P. A., Ceccaldi, R., Shapiro, G. I. & D'Andrea, A. D. Homologous recombination deficiency: exploiting the fundamental vulnerability of ovarian cancer. *Cancer Discov.* **5,** 1137–1154 (2015).
5. Moynahan, M. E., Cui, T. Y. & Jasin, M. Homology-directed DNA repair, mitomycin-C resistance, and chromosome stability is restored with correction of a *Brca1* mutation. *Cancer Res.* **61,** 4842–4850 (2001).
6. Schlacher, K. *et al.* Double-strand break repair-independent role for BRCA2 in blocking stalled replication fork degradation by MRE11. *Cell* **145,** 529–542 (2011).
7. Bouwman, P. *et al.* 53BP1 loss rescues BRCA1 deficiency and is associated with triple-negative and BRCA-mutated breast cancers. *Nat. Struct. Mol. Biol.* **17,** 688–695 (2010).
8. Alabert, C. & Groth, A. Chromatin replication and epigenome maintenance. *Nat. Rev. Mol. Cell Biol.* **13,** 153–167 (2012).
9. Clemente-Ruiz, M. & Prado, F. Chromatin assembly controls replication fork stability. *EMBO Rep.* **10,** 790–796 (2009).
10. Göllner, S. *et al.* Loss of the histone methyltransferase EZH2 induces resistance to multiple drugs in acute myeloid leukemia. *Nat. Med.* **23,** 69–78 (2016).
11. de Vries, N. A. *et al.* Prolonged Ezh2 depletion in glioblastoma causes a robust switch in cell fate resulting in tumor progression. *Cell Rep.* **10,** 383–397 (2015).
12. Morey, L. & Helin, K. Polycomb group protein-mediated repression of transcription. *Trends Biochem. Sci.* **35,** 323–332 (2010).
13. Bracken, A. P. *et al.* EZH2 is downstream of the pRB-E2F pathway, essential for proliferation and amplified in cancer. *EMBO J.* **22,** 5323–5335 (2003).
14. Campbell, S., Ismail, I. H., Young, L. C., Poirier, G. G. & Hendzel, M. J. Polycomb repressive complex 2 contributes to DNA double-strand break repair. *Cell Cycle* **12,** 2675–2683 (2013).
15. Chou, D. M. *et al.* A chromatin localization screen reveals poly (ADP ribose)-regulated recruitment of the repressive polycomb and NuRD complexes to sites of DNA damage. *Proc. Natl Acad. Sci. USA* **107,** 18475–18480 (2010).
16. Hansen, K. H. *et al.* A model for transmission of the H3K27me3 epigenetic mark. *Nat. Cell Biol.* **10,** 1291–300 (2008).
17. Ceccaldi, R. *et al.* Homologous-recombination-deficient tumours are dependent on Polh-mediated repair. *Nature* **518,** 258–262 (2015).
18. Kais, Z. *et al.* FANCD2 maintains fork stability in BRCA1/2-deficient tumors and promotes alternative end-joining DNA repair. *Cell Rep.* **15,** 2488–2499 (2016).
19. Cancer, T. & Atlas, G. Integrated genomic analyses of ovarian carcinoma. *Nature* **474,** 609–615 (2011).
20. McCabe, M. T. *et al.* EZH2 inhibition as a therapeutic strategy for lymphoma with EZH2-activating mutations. *Nature* **492,** 108–112 (2012).
21. Kim, K. H. & Roberts, C. W. M. Targeting EZH2 in cancer. *Nat. Med.* **22,** 128–134 (2016).
22. Branzei, D. & Foiani, M. Maintaining genome stability at the replication fork. *Nat. Rev. Mol. Cell Biol.* **11,** 208–219 (2010).
23. Alabert, C. *et al.* Nascent chromatin capture proteomics determines chromatin dynamics during DNA replication and identifies unknown fork components. *Nat. Cell Biol.* **16,** 281–293 (2014).
24. Piunti, A. *et al.* Polycomb proteins control proliferation and transformation independently of cell cycle checkpoints by regulating DNA replication. *Nat. Commun.* **5,** 3649 (2014).
25. Alabert, C. *et al.* Two distinct modes for propagation of histone PTMs across the cell cycle. *Genes Dev.* **29,** 585–590 (2015).
26. Thomas Leung, K. H., El Hassan, M. A. & Bremner, R. A rapid and efficient method to purify proteins at replication forks under native conditions. *Biotechniques* **55,** 204–206 (2013).
27. Vassin, V. M., Anantha, R. W., Sokolova, E., Kanner, S. & Borowiec, J. A. Human RPA phosphorylation by ATR stimulates DNA synthesis and prevents ssDNA accumulation during DNA-replication stress. *J. Cell Sci.* **122,** 4070–4080 (2009).
28. Petermann, E. & Helleday, T. Pathways of mammalian replication fork restart. *Nat. Rev. Mol. Cell Biol.* **11,** 683–687 (2010).
29. Cortez, D. Preventing replication fork collapse to maintain genome integrity. *DNA Repair* **32,** 149–157 (2015).
30. Petermann, E., Orta, M. L., Issaeva, N., Schultz, N. & Helleday, T. Hydroxyurea-stalled replication forks become progressively inactivated and require two different RAD51-mediated pathways for restart and repair. *Mol. Cell* **37,** 492–502 (2010).
31. Mirzoeva, O. K. & Petrini, J. H. J. DNA replication-dependent nuclear dynamics of the Mre11 complex. *Mol. Cancer Res.* **1,** 207–218 (2003).
32. Jonkers, J. *et al.* Synergistic tumor suppressor activity of BRCA2 and p53 in a conditional mouse model for breast cancer. *Nat. Genet.* **29,** 418–425 (2001).
33. Schwartzentruber, J., Korshunov, A. & Liu, X. Y. Driver mutations in histone H3.3 and chromatin remodelling genes in paediatric glioblastoma. *Nature* **482,** 226–231 (2012).
34. Hanada, K. *et al.* The structure-specific endonuclease Mus81 contributes to replication restart by generating double-strand DNA breaks. *Nat. Struct. Mol. Biol.* **14,** 1096–1104 (2007).
35. Chen, H. *et al.* Sae2 promotes DNA damage resistance by removing the Mre11–Rad50–Xrs2 complex from DNA and attenuating Rad53 signaling. *Proc. Natl Acad. Sci. USA* **112,** E1880–E1887 (2015).

METHODS

Bioinformatic analyses. The chromatin-modifiers gene list analysed is described in Supplementary Table 1. TCGA data sets were accessed through the public TCGA data portal (https://tcga-data.nci.nih.gov). Figure 1a and Supplementary Fig. 1b depict *EZH2* and *MKi67* gene expression respectively in the ovarian carcinoma data set GSE9891, breast carcinoma TCGA and uterine carcinoma TCGA. Normalization of expression values was performed using *z*-score transformation. mRNA expression values were subdivided into subgroups reflecting the stage of the disease (for GSE9891: grade 3 ovarian serous carcinoma, $n = 143$ compared with type 1 (grade 1) ovarian cancers, $n = 20$; for uterine: serous-like tumours, $n = 60$ compared with the rest of the tumours, $n = 172$; for breast: basal-like breast carcinoma, $n = 80$ compared with the rest of the tumours, $n = 421$). In the ovarian[1] and breast TCGA data sets, all tumours were analysed. In the uterine TCGA, we curated all tumours except the ultra- and hyper-mutated group (that is, POLE-mutated and MSI (microsatellite instability) tumours). Disease-free survival curves of TCGA ovarian carcinoma patients were generated by the Kaplan–Meier method and differences between survival curves were assessed for statistical significance with the log-rank test. We divided the TCGA ovarian carcinoma patients into three cohorts according to their BRCA1/2 mutational status: BRCA1/2-wild-type, BRCA1-mutated and BRCA2-mutated. In each of these three cohorts, we analysed the correlation between EZH2 or MUS81 expression with outcome. To do so, we arbitrarily established a cutoff point for EZH2 or MUS81 expression levels that was represented by their median. On the basis of this cutoff, we divided patients into two groups: those with higher than median EZH2 or MUS81 mRNA levels (EZH2 or MUS81 high group) and those with lower than median levels (EZH2 or MUS81 low group).

Chromosomal breakage analysis. HeLa and VU423 cells were transfected twice with siRNAs. GSK126 (5 μM) was added to cell cultures at the time of the first transfection. Next, cells were incubated for 48 h with or without the indicated concentrations of MMC. Cells were exposed for 2 h to 100 ng ml^{-1} of colcemid and treated with a hypotonic solution (0.075 M KCl) for 20 min and fixed with 3:1 methanol/acetic acid. Slides were stained with Wright's stain. Fifty metaphase spreads were scored for aberrations for each experiment. The number of chromosomal aberrations per cell is reported.

Clonogenic survival assay. Cells were seeded at 1,000–5,000 per well into 6-well plates and continuously treated with the PARP inhibitor rucaparib or with cisplatin (CDDP). GSK126 (5 μM) was added where indicated. Colony formation was scored 12–14 days after treatment using 0.5% (w/v) crystal violet in methanol. For each treated sample, survival curves were expressed as the number of colonies compared with the untreated control, which was arbitrarily set to 1. Error bars represent the standard error of the mean (s.e.m.) over $n = 3$ independent experiments performed.

Immunoblot analysis. For protein detection, cell pellets were washed and lysed with RIPA buffer (20 mM TRIS-HCl (pH 8.0); 150 mM NaCl; 1 mM EDTA; 1 mM EGTA; 1% Triton X-100; 0.5% Sodium deoxycholate; 0.1% SDS) supplemented with protease inhibitor cocktail (Roche). For detection of BRCA1 and BRCA2, cells were lysed in PD buffer (20 mM Tris pH 8.0, 300 mM NaCl, 2% NP40, 20% glycerol, 10 mM EDTA) supplemented with protease inhibitor cocktail (Roche). Protein lysates were then resolved on NuPAGE (Invitrogen) gels and transferred onto nitrocellulose membrane (or PVDF, in the case of BRCA1 and BRCA2 detection), followed by detection using Western Lighting Plus ECL (Perkin Elmer).

Immunofluorescence. Cells were fixed with 4% paraformaldehyde (PFA) for 10 min at room temperature, followed by permeabilization with 0.3% Triton X-100 for 10 min and blocking with 3% BSA for 30 min. Primary antibody staining was performed overnight at 4 °C while secondary antibody staining was performed at room temperature for 1 h. When indicated, cells were transfected with siRNAs 48 h before treatments. For RAD51, cells were treated with 2 mM hydroxyurea (HU) for 6 h and fixed immediately. For MUS81 and MRE11 foci, replication stress was induced with 1 mM HU for 24 h. Afterwards, cytosoluble material was extracted with cytoskeletal (CSK) buffer + 0.5% Triton X-100 for 5 min on ice. Fixation and antibody staining were then performed as indicated above. The number of cells with more than ten RAD51 or five MUS81/MRE11 foci was calculated relative to control cells (SiScr or EV+SiScr). At least 100 cells were counted for each sample. Images were captured using a Zeiss AX10 fluorescence microscope and AxioVision software. Co-localization of MRE11 and MUS81 with stalled replication sites was performed as in ref. 2.

Proximity ligation assay (PLA). Whole cells, treated with 3 mM HU for 4 h or untreated, were fixed, permeabilized and stained with primary antibody as indicated for immunofluorescence. Afterwards, *in situ* proximity ligation assay was performed using the Duolink Detection Kit (Sigma Aldrich Duolink) in combination with anti-Mouse PLUS and anti-Rabbit MINUS oligonucleotide labelled secondary antibodies (PLA probes). Briefly, PLA probes were bound to primary antibodies during a 60 min reaction at 37 °C; then PLA probe-coupled oligonucleotides were ligated during a 30 min reaction performed at 37 °C. An amplification reaction was performed for 140 min at 37 °C to allow generation of a fluorescent signal (PLA signal) at sites where two oligonucleotide probes were ligated. The percentage of cells with more than ten nuclear PLA foci was calculated by using a Zeiss AX10 fluorescence microscope.

Reporter assays. HR efficiency was measured using the DR-GFP reporter assay. Briefly, 48 h before transfection of Sce-I cDNA, U2OS-DR-GFP cells were transfected with the indicated siRNA and/or treated with GSK126 (5 μM). The HR activity was determined by fluorescence-activated cell sorting (FACS)-mediated quantification of viable GFP-positive cells 72 h after Sce-I was transfected.

DNA fibre analysis. Fork degradation and restart experiments were performed as in ref. 3. Briefly, for fork degradation analysis, VU423 cells, untransduced or transduced with pOZ vectors, were transfected twice with the indicated siRNAs. GSK126 (5 μM) was added to cultures at the time of the first transfection. At 72 h after transfection, cells were incubated with 250 μM iododeoxyuridine (IdU) (Sigma, I7125) for 30 min, followed by 25 μM chlorodeoxyuridine (CldU) (Sigma, C6891) for 30 min. Cells were then incubated with 4 mM HU for 2.5 hours. For fork restart analysis, cells were incubated with 250 μM IdU for 30 min. Cells were then treated with 1 μM HU for 1 h and incubated in 25 μM CldU for 30 min. Preparation of DNA plugs from cells and molecular combing of DNA fibres were performed with the Molecular Combing Platform by Genomic Vision. Next, denaturation of DNA was achieved by treatment of fibre slides with 2.5 M HCl for 2 h. Immunostaining was performed by following the immunofluorescence protocol and by using two anti-BrdU antibodies, one specific for IdU and the other for CldU (see the Antibodies section). Both fork stability and restart are expressed as ratios between the second and the first incorporated analogues. This ratio is set to 1 in the case of the control (siScr, EV or EV+siScr) and all the other samples are expressed relative to it. The number of stalled forks is calculated as numbers of DNA fibres that have incorporated only CldU in the fork restart experiments. The ratio of stalled forks is expressed as a fold change relative to the number of stalled forks counted for the control (siScr), which was arbitrarily set to 1. Pictures were taken with an Olympus confocal microscope and fibre length was measured by ImageJ software. At least 100 stretched fibres were counted per condition.

aniPOND (accelerated native isolation of protein on nascent DNA). A modified version of iPOND was exploited to detect proteins at stalled forks[36]. Briefly, exponentially growing 293T cells were subjected to EdU incorporation (15 min). This was followed by stalling of replicating forks with 3 mM HU for 4 h and by lysis of whole cells in NEB buffer (20 mM Hepes pH 7.2, 50 mM NaCl, 3 mM MgCl, 300 mM sucrose and 0.5% IGEPAL CA630). Nuclear unsoluble, chromatin-bound material was then subjected to the Click-iT reaction (Thermo Scientific, reaction in 25 μM biotin–azide, 10 mM (+)-sodium L-ascorbate, 2 mM $CuSO_4$). Afterwards, sonication of chromatin-bound material was performed in B1 buffer (25 mM NaCl, 2 mM EDTA, 50 mM Tris-HCl pH 8.0, 1% IGEPAL CA630 plus protease inhibitors) by performing 2′ of 10″ ON + 10″ OFF cycles at a power of 18 W. The sonicator used was an Ultrasonic Homogenizer Sonicator. After sonication, the NaCl concentration was lowered by adding to the lysate one volume of buffer B2 (150 mM NaCl, 2 mM EDTA, 50 mM Tris-HCl pH 8.0, 0.5% IGEPAL CA630 plus protease inhibitors). Fragmented chromatin was then subjected to overnight immunoprecipitation with streptavidin-coated beads (Thermo Scientific). A total input aliquot (0.5% of total lysate) was taken from the lysate before overnight streptavidin capture. The day after, extensive washes with buffer B2 were performed and then the EdU/streptavidin-bound material (capture sample) was eluted with 2× Laemmli sample buffer (Biorad, with 5% β-mercaptoethanol added) by boiling at 99 °C for 15 min. Both capture and total input samples were loaded on acrylamide gels for protein detection. Where indicated, cells were treated for 72 h with GSK126 (5 μM) before EdU incorporation and fork stalling with HU.

Pulldown assay. Exponentially growing 293T cells were lysed in Cyto buffer (10 mM Tris-Cl pH 7.6, 100 mM NaCl, 2 mM $MgCl_2$, 0.3 M sucrose, 0.25% v/v Igepal/NP40 and inhibitors) for 20 min on ice and subsequently centrifuged. The nuclear pellet was washed once with Cyto buffer without detergent. Nuclei were then resuspended in high-salt buffer (50 mM Tris pH 7.2, 300 mM NaCl , 1 mM dithiothreitol, 0.5% (w/v) Igepal/NP40, 1 mM EDTA and inhibitors) and sonicated 4 × 10″ at 12 W of power, each time intercalated by a 1 min pause. After centrifugation, nuclear lysates were pre-cleared with washed streptavidin beads by rotating for 1 h at 4 °C. Cleared supernatant was incubated overnight at 4 °C on the wheel with 5 μg of H3, H3K27me2 or H3K27me3 biotinylated peptides (Millipore). The morning

DOI: 10.1038/ncb3626

after, after extensive washes in high-salt nuclear buffer, peptide-bound protein complexes were eluted with 2× Laemmli buffer (Biorad, with 5% β-mercaptoethanol added) by boiling at 99 °C for 15 min and loaded on a acrylamide gel for protein detection.

Immunohistochemistry. Immunohistochemical staining of EZH2 was performed using formalin-fixed paraffin-embedded tissues of olaparib-naive and -resistant KB2P tumours. Antigen retrieval was performed by cooking in citrate buffer pH 6.0 for 30 min and endogenous peroxidase activity was blocked by incubation with methanol solution of 3% H_2O_2 for another 20 min. To minimize the background, 10% milk solution in PBS was used as a blocking buffer (30 min, room temperature). Furthermore, samples were incubated with primary antibody (Cell Signaling no. 5246, diluted 1:200 in 1% BSA, 1.25% goat serum in PBS) overnight at 4 °C and with a peroxidase-labelled anti-rabbit polymer (DakoCytomation, K4011) for 30 min at room temperature. For detection, we used DAKO Liquid DAB+ Substrate Chromogen System (DAKO, K3468), according to the manufacturer's protocol, and haematoxylin counterstaining. The analysis was done in a blind, semi-quantitative manner, using the following scores: 0, 0–25%; 1, 25–50%; 3, 50–75%; and 4, 75–100% relative expression.

RNA-sequencing. RNA libraries derived from the panel of PARPi-naive and -resistant KB2P tumours were analysed on a 2100 Bioanalyzer (Agilent) using a 7500 chip (Agilent). Expression of Ezh2 and Mus81 in KB2P-derived tumours was expressed as $\log_2$ reads.

***In vivo* studies.** This study is compliant with all relevant ethical regulations regarding animal research; all animal experiments were approved by the Animal Ethics Committee of The Netherlands Cancer Institute (Amsterdam, the Netherlands) and performed in accordance with the Dutch Act on Animal Experimentation (November 2014). Orthotopic transplantations, tumour monitoring and sampling were performed as described before[37]. Briefly, KB2P PARPi-naive tumour was transplanted into 40 NMRI-nude females and treatments were initiated following tumour outgrowth to approximately 200 mm^3 (100%). Tumour-bearing mice, randomized into treatment groups blindly as described previously[5], were treated with vehicle, olaparib (100 mg kg^{-1}, intraperitoneally) and GSK126 inhibitor (50 mg kg^{-1}, intraperitoneally) alone or in combination for 28 consecutive days. Animals were euthanized with CO_2 when the tumour reached a volume of 1,500 mm^3. All of the procedures were carried out by animal technicians who were blinded regarding the hypothesis of the treatment outcome.

Plasmid construction and generation of stable cell lines. Codon-optimized, siRNA-resistant wild-type (EZH2 WT) or catalytic-dead (F672I/H694A/R732K, named ΔHMT) EZH2 cDNAs were kindly provided by S. Orkin's laboratory (DFCI, Boston, USA) and subcloned into pOZ-C-FLAG-HA, a retroviral expression vector that also encodes for IL2Receptor. Retroviral particles were produced and VU423 cells were transduced. Transduced VU423 cells were selected by two consecutive rounds of positive selection with magnetic beads coated with anti-IL2 receptor antibody. Stable VU423 cell lines expressing either empty vector (EV), WT EZH2 (WT) or ΔHMT EZH2 (ΔHMT) were used for complementation studies following siRNA-mediated knockdown of the endogenous EZH2 protein. Stable knockdown HEK 293T cell lines used for aniPOND experiments were generated by production of lentiviral particles and transduction. Briefly, shScr, EZH2_1 and EZH2_4 plKO-Puro-shRNA plasmids were obtained from the Mission library by Sigma Aldrich. EZH2_1 sequence was 5′-CCGGTATGATGGTTAACGGTGATCACTGAGTGAT CACCGTTAACCATCATATTTTTG-3′ while EZH2_4 was 5′-CCGGGCGTATA AAGACACCACCTAACTCGAGTTAGGTGGTGTCTTTATACGCTTTTTG-3′ .

Wild-type MUS81 was kindly provided by M. I. Aladjem's laboratory (NCI, NIH, Bethesda, Maryland, USA). Amino acids 1–128, 1–170 and 1–256 truncated MUS81 mutants were amplified by PCR from the provided full-length cDNA and subcloned into pCDNA3.1-N-FLAG vector (Addgene). At this point, truncated MUS81 cDNAs were either *in vitro* transcribed and translated by using the TNT T7 Quick Coupled Transcription–Translation System (Promega) or transiently transfected into 293Ts for *in vivo* pulldowns. The 128–170 MUS81 deletion mutant (deletion 128–170) of MUS81 was generated by mutagenesis PCR from the full-length MUS81 cDNA.

Cell culture, transfections and siRNA sequences. HeLa, VU423 (*BRCA2*$^{-/-}$), A2780, U2OS, HEK 293T and the respective virally transduced cell lines were purchased from ATCC and maintained in DMEM plus 10% fetal calf serum (FCS), L-glutamine (2 mM) and penicillin–streptomycin (1%). KURAMOCHI (*BRCA2*$^{-/-}$), MDA-MB-436 (*BRCA1*$^{-/-}$), MDA-MB-436 (called MDA436) corrected with EV or HA-BRCA1, and HCC1937 (*BRCA1*$^{-/-}$) cells were purchased from ATCC and maintained in RPMI medium plus 10% FCS, L-glutamine (2 mM) and penicillin–streptomycin (1%). None of the cell lines used in this paper is currently listed in the database of commonly misidentified cell lines maintained by ICLAC. Cell lines were tested for mycoplasma contamination at the beginning of the study. When indicated, cells were transfected with RNAi Max (Invitrogen) with the following siRNA sequences (sense sequences):

BRCA1: 5′-CAGCAGTTTATTACTCACTAATT-3′;
BRCA2: 5′-GAAGAATGCAGGTTTAATATT-3′;
53BP1: 5′-CAGGACAGTCTTTCCACGA-3′;
EZH2si_4: 5′-TTCGAGCTCCTCTGAAGCA-3′;
MUS81_5: 5′-GGAGCACCTGAATCCTAATTT-3′;
MUS81_8: 5′-AGTTGGTCCTCATCAAATATT-3′;
Exo1: 5′-GGATGTACTTTACCTTCTATT-3′;
Mre11: 5′-GGGTTATTTGAGCAAGTAATT-3′;
FAN1: 5′-GGTGGACGCCTTTCTCAAATT-3′;
CtIP: 5′-GCTAAAACAGGAACGAATCTT-3′;
SUZ12: 5′-GCATAATGTCAATAGATAATT-3′. All of these sequences were from Qiagen.

The following siRNA sequences were derived from published works as indicated:
FANCD2: 5′-GGAGAUUGAUGGUCUACUATT-3′[18];
DNA2: 5′-CAGUAUCUCCUCUAGCUAGTT-3′[38];
PTIP: 5′-TAATCCGCAATTGCAAACA-3′[39].

Antibodies. The antibodies used in this study were: anti-EZH2 (for western blot: Millipore, clone BD43, 1:1,000; for PLA: Cell Signaling, clone AC22, 1:500; for IHC: Cell Signaling, no. 5246, 1:500), anti-H3K27me2 (Cell Signaling, 1:2,000), anti-H3K27me3 (Cell Signaling, no. 9733, 1:2,000), anti-H3 (Santa Cruz, clone FL136, 1:10,000), anti-BRCA1 (Calbiochem, OP-92, 1:250), anti-BRCA2 (Calbiochem, OP-95, 1:250), anti-53BP1 (Abcam, no. 36823, 1:1,000), anti-tubulin (Santa Cruz, clone B7, 1:500), anti-PCNA (clone PC-10, 1:250), anti-FANCD2 (Santa Cruz, clone FI17, 1:250), anti-FLAG (Sigma, clone M2, 1:2,000), RPA pSer33 and pSer4/8 (Novus Biologicals, 1:500 and 1:250), anti-MUS81 (western blot: Abcam, 97391, 1:1,000; IF: Abcam, MTA30 2G1073, 1:250), anti-MRE11 (Novus Biologicals, 1:1,000), anti-EXO1 (Bethyl, 1:1,000), anti-DNA2 (Abcam, 1:500), anti-CTIP (Bethyl, 1:1,000), anti-FAN1 (Abcam, 1:500), anti-RAD51 (Santa Cruz, clone H92, 1:250), anti-EED (Santa Cruz, clone H300, 1:250), anti-BrdU (for detection of ssDNA in PLA assay and of IdU in fibre assay, no. 347580, clone B44, Becton Dickinson, 1:50), anti-BrdU (for detection of CldU, Abcam no. 6326, 1:100). Secondary antibodies used for immunoblot were HRP-linked anti-goat (Santa Cruz, 1:1,000), anti-mouse or anti-rabbit (Life Technologies, 1:5,000) while for immunofluorescence we used Alexa-Fluor antibodies (Life Technologies, 1:1,000).

Chemicals. Mitomycin C (MMC), cis-diamminedichloroplatinum(II) (cisplatin, CDDP), hydroxyurea (HU), 5-iodo-2′-deoxyuridine (IdU), 5-chloro-2′-deoxyuridine (CldU) and 5-ethynyl-2′-deoxyuridine (EdU) were purchased from Sigma. The PARP inhibitor rucaparib and the EZH2 inhibitor GSK126 were purchased from Selleckchem. Olaparib was purchased from Syncom.

Statistical analysis and reproducibility. Statistical tests used in this manuscript are justified as appropriate and the data do meet the assumptions of the used tests. No estimate of variation within each group of data was considered. The variance between the groups that were statistically compared was similar. Data are represented as mean ± standard error of the mean (s.e.m.) over $n = 3$ independent experiments performed or as mean ± standard deviation (s.d.) for panels in Fig. 5a,b and Supplementary Fig. 5c. Unless otherwise stated, significance was calculated using the unpaired, two-sided. Student's *t*-test or the χ^2 test for trends in proportions. For sample sizes of $n < 10$, individual data points were superimposed on bar graphs. In DNA fibre assay experiments, the D'Agostino and Pearson normality test was performed. When the normality test was not passed, significance was assessed with the one-sided Kruskal–Wallis test. Analyses were performed by the use of GraphPad Prism 6 software. A P value less than 0.05 was considered statistically significant (NS, not significant; $^{*}P < 0.05$, $^{**}P < 0.01$ and $^{***}P < 0.001$, with exact values as indicated in figure legends). *In vivo* experiments were run with $n = 9$ mice for vehicle, GSK126 and olaparib treatment groups and $n = 8$ mice for the olaparib + GSK126 group. Experiments were independently reproduced in the laboratory at least three times.

Ethical compliance. All animal experiments were approved by the Animal Ethics Committee of The Netherlands Cancer Institute (Amsterdam, the Netherlands).

Data availability. RNA-seq data that support the findings of this study have been deposited in the European Nucleotide Archive (ENA, http://www.ebi.ac.uk/ena) under accession number PRJEB20535 and can be downloaded from the 'ena' subfolder from Globus (www.globus.org). The human ovarian, breast and uterine carcinoma data sets that support the findings of this study were derived

from and are available at the CDG/TCGA portals at the following links: https://tcga-data.nci.nih.gov/docs/publications/ov_2011 for ovarian, https://tcga-data.nci.nih.gov/docs/publications/brca_2012 for breast, and https://tcga-data.nci.nih.gov/docs/publications/ucec_2013 for uterine. TCGA publications generated from analysis of these data sets are 'Integrated genomic analyses of ovarian carcinoma'[19], 'Comprehensive molecular portraits of human breast tumours'[36] and 'Integrated genomic characterization of endometrial carcinoma'[40], respectively.

36. The Cancer Genome Atlas Network. Comprehensive molecular portraits of human breast tumours. *Nature* **490,** 61–70 (2012).
37. Rottenberg, S. *et al*. Selective induction of chemotherapy resistance of mammary tumors in a conditional mouse model for hereditary breast cancer. *Proc. Natl Acad. Sci. USA* **104,** 12117–12122 (2007).
38. Thangavel, S. *et al*. DNA2 drives processing and restart of reversed replication forks in human cells. *J. Cell Biol.* **208,** 545–562 (2015).
39. Gong, Z., Cho, Y.-W., Kim, J.-E., Ge, K. & Chen, J. Accumulation of Pax2 transactivation domain interaction protein (PTIP) at sites of DNA breaks via RNF8-dependent pathway is required for cell survival after DNA damage. *J. Biol. Chem.* **284,** 7284–7293 (2009).
40. The Cancer Genome Atlas Network. Integrated genomic characterization of endometrial carcinoma. *Nature* **497,** 67–73 (2013).

nature cell biology

DOI: 10.1038/ncb3626

In the format provided by the authors and unedited.

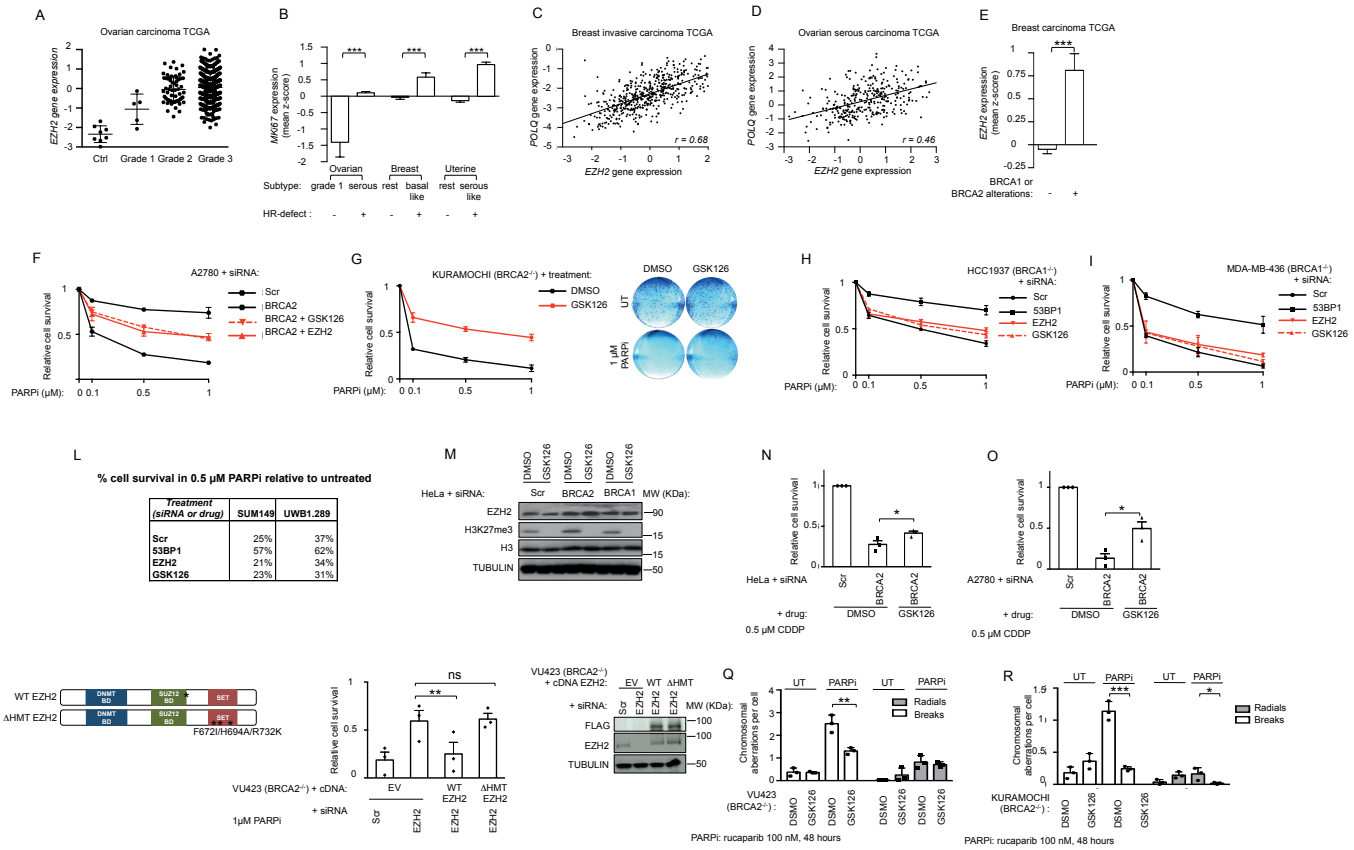

Supplementary Figure 1 EZH2-mediated drug resistance depends on its methyltransferase activity and extends to cisplatin. **a,** EZH2 expression in OvCa TCGA (n=494 OvCa (grade 1, n=5; grade 2, n=61; grade 3, n=428) and n=8 control samples). Each dot represents a Z-score for a tumor. Error bars represent s.e.m. and the black bar represents the median. P=0.00063. **b**, MKi67 gene expression in ovarian (grade 2/3 serous n=143 and grade 1 n=20; ***P=0.00034), breast (basal-like n=80 and rest n=421; ***P=0.00045) and uterine (serous-like n=60 compared to the rest n=172; ***P=0.00067) cancers. Expression values are represented as the mean ± s.e.m. of Z-scores. **c-d,** EZH2 expression in breast carcinoma TCGA (**c**) and in ovarian TCGA (**d**). **e,** EZH2 expression in breast TCGA (n=501.samples). Bars represent mean ± s.e.m. and ***P=0.000136. **f-l,** Clonogenic assays in A2780 (**f**), KURAMOCHI (**g**) or in HCC1937 (**h**), MDA-MB-436 (**i**), SUM149 or UWB1.289 (**l**). **m**, Immunoblot of one out of 3 representative experiment of HeLa cells treated with vehicle (DMSO) or GSK126. **n** and **o**, Clonogenic assay in HeLa (**n**), A2780 (**o**) treated with DMSO or GSK126 under cisplatin. **p**, EZH2 domains with the F672I/H694A/R732K mutations of DHMT mutant. **m**, Clonogenic assays in EV, WT or DHMT VU423 cells treated with rucaparib. **q** and **r**, Chromosome breakage analysis of VU423 (**q**) and KURAMOCHI cells (**r**) treated with DMSO or GSK126 and with rucaparib. For **a**, **b**, significance was assessed with one-way Anova. Correlation was assessed with Pearson test r=0.68, P=0.00026 (**c**) and r=0.46, P=0.00067 (**d**). Data in **f**, **g**, **h** and **i** represent mean ± s.e.m of n=3 independent experiments. Data in **n**, **o**, **p, q** and **r** represent mean ± s.e.m of n=3 independent experiments. **n**: *P=0.016, **o**: *P=0.028, **p**: **P=0.00045, **q**: **P=0.0021 and **r**: from left, ***P=0.00011 and *P=0.038 Significance in **e**, **n**, **o**, **p**, **q** and **r** was assessed with the two-sided Student's t test. In **b, e, n, o, p, q, r**, *P<0.05, **P<0.01 and ***P<0.001, ns=non significant with exact P values (with a confidence interval of 95%) noted in legends for relevant panels Unprocessed original scans of blots are shown in Supplementary Fig. S6.

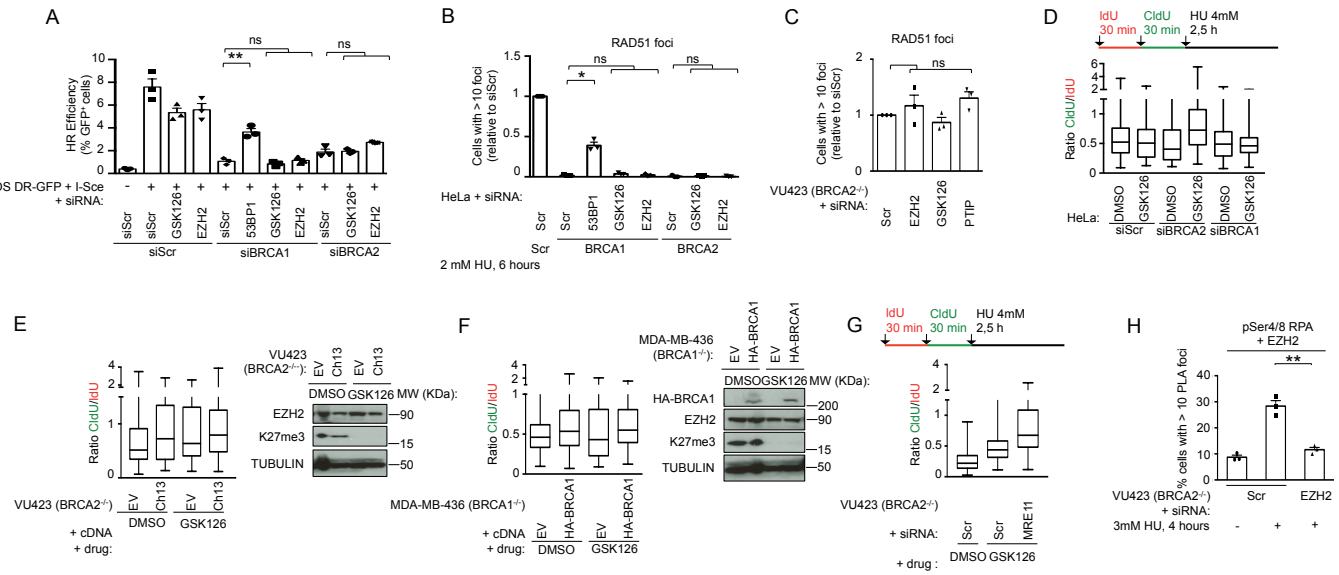

Supplementary Figure 2 Fork protection and not HR restoration is associated with EZH2 loss at stalled forks. **a**, DR-GFP assay in cells transfected with siRNAs and/or treated with GSK126. **b** and **c,** Quantification of RAD51 foci in HeLa (**b**) and VU423 (**c**) cells treated as indicated and subjected to HU treatment. The number of RAD51 positive cells is expressed as fold change of siScr-transfected sample, whose value is set to 1. **d,** Schematic for fork protection experiments. Box and whiskers plot show CldU to IdU ratio. P=0.001. **e**, Fork protection experiment and immunoblot analysis of VU423 cells stably expressing empty vector (EV) or Chromosome 13 (containing BRCA2 gene) and treated with DMSO or GSK126. P=0.04. **f**, Fork protection experiment and immunoblot analysis of MDA436 cells stably expressing an empty vector (EV) or a vector expressing HA-BRCA1 and treated with DMSO or GSK126. P = ns, not significant. **g**, Schematic for the labeling of cells with IdU and CldU for fork protection experiments. Box plot show CldU to IdU ratio. P = 0.0002. **h,** PLA assays in VU423 cells transfected with the indicated siRNAs and co-stained with antibodies against pSer4/8 RPA and EZH2. Bars indicate the number of cells with more than 10 PLA foci. n=100 cells were counted per condition. Data in **a**, **h** represent mean ± s.e.m of n=3 independent experiments. Significance was assessed with the χ^2 significance test for trend in proportions. **a**: **P=0.0049, **h**: **P=0.0064. Data in **b, c** represent mean ± s.e.m of n=3 independent experiments. Significance was assessed with two-sided Student's t test. *P=0.021. Box plots in **d, e, f** and **g** display median bar, first-third quartile box and min-to-max value whiskers. Analysis was performed by measuring analogue tracts on n=100 fibers per condition on n=3 independent experiments. Significance of difference among all the groups was assessed with the one-sided Kruskal-Wallis test. In **a, b, c** and **h**, *P<0.05, **P<0.01, ns=non significant with exact P values (with a confidence interval of 95%) noted in legends for relevant panels. Unprocessed original scans of blots are shown in Supplementary Fig. S6.

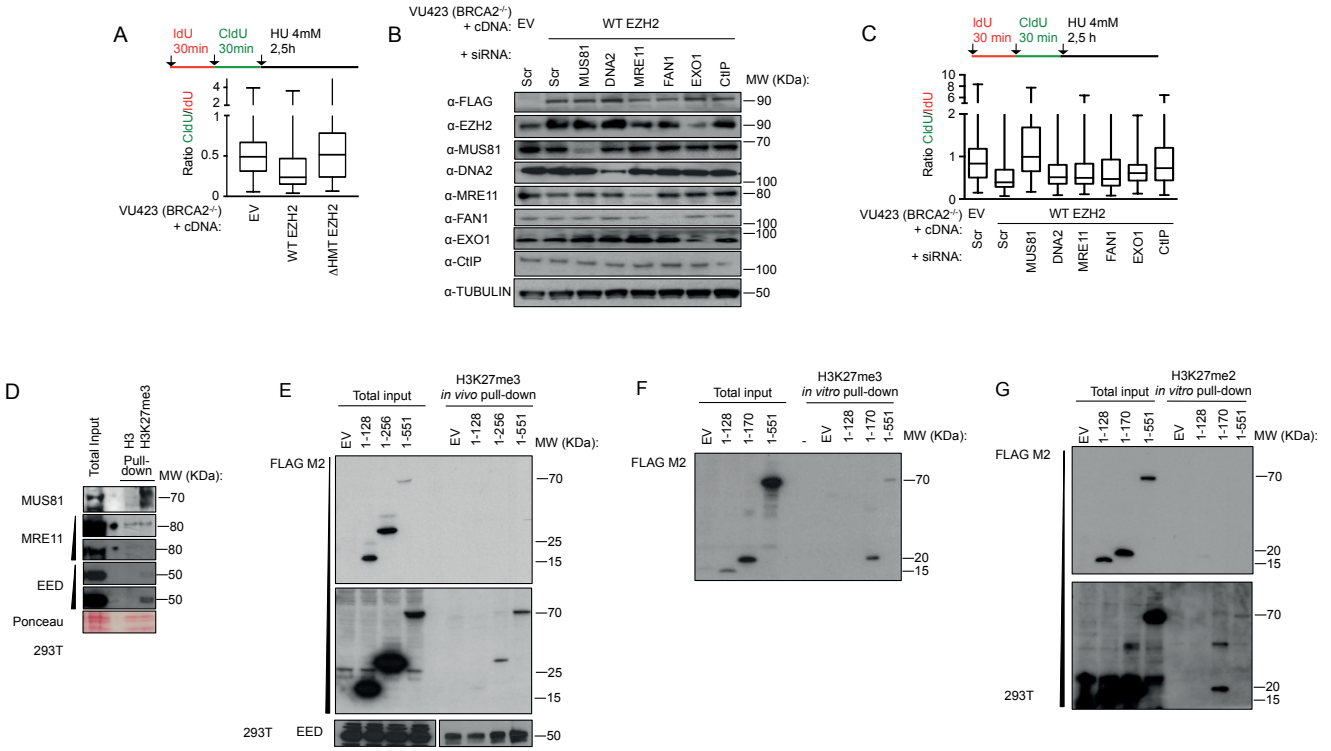

Supplementary Figure 3 EZH2 mediates fork degradation by specifically recruiting the endonuclease MUS81 through H3K27 methylation. **a**, Schematic of fork protection experiments with CldU and IdU incorporation for VU423 cells. Box plots for CldU to IdU ratio of VU423 cells transduced with EV, WT or DHMT are shown. P = 0.0006. **b**, One representative Immunoblot analysis of three independently performed and with similar results of VU423 cell transduced with EV or WT EZH2 and transfected with the indicated siRNAs. **c**, Schematic for the labeling with IdU and CldU of cells expressing EV or WT EZH2 for fork protection experiments. Box plots show CldU/IdU ratio of cells expressing the indicated cDNA and transfected with nuclease siRNAs (MUS81_5 was used). P=0.000012. **d**, Pull-down in 293T whole cell lysate with unmethylated or trimethylated histone H3 at lysine 27 (H3 or H3K27me3) depicting differential MUS81 but not MRE11 pull-down. EED binding to H3K27me3 is used as a positive control. **e** and **f**, Pull-down with trimethylated histone H3 at lysine 27 (H3K27me3) in 293T whole cell lysate expressing full-length or truncated MUS81 (**e**) or after in vitro transcription and translation of the MUS81 constructs (TnT, **f**). EED binding to H3K27me3 is used as a positive control. **g**, Pull-down after in vitro transcription and translation of the MUS81 constructs (TnT) performed with dimethylated histone H3 at lysine 27 (H3K27me2). Box plots in **a** and **c** display median bar, first-third quartile box and min-to-max value whiskers. Analysis was performed by measuring analogue tracts on n=100 fibers per condition on n=3 independent experiments. Significance of difference among all the groups was assessed with the one-sided Kruskal-Wallis test. Data in **e**, **f**, **g** and **h** represent one out of 3 independent experiments with similar results. Unprocessed original scans of blots are shown in Supplementary Fig. S6.

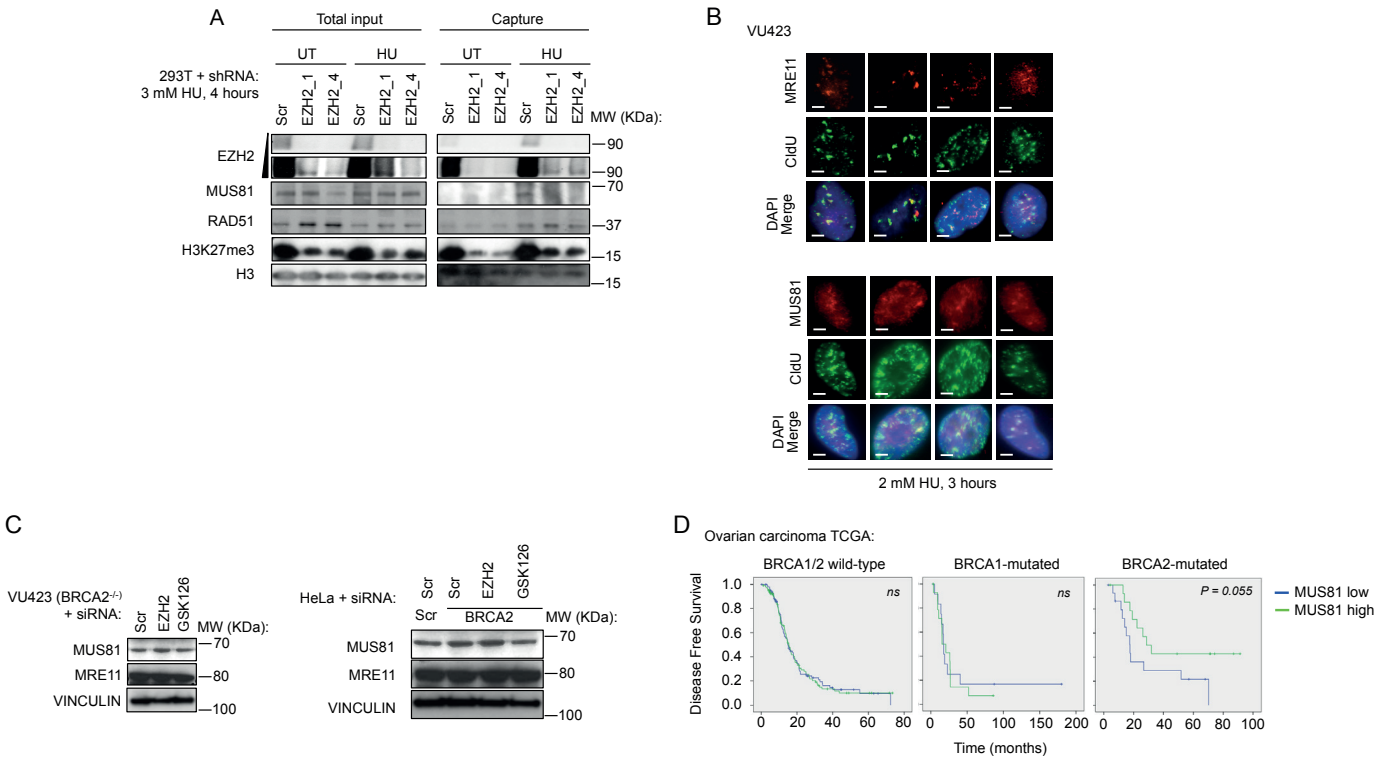

Supplementary Figure 4 MUS81 levels are not dependent on EZH2-mediated transcriptional activity and separate BRCA2-mutated ovarian carcinoma patients based on their PFS after chemotherapy. **a,** aniPOND of one out of 3 independent experiments with similar results were performed in 293T cells transduced with control (shScr) or EZH2 specific shRNAs (EZH2_1 and EZH2_4) showing recruitment of proteins at replicating (untreated, UT) and stalled (HU treated) forks. **b**, Immunofluorescence analysis of one out of 3 independent experiments with similar results of colocalization of MRE11 and MUS81 with sites of stalled replication, as marked by CldU incorporation upon HU treatment. Scale bar, 1 mm. **c**, Immunoblot analysis of one out of 3 independent experiments with similar results of VU423 and HeLa cells transfected with the indicated siRNAs. **d**, Progression-free survival (PFS) after platinum chemotherapy of TCGA patients harboring BRCA wild-type (n=82 samples), BRCA1-mutated (n=27 samples) or BRCA2-mutated (n=34 samples) ovarian carcinomas. Statistical significance was assessed by the two-sided log-rank test, P=0.055 with a 95% confidence interval. Unprocessed original scans of blots are shown in Supplementary Fig. S6.

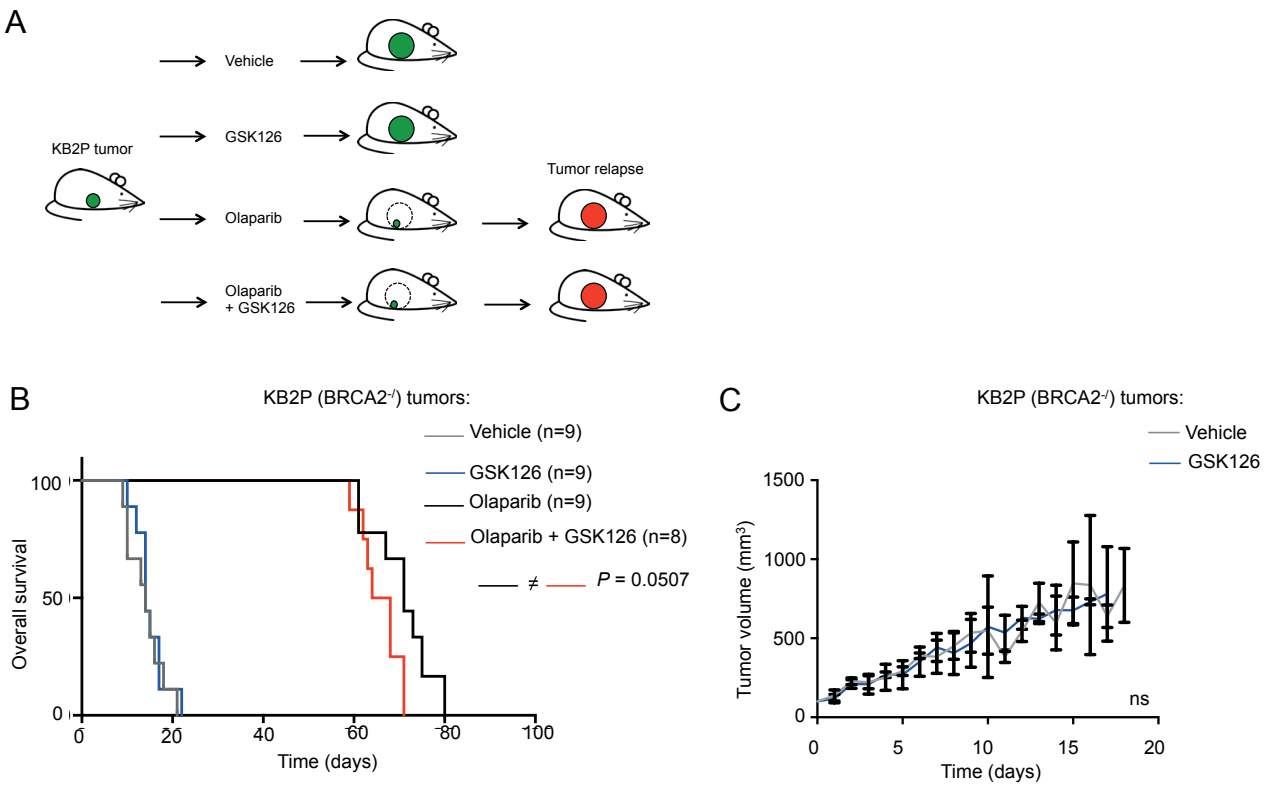

Supplementary Figure 5 Ezh2 inhibition shortens the overall survival of mice harboring KB2P-derived tumors without affecting tumor proliferation a, Outline of the PARPi in vivo intervention study. A spontaneous Brca2-/ p53-deficient tumor was generated and re-transplanted into syngenic WT mice. When the tumors reached 200 mm3, they were treated with either vehicle (n=9), GSK126 (n=9), olaparib (n=9) or olaparib + GSK126 (n=8). b, Overall survival of mice orthotopically injected with KB2P-derived tumors. c, Tumor growth curve of tumors treated with vehicle (grey) or GSK126 (blue). Data are represented as mean +/- s.d. In b, the two-sided log-rank (Mantel-Cox) P value is indicated, with a confidence interval of 95%. In c, significance was assessed by the two-sided Student's t test, ns=non significant.

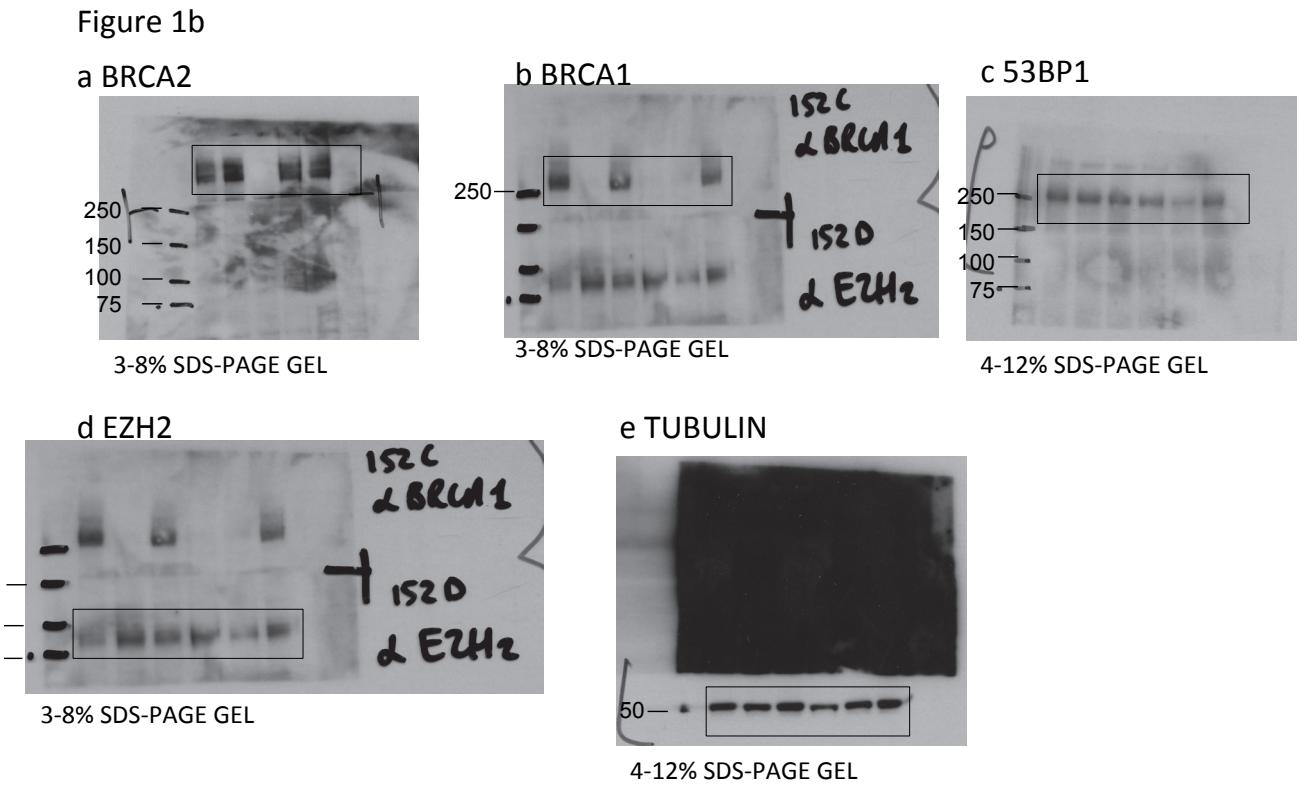

Supplementary Figure 6 Full scans of key Western blots. See blots of Figures 1B, 1C, 1F, Figures 2A, 2D, 2F, Figures 3A, 3C, 3E, 3F, Figure 4A, 4B, Supplementary Figures S1M, S1P, S2E, S2F, S3B, S3D, S3E, S3F, S3G and Supplementary Figure S4A and C.

Figure 1c

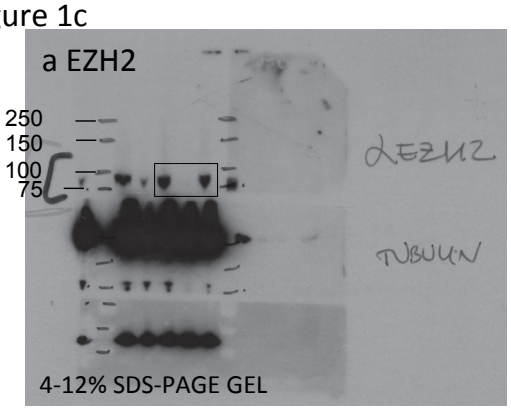

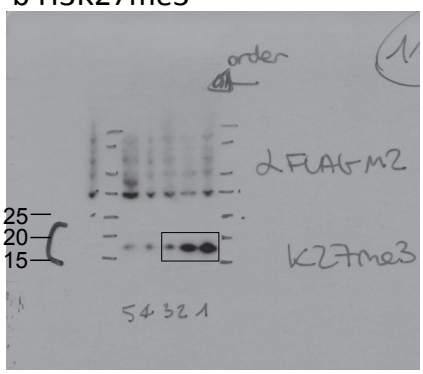

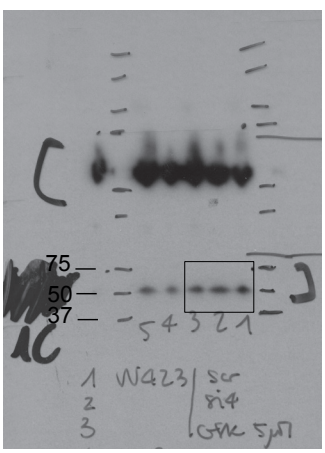

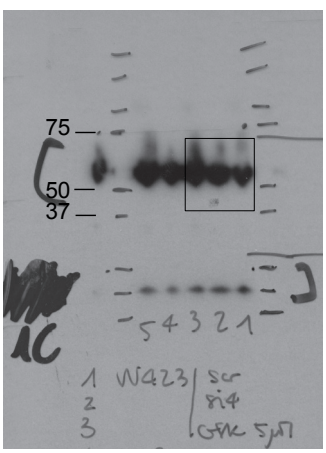

Supplementary Figure 6 Continued

Figure 1f

a BRCA2

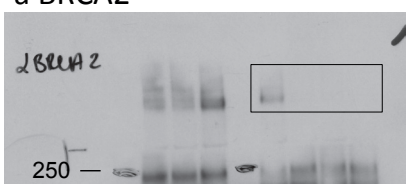

3-8% SDS-PAGE GEL

b SUZ12

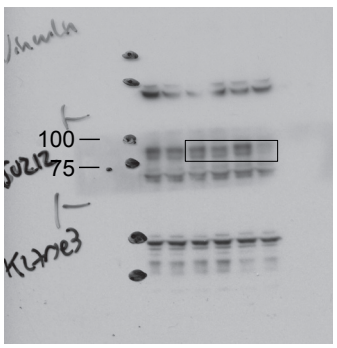

4-12% SDS-PAGE GEL

c TUBULIN

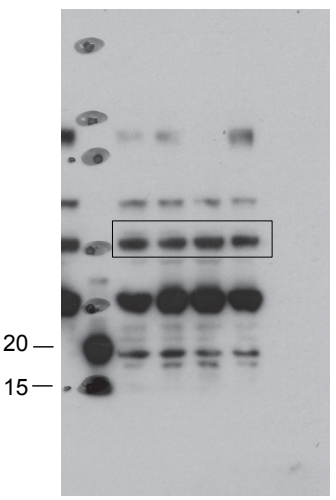

4-12% SDS-PAGE GEL

d H3K27me3

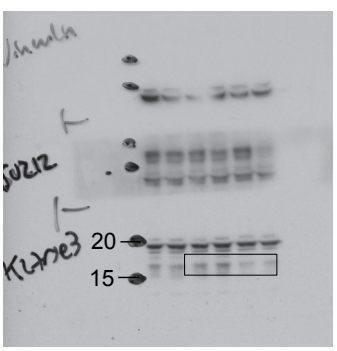

4-12% SDS-PAGE GEL

e H3

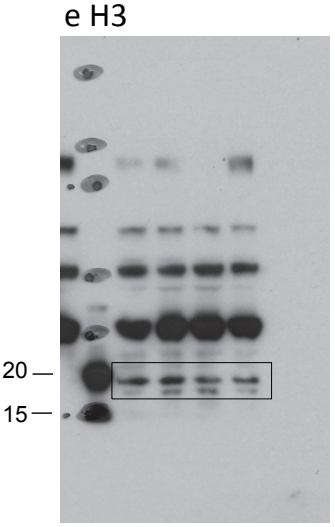

4-12% SDS-PAGE GEL

Supplementary Figure 6 Continued

Figure 2a

a PTIP

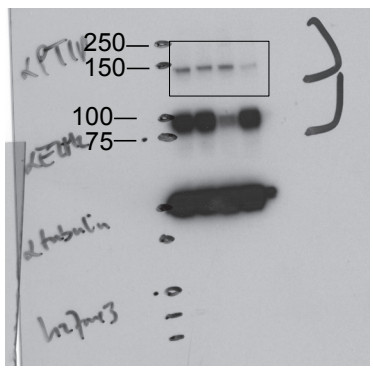

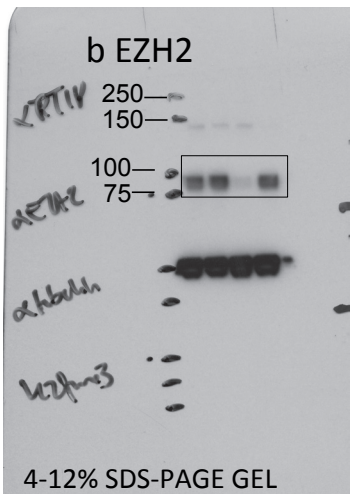

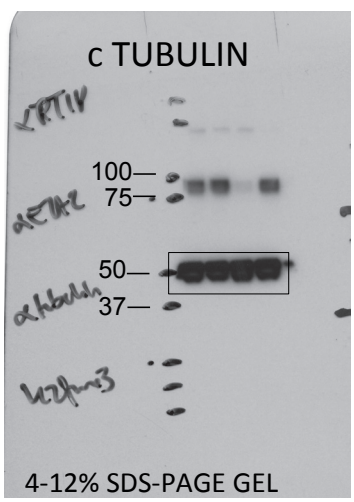

Supplementary Figure 6 Continued

Figure 2d

a FANCD2

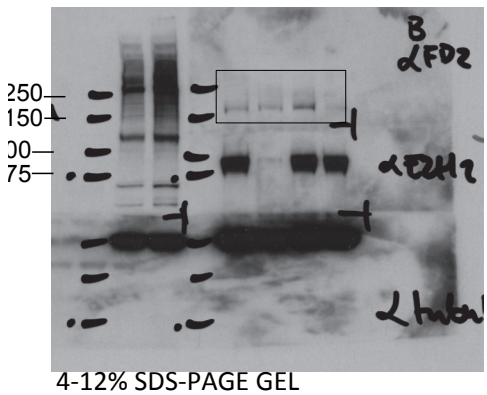

4-12% SDS-PAGE GEL

b EZH2

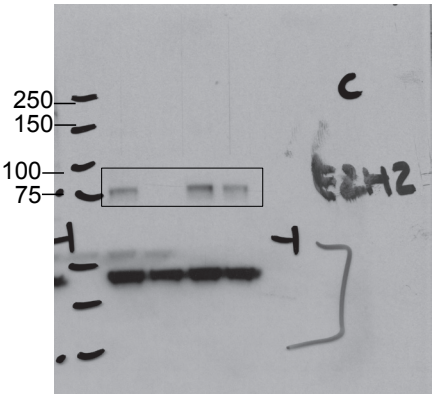

4-12% SDS-PAGE GEL

c TUBULIN

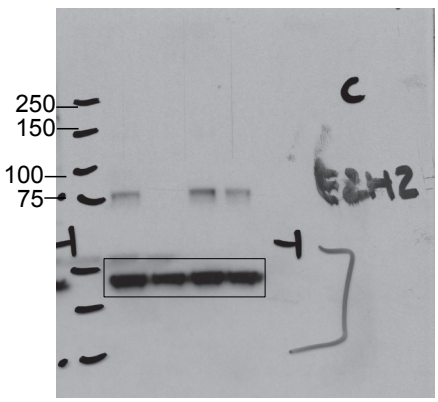

4-12% SDS-PAGE GEL

Supplementary Figure 6 Continued

Figure 2f - total input

a EZH2

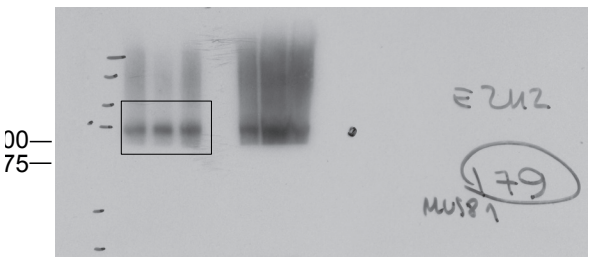

4-12% SDS-PAGE GEL

b PCNA

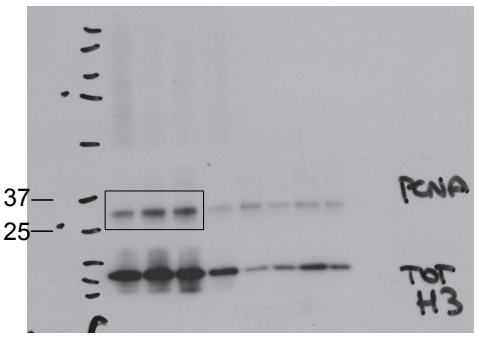

4-12% SDS-PAGE GEL

c H3K27me3

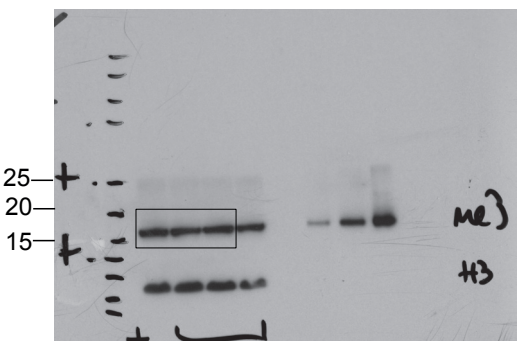

4-12% SDS-PAGE GEL

d H3

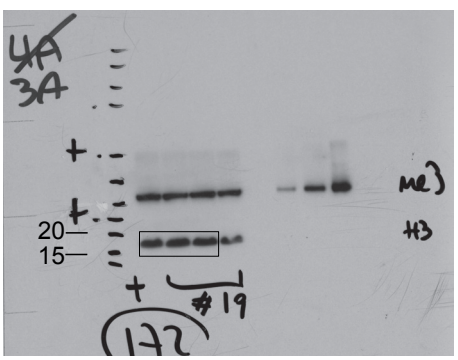

4-12% SDS-PAGE GEL

Supplementary Figure 6 Continued

Figure 2f – capture

a EZH2

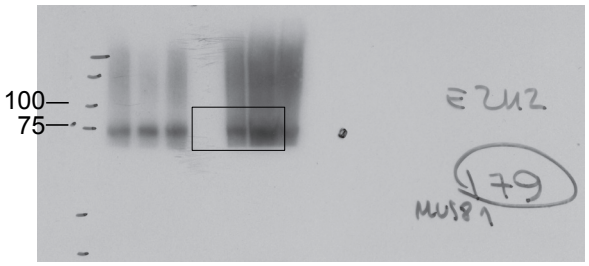

4-12% SDS-PAGE GEL

b PCNA

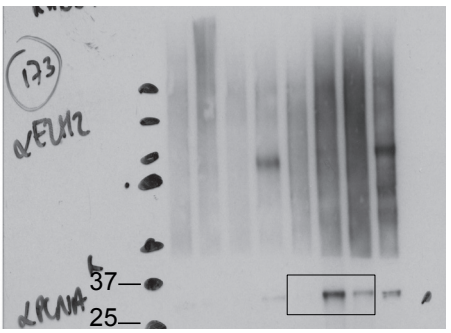

4-12% SDS-PAGE GEL

c H3K27me3

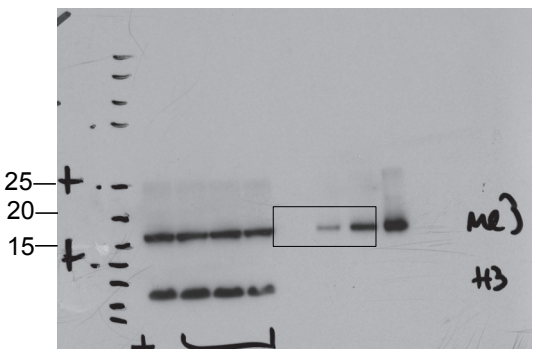

4-12% SDS-PAGE GEL

d H3

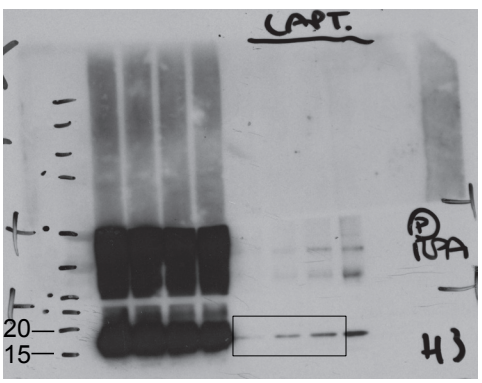

4-12% SDS-PAGE GEL

Supplementary Figure 6 Continued

Figure 3a

a Flag- EZH2

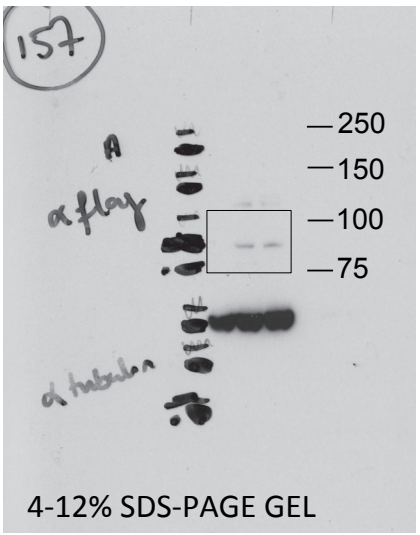

b TUBULIN

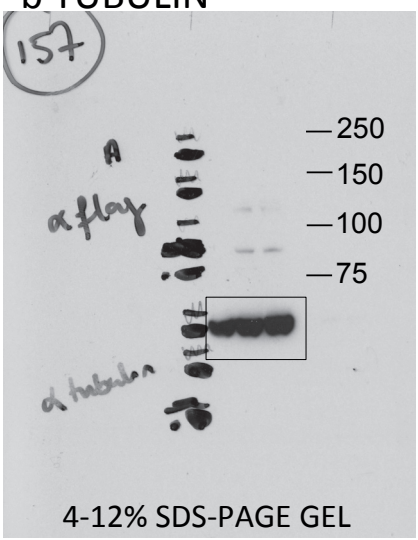

Supplementary Figure 6 Continued

Figure 3c

a MUS81

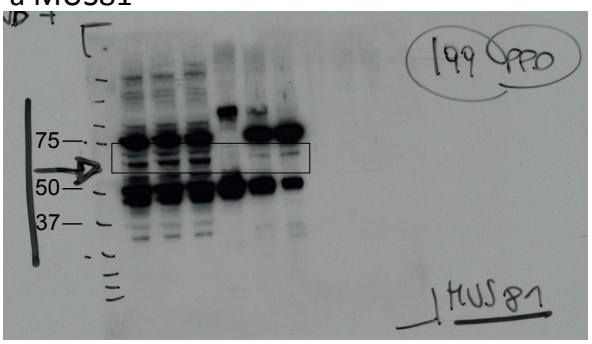

4-12% SDS-PAGE GEL

b EED

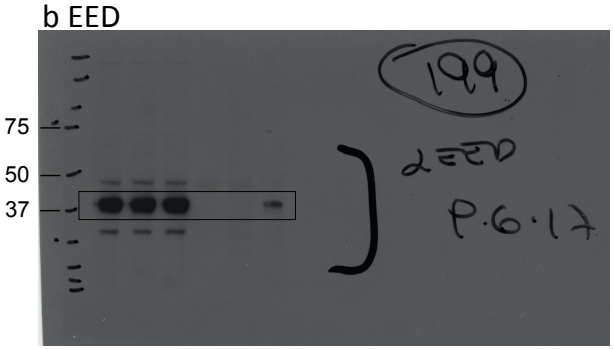

4-12% SDS-PAGE GEL

Figure 3e

a FLAG

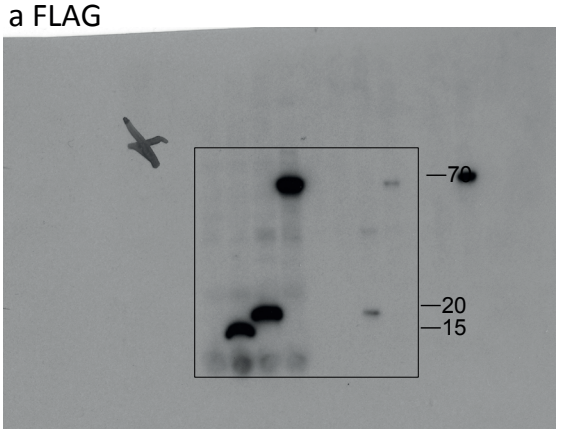

4-12% SDS-PAGE GEL

Figure 3f

a FLAG

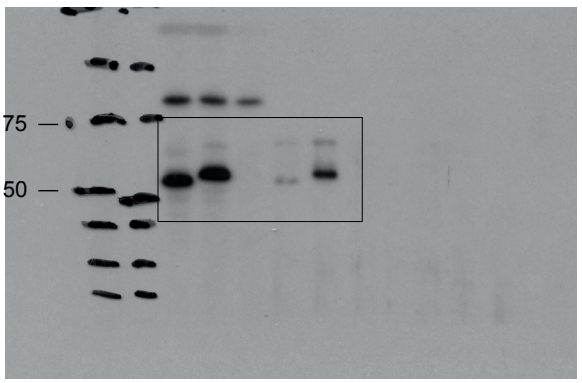

4-12% SDS-PAGE GEL

Supplementary Figure 6 Continued

Figure 4a - total input

a EZH2

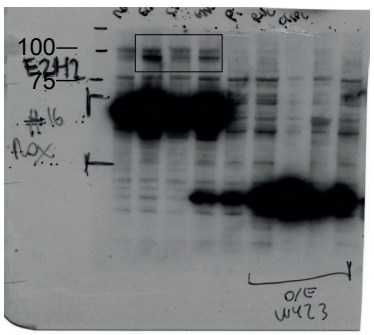

4-12% SDS-PAGE GEL

b MRE11

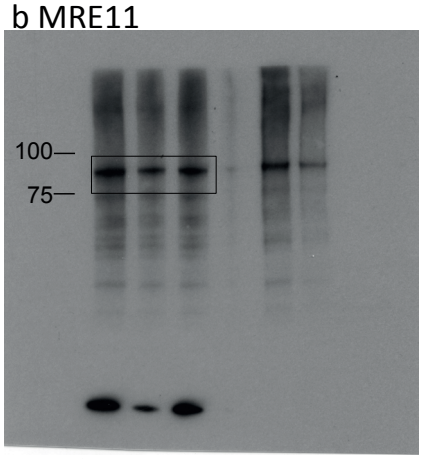

4-12% SDS-PAGE GEL

c MUS81

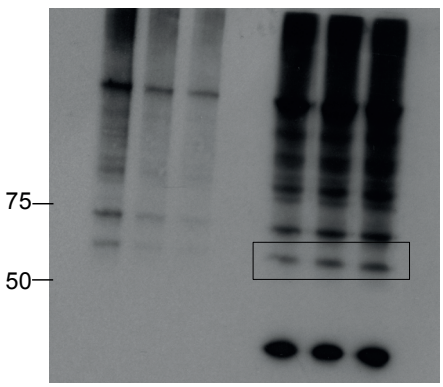

4-12% SDS-PAGE GEL

d H3

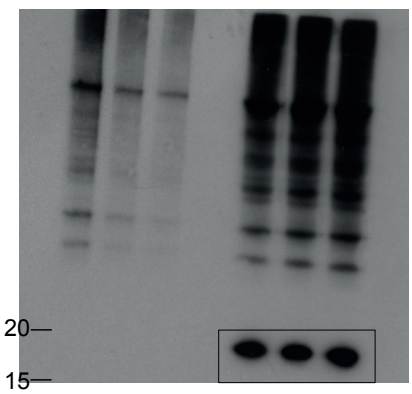

4-12% SDS-PAGE GEL

Supplementary Figure 6 Continued

Figure 4a – capture

a EZH2

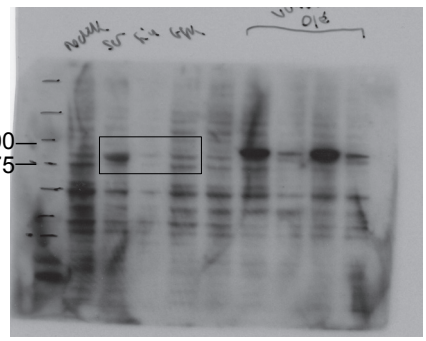

4-12% SDS-PAGE GEL

b MRE11

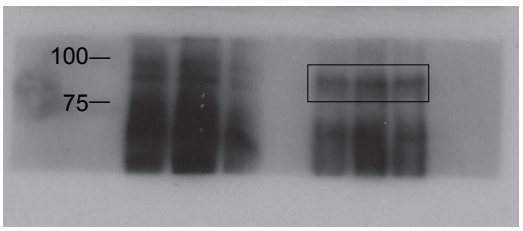

4-12% SDS-PAGE GEL

c MUS81

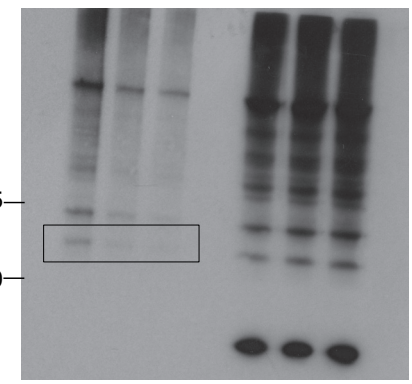

4-12% SDS-PAGE GEL

d H3

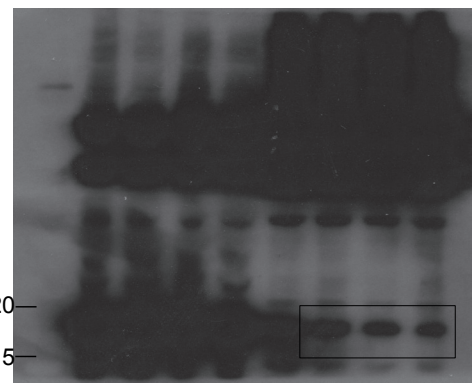

4-12% SDS-PAGE GEL

Supplementary Figure 6 Continued

Figure 4a - total input and capture

e H3K27me3 - total input

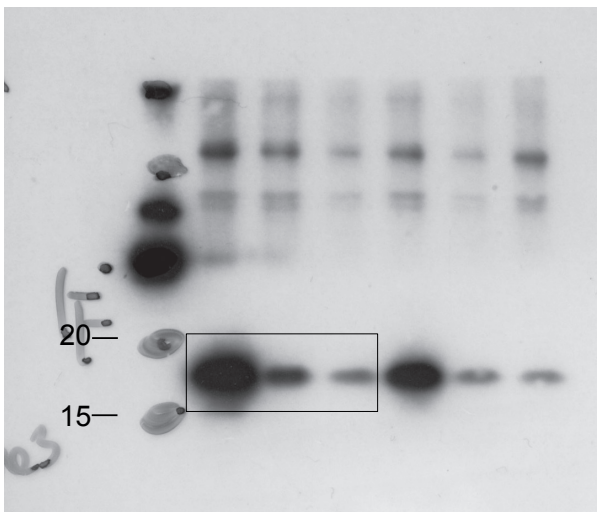

e H3K27me3 - capture

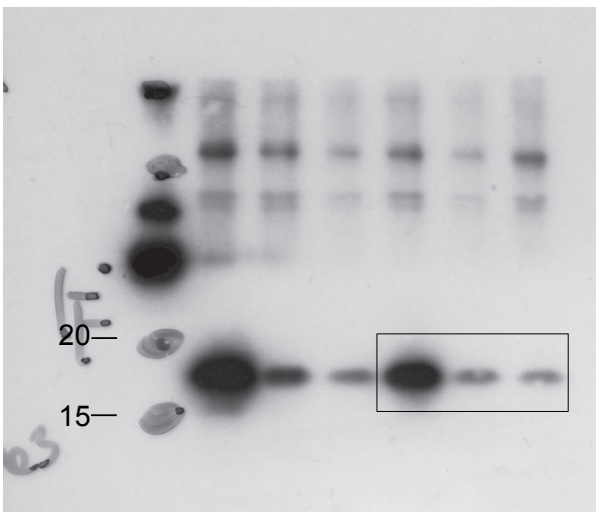

Supplementary Figure 6 Continued

Figure 4b

a EZH2

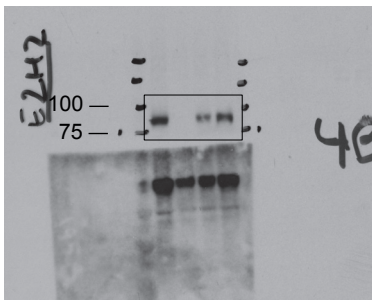

4-12% SDS-PAGE GEL

b MUS81

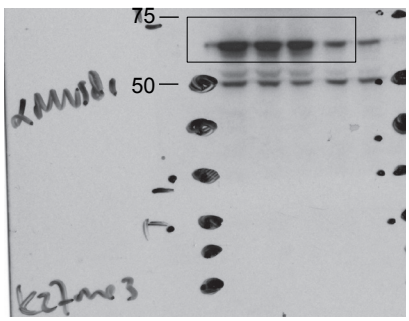

4-12% SDS-PAGE GEL

c TUBULIN

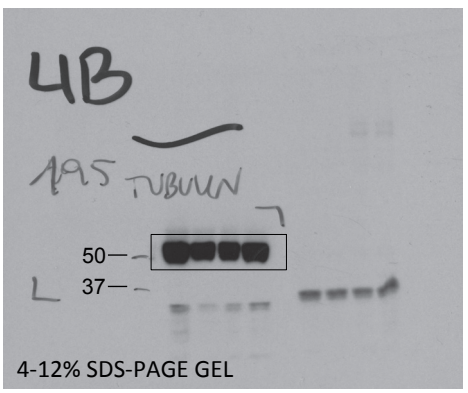

4-12% SDS-PAGE GEL

d H3K27me2

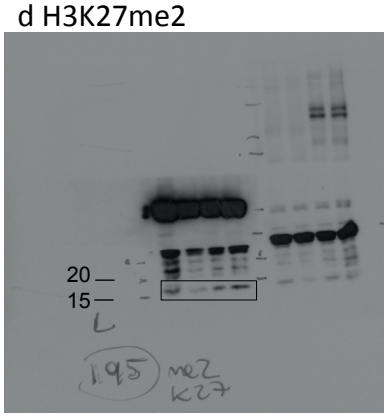

4-12% SDS-PAGE GEL

e H3K27me3

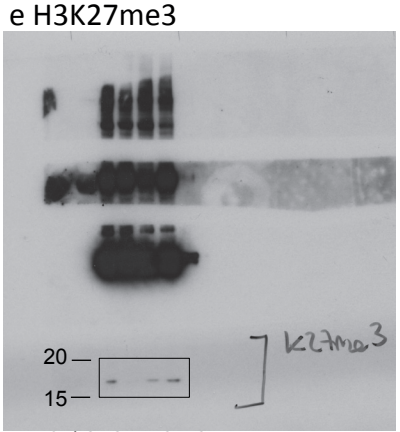

4-12% SDS-PAGE GEL

Supplementary Figure 6 Continued

Figure S1m

a EZH2

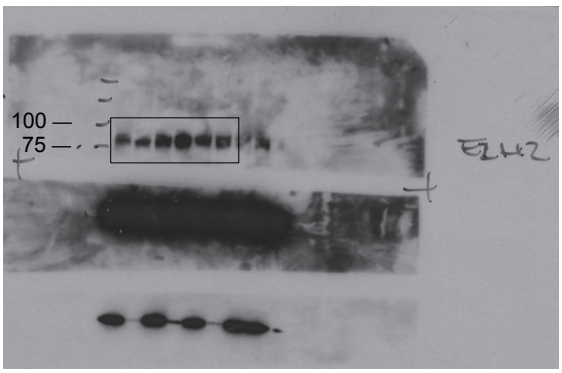

4-12% SDS-PAGE GEL

b TUBULIN

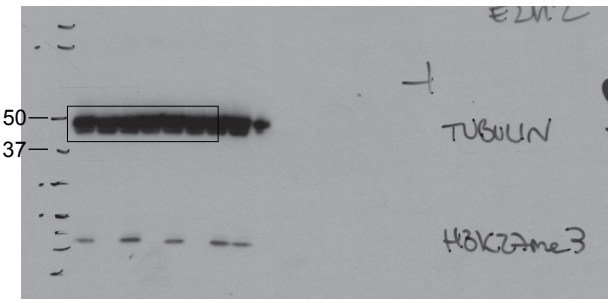

4-12% SDS-PAGE GEL

c H3K27me3

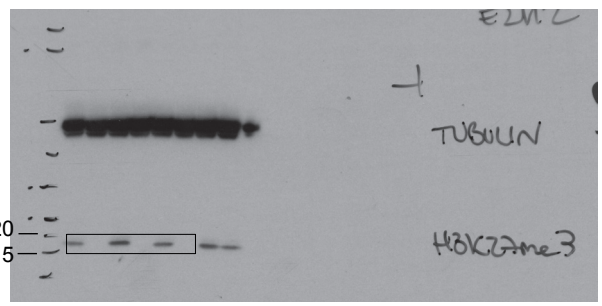

4-12% SDS-PAGE GEL

d H3

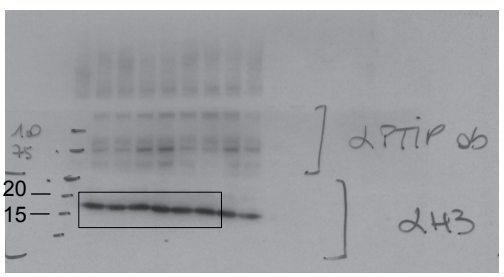

4-12% SDS-PAGE GEL

Supplementary Figure 6 Continued

Figure S1p

a FLAG

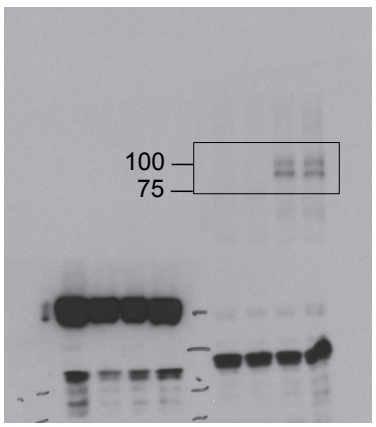

4-12% SDS-PAGE GEL

b TUBULIN

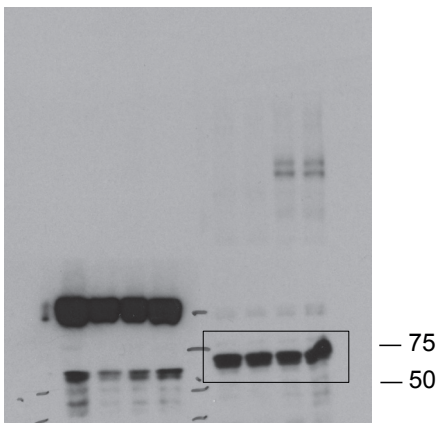

4-12% SDS-PAGE GEL

c EZH2

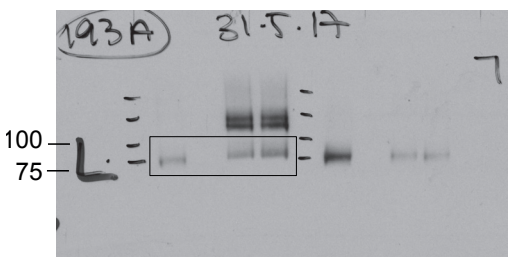

4-12% SDS-PAGE GEL

Supplementary Figure 6 Continued

Figure S2e

a EZH2

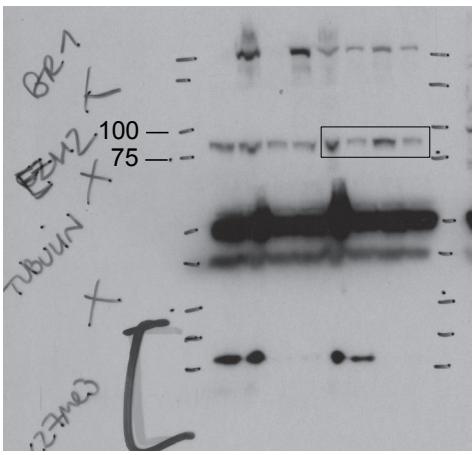

4-12% SDS-PAGE GEL

b H3K27me3

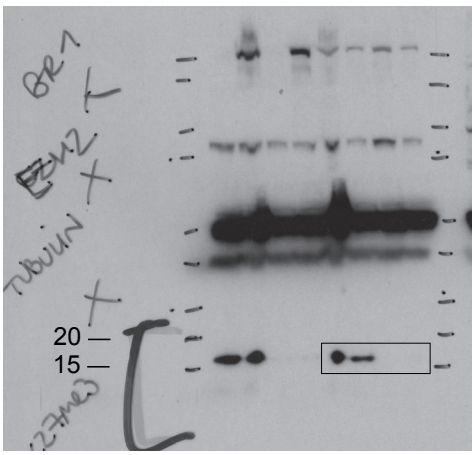

4-12% SDS-PAGE GEL

c TUBULIN

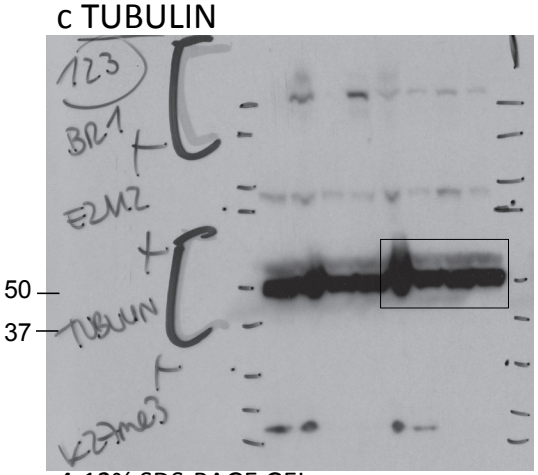

4-12% SDS-PAGE GEL

Supplementary Figure 6 Continued

Figure S2f

a HA-BRCA1

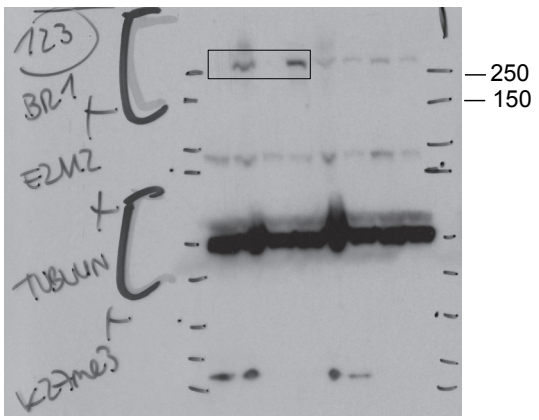

4-12% SDS-PAGE GEL

b EZH2

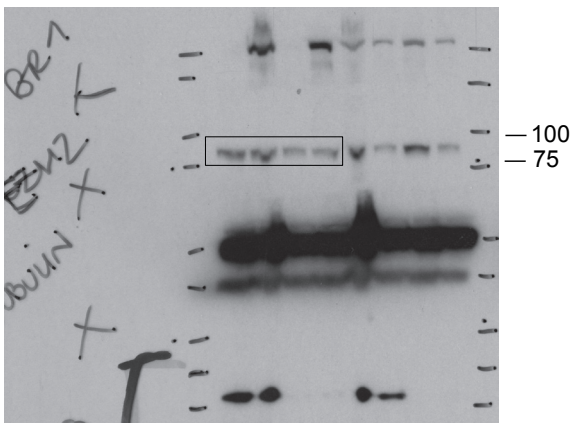

4-12% SDS-PAGE GEL

c K27me3

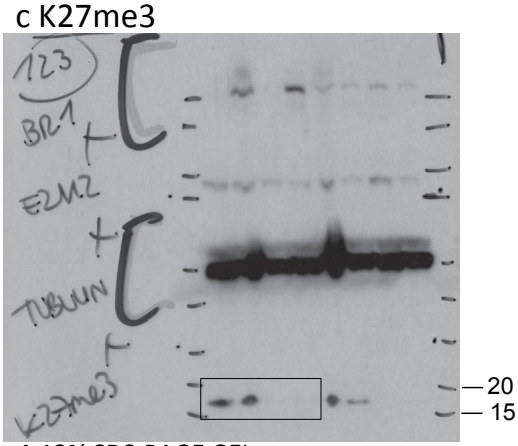

4-12% SDS-PAGE GEL

d TUBULIN

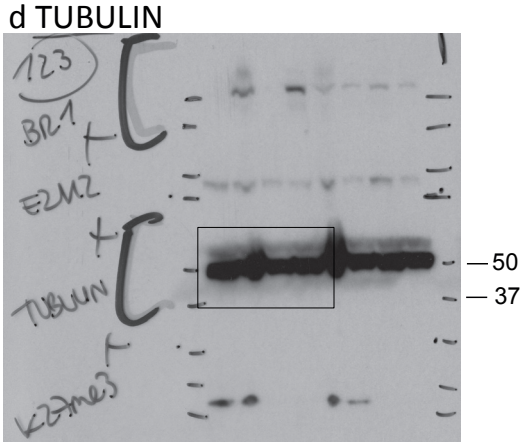

4-12% SDS-PAGE GEL

Supplementary Figure 6 Continued

Figure S3b

a FLAG

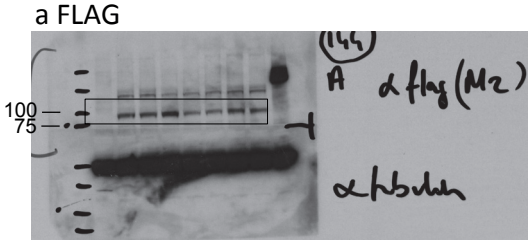

4-12% SDS-PAGE GEL

b EZH2

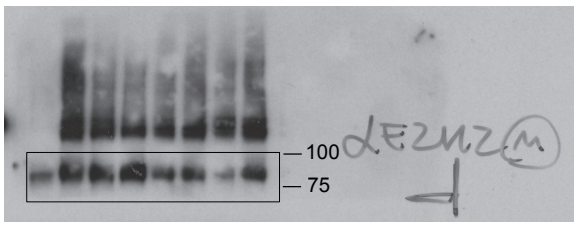

4-12% SDS-PAGE GEL

c MUS81

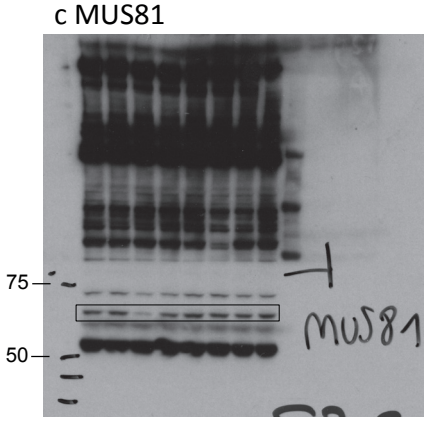

4-12% SDS-PAGE GEL

d DNA2

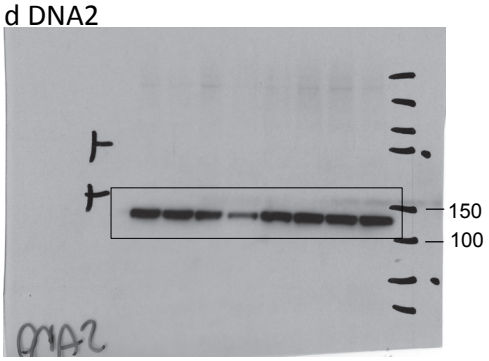

4-12% SDS-PAGE GEL

Supplementary Figure 6 Continued

Figure S3b

e MRE11

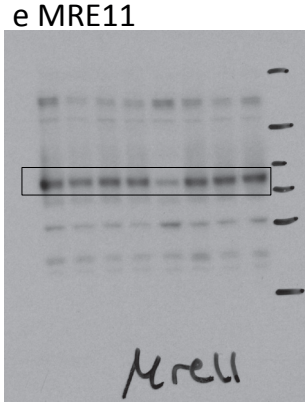

4-12% SDS-PAGE GEL

f FAN1

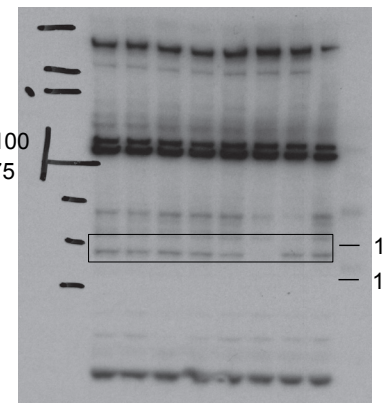

4-12% SDS-PAGE GEL

g TUBULIN

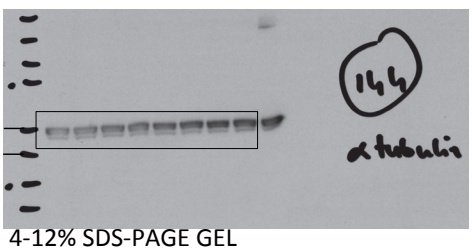

4-12% SDS-PAGE GEL

h EXO1

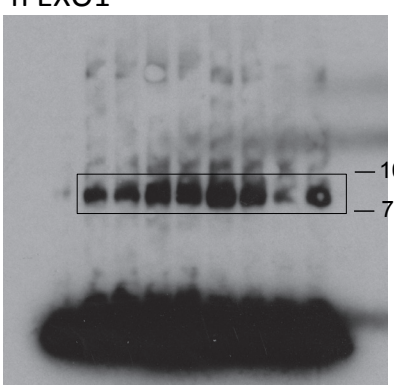

4-12% SDS-PAGE GEL

i CtIP

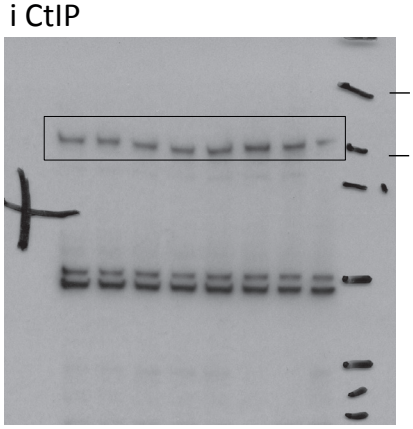

4-12% SDS-PAGE GEL

Supplementary Figure 6 Continued

Figure S3d

a MUS81

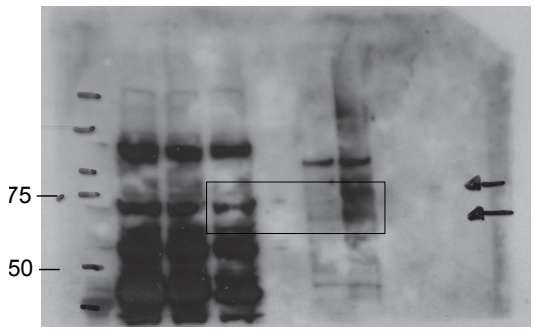

4-12% SDS-PAGE GEL

b MRE11

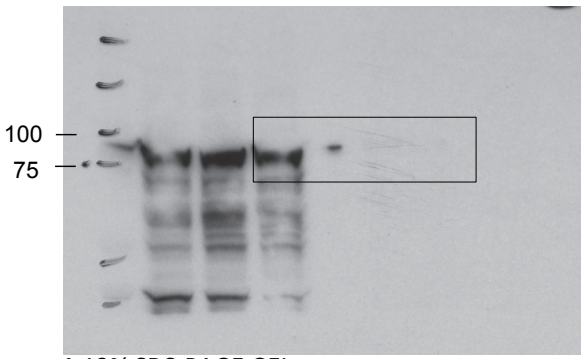

4-12% SDS-PAGE GEL

c EED

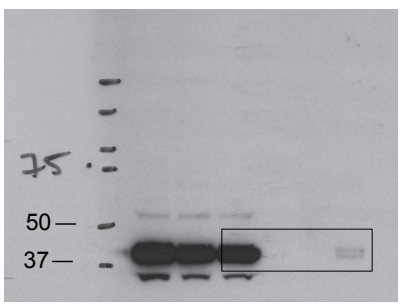

4-12% SDS-PAGE GEL

b MRE11 – high exposure

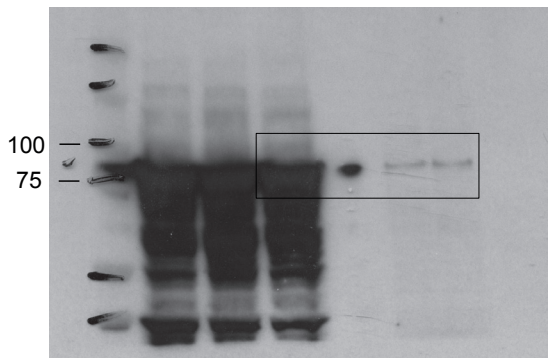

4-12% SDS-PAGE GEL

Supplementary Figure 6 Continued

Figure S3e

a FLAG

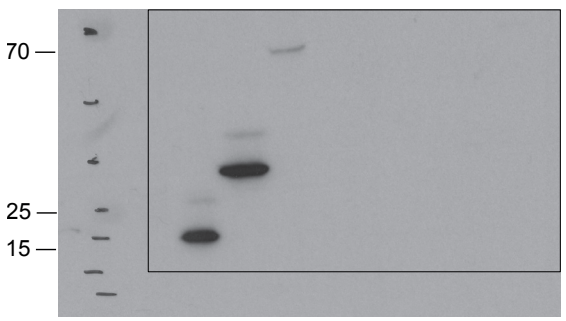

4-12% SDS-PAGE GEL

a FLAG – high exposure

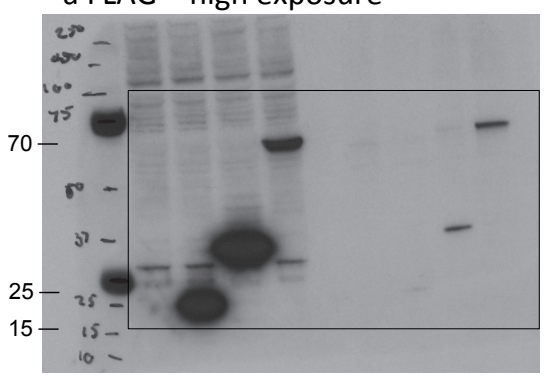

4-12% SDS-PAGE GEL

b EED

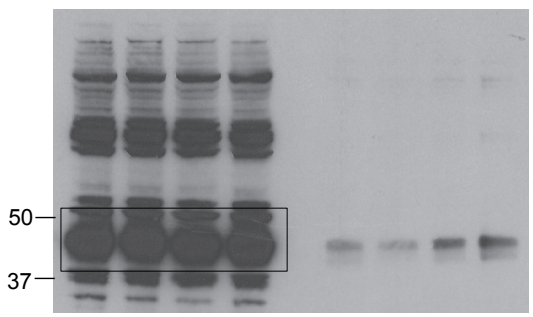

4-12% SDS-PAGE GEL

b EED – high exposure

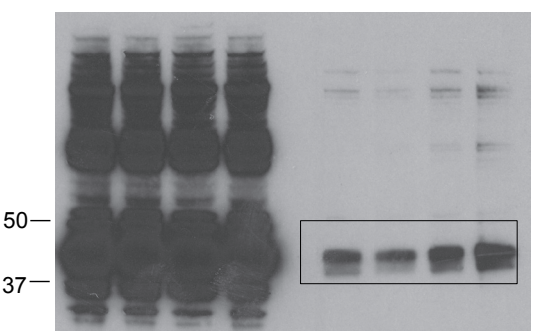

4-12% SDS-PAGE GEL

Supplementary Figure 6 Continued

Figure S3f
FLAG

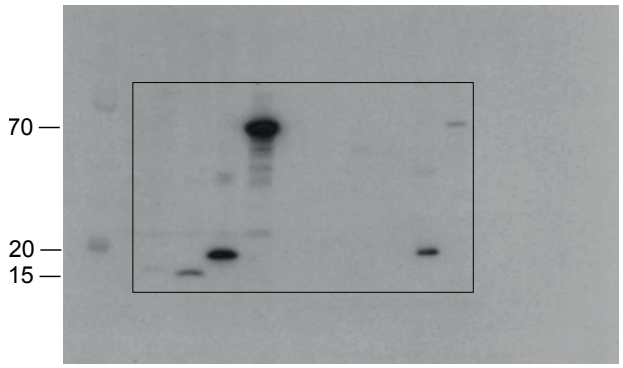

4-12% SDS-PAGE GEL

Figure S3g
FLAG

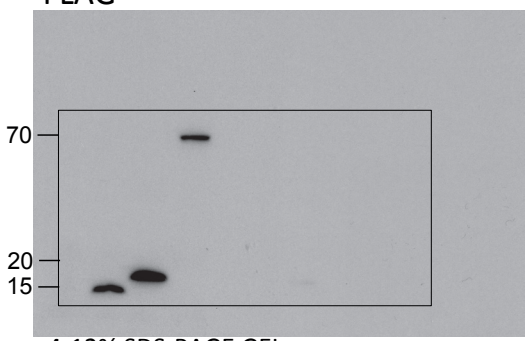

4-12% SDS-PAGE GEL

FLAG – high exposure

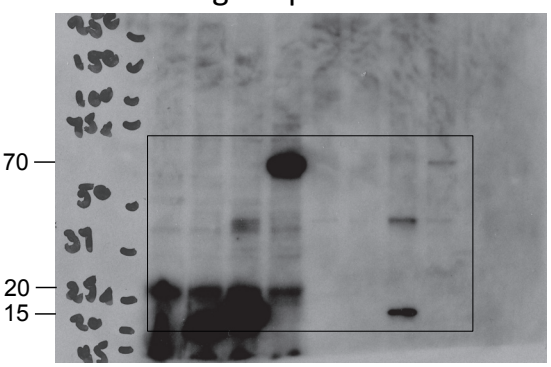

4-12% SDS-PAGE GEL

Supplementary Figure 6 Continued

Figure S4a – total inputs

a EZH2

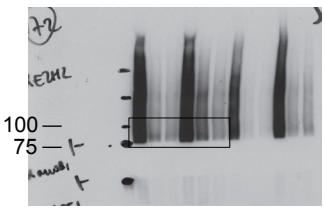

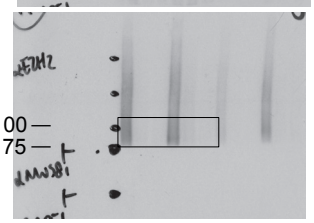

4-12% SDS-PAGE GEL

b MUS81

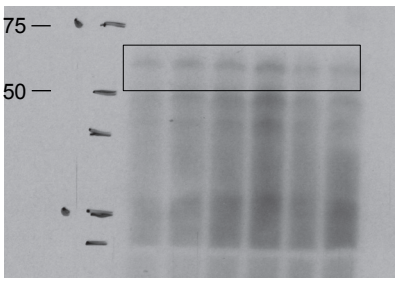

4-12% SDS-PAGE GEL

c RAD51

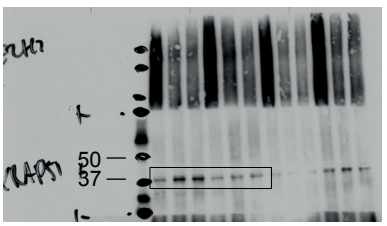

4-12% SDS-PAGE GEL

d H3K27me3

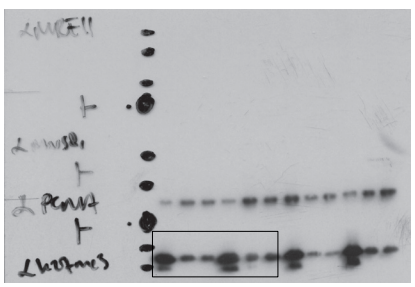

4-12% SDS-PAGE GEL

e H3

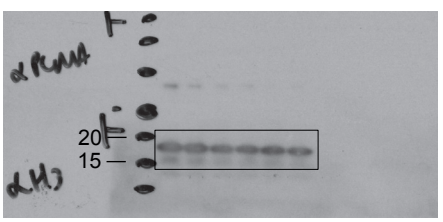

4-12% SDS-PAGE GEL

Supplementary Figure 6 Continued

Figure S4a – capture samples

a EZH2

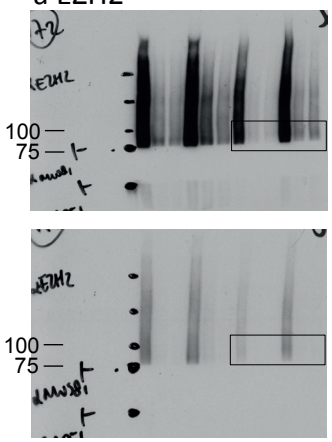

4-12% SDS-PAGE GEL

b MUS81

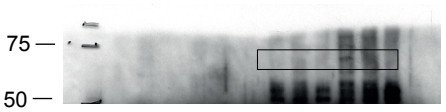

4-12% SDS-PAGE GEL

c RAD51

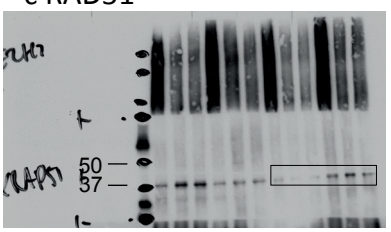

4-12% SDS-PAGE GEL

d H3K27me3

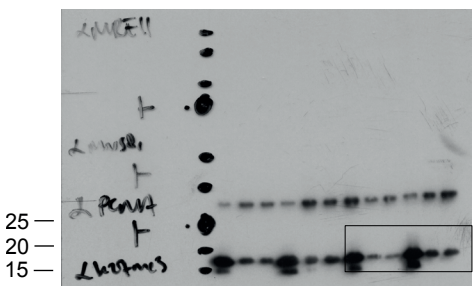

4-12% SDS-PAGE GEL

e H3

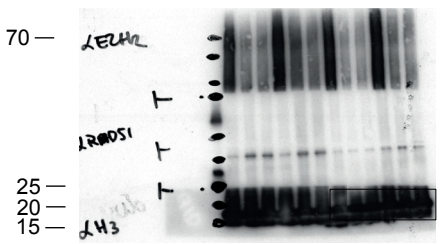

4-12% SDS-PAGE GEL

Supplementary Figure 6 Continued

Figure S4c - left

a MUS81

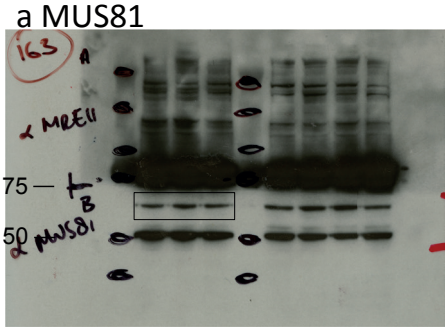

4-12% SDS-PAGE GEL

b MRE11

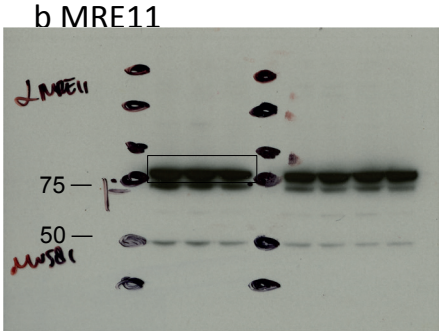

4-12% SDS-PAGE GEL

c VINCULIN

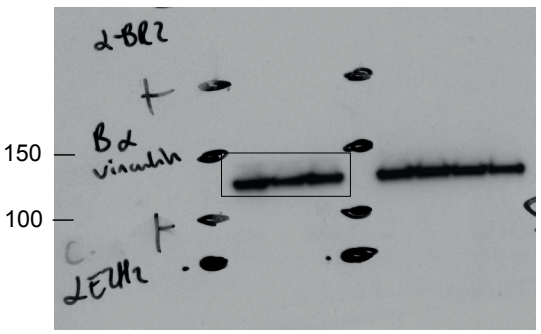

4-12% SDS-PAGE GEL

Supplementary Figure 6 Continued

Figure S4c - right

a MUS81

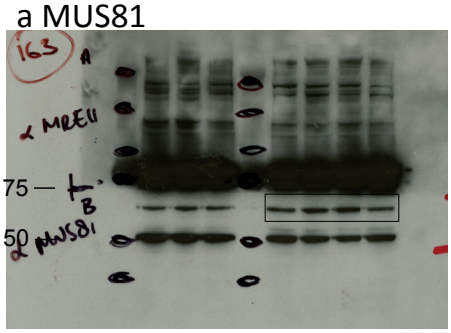

4-12% SDS-PAGE GEL

b MRE11

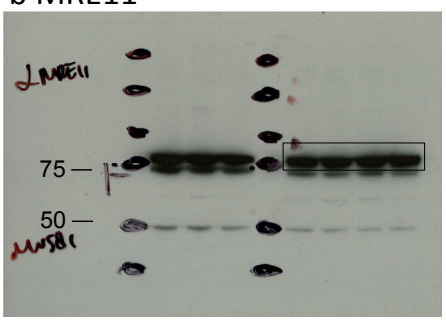

4-12% SDS-PAGE GEL

c VINCULIN

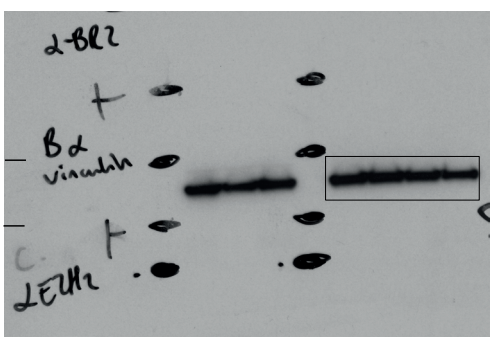

4-12% SDS-PAGE GEL

Supplementary Figure 6 Continued

Supplementary Table Legend

Supplementary Table 1 Gene list of chromatin modifiers analyzed. The table depicts the chromatin modifiers gene list analyzed from the TCGA data sets that are reported in the Methods section.

nature research

Corresponding author(s): Alan D'Andrea

☐ Initial submission ☐ Revised version ☒ Final submission

Life Sciences Reporting Summary

Nature Research wishes to improve the reproducibility of the work that we publish. This form is intended for publication with all accepted life science papers and provides structure for consistency and transparency in reporting. Every life science submission will use this form; some list items might not apply to an individual manuscript, but all fields must be completed for clarity.

For further information on the points included in this form, see Reporting Life Sciences Research. For further information on Nature Research policies, including our data availability policy, see Authors & Referees and the Editorial Policy Checklist.

Experimental design

1. Sample size

   Describe how sample size was determined. — No sample size calculation was performed.

2. Data exclusions

   Describe any data exclusions. — No data were excluded from the analysis.

3. Replication

   Describe whether the experimental findings were reliably reproduced. — All attempts of replication were successful.

4. Randomization

   Describe how samples/organisms/participants were allocated into experimental groups. — Tumor-bearing mice were randomized blindly and irrespective of their characteristics.

5. Blinding

   Describe whether the investigators were blinded to group allocation during data collection and/or analysis. — All the in vivo procedures were carried out by animal technicians who were blinded to the hypothesis of the treatment outcome.

   Note: all studies involving animals and/or human research participants must disclose whether blinding and randomization were used.

6. Statistical parameters

   For all figures and tables that use statistical methods, confirm that the following items are present in relevant figure legends (or in the Methods section if additional space is needed).

n/a	Confirmed
☐	☒ The exact sample size (*n*) for each experimental group/condition, given as a discrete number and unit of measurement (animals, litters, cultures, etc.)
☐	☒ A description of how samples were collected, noting whether measurements were taken from distinct samples or whether the same sample was measured repeatedly
☐	☒ A statement indicating how many times each experiment was replicated
☐	☒ The statistical test(s) used and whether they are one- or two-sided (note: only common tests should be described solely by name; more complex techniques should be described in the Methods section)
☒	☐ A description of any assumptions or corrections, such as an adjustment for multiple comparisons
☐	☒ The test results (e.g. *P* values) given as exact values whenever possible and with confidence intervals noted
☐	☒ A clear description of statistics including central tendency (e.g. median, mean) and variation (e.g. standard deviation, interquartile range)
☐	☒ Clearly defined error bars

See the web collection on statistics for biologists for further resources and guidance.

Software

Policy information about availability of computer code

7. Software

Describe the software used to analyze the data in this study.	Analyses were performed with the use of GraphPad Prism 6 software.

For manuscripts utilizing custom algorithms or software that are central to the paper but not yet described in the published literature, software must be made available to editors and reviewers upon request. We strongly encourage code deposition in a community repository (e.g. GitHub). *Nature Methods* guidance for providing algorithms and software for publication provides further information on this topic.

Materials and reagents

Policy information about availability of materials

8. Materials availability

Indicate whether there are restrictions on availability of unique materials or if these materials are only available for distribution by a for-profit company.	All unique materials used are readily available from the authors or from standard commercial sources.

9. Antibodies

Describe the antibodies used and how they were validated for use in the system under study (i.e. assay and species).	Antibodies. Antibodies used in this study were: anti-EZH2 (for Western blot: Millipore, clone BD43, 1:1000, for PLA: Cell Signal, clone AC22, 1:500, for IHC: Cellsignal, #5246, 1:500), anti-H3K27me2 (Cell Signal, 1:2000), anti-H3K27me3 (Cell Signal, #9733, 1:2000), anti-H3 (Santa Cruz, clone FL136, 1:10000), anti-BRCA1 (Calbiochem, OP-92, 1:250), anti-BRCA2 (Calbiochem, OP-95, 1:250), anti-53BP1 (Abcam, #36823, 1:1000), anti-tubulin (Santa Cruz, clone B7, 1:500), anti-PCNA (clone PC-10, 1:250), anti-FANCD2 (Santa Cruz, clone FI17, 1:250), anti-FLAG (Sigma, clone M2, 1:2000), RPA pSer33 and pSer4/8 (Novus Biologicals, 1:500 and 1:250), anti-MUS81 (Western blot: Abcam, 97391, 1:1000; IF: Abcam, MTA30 2G1073, 1:250), anti-MRE11 (Novus Biologicals, 1:1000), anti-EXO1 (Bethyl, 1:1000), anti-DNA2 (Abcam, 1:500), anti-CTIP (Bethyl, 1:1000), anti-FAN1 (Abcam, 1:500), anti-RAD51 (Santa Cruz, clone H92, 1:250), anti-EED (Santa Cruz, clone H300, 1:250) anti-BrdU (for detection of ssDNA in PLA assay and of IdU in fiber assay, #347580, clone B44, Becton Dickinson, 1:50), anti-BrdU (for detection of CldU, Abcam #6326, 1:100). Secondary antibodies used for immunoblot were HRP-linked anti-goat (Santa Cruz, 1:1000), anti-mouse or anti-rabbit (Life Technologies, 1:5000) while for immunofluorescence we used Alexa-Fluor antibodies (Life Technologies, 1:1000). Only antibodies previously validated for the assay of interest were used. In addition, antibodies were validated by comparing the signal of Scr cells with the signal of cells knocked-down for the antigen against which the antibody was raised.

10. Eukaryotic cell lines

a. State the source of each eukaryotic cell line used.	The eukaryotic cell lines used were purchased from ATCC (American Type Culture Collection).
b. Describe the method of cell line authentication used.	None of the cell lines used were authenticated.
c. Report whether the cell lines were tested for mycoplasma contamination.	Cell lines were tested for mycoplasma at the beginning of the study and resulted negative (mycoplasma-specific PCR test). This is also indicated in the "Materials and Methods" section.
d. If any of the cell lines used are listed in the database of commonly misidentified cell lines maintained by ICLAC, provide a scientific rationale for their use.	None of the cell lines used in this paper are currently listed in the database of commonly misidentified cell lines maintained by ICLAC. This is indicated in the "Materials and Methods" section.

Animals and human research participants

Policy information about studies involving animals; when reporting animal research, follow the ARRIVE guidelines

11. Description of research animals

Provide details on animals and/or animal-derived materials used in the study.	Mice used were NMRI-nude females of 7-8 weeks of age

Policy information about studies involving human research participants

12. Description of human research participants

Describe the covariate-relevant population characteristics of the human research participants.	The study did not involve any human research participants.